Master's thesis

NTNU
Norwegian University of Science and Technology
Faculty of Natural Sciences
Department of Chemical Engineering

Vilde Rolland Svensen

The Effect of Metal Promoters on Supported Cobalt Catalysts for the Fischer-Tropsch Synthesis

Master's thesis in Chemical Engineering
Supervisor: Edd Anders Blekkan
Co-supervisor: Ingeborg-Helene Svenum and Rune Myrstad
June 2021

NTNU
Norwegian University of
Science and Technology

Vilde Rolland Svensen

The Effect of Metal Promoters on Supported Cobalt Catalysts for the Fischer-Tropsch Synthesis

Master's thesis in Chemical Engineering
Supervisor: Edd Anders Blekkan
Co-supervisor: Ingeborg-Helene Svenum and Rune Myrstad
June 2021

Norwegian University of Science and Technology
Faculty of Natural Sciences
Department of Chemical Engineering

NTNU
Norwegian University of
Science and Technology

Preface

This thesis was a continuation of the specialization course TKP4580. Hence, a lot of the contents in the first three chapters, in addition to some of the contents in the appendices originates from the report produced in the course TKP4580. The work was performed at the Department of Chemical Engineering, at the Norwegian University of Science and Technology (NTNU).

I would like to express my deepest gratitude towards my supervisor Professor Edd A. Blekkan for guidance and mentoring during this project. I am impressed by the amount of knowledge and interest he has on the Fischer-Tropsch process, and that he always takes time to answer my questions. Thanks also goes out to my co-supervisors Dr. Ingeborg-Helene Svenum and researcher Rune Myrstad from SINTEF for their help and our discussions during the project, as well as Rune's much appreciated technical aid with the operation of the Fischer-Tropsch rig. Furthermore, I would like to thank Estelle and Karin for instrument training and helping out whenever there are problems with an instrument in the lab, and Merethe Christensen Vadseth for providing crucial chemicals.

I would like to thank my fellow master students at the catalysis group, as well as the Ph.D candidates, for creating a good social environment and helping each other out when needed. Finally, I would like to thank my parents and my boyfriend, Jostein Lund, for their unconditional support throughout my time as a master student at NTNU.

Vilde Rolland Svensen
Trondheim, June, 2021

Summary

In this work, the effect of different metal promoters on supported 20 wt% Co catalysts for the Fischer-Tropsch synthesis (FTS) was investigated. The metals studied were Ru, Re and Pt, on Co/Al_2O_3 and Co/TiO_2 catalysts, prepared by incipient wetness impregnation. The atomic ratio between the promoters and Co was 0.01 for all the promoted catalysts. All of the prepared catalysts were characterized by X-Ray Fluorescence (XRF), X-Ray Diffraction (XRD), Temperature Programmed Reduction (TPR), N_2-physisorption, and H_2-chemisorption. The catalysts activity and selectivity were then tested in in a fixed bed reactor at 20 bar and 210 ^oC (H_2/CO=2.0). The Pt-promoted Co/Al_2O_3 catalyst was prepared from two different precursors; $Pt(NH_3)_4(NO_3)_2$ and $H_2PtCl_6 \cdot 6\,H_2O$, where the catalyst containing chloride was not analysed by TPR or the FTS experiments, due to the observed blocking of active sites by chloride.

FTS is the most studied technology for the production of synthetic hydrocarbon chemicals and fuels, but is highly dependent on active catalysts. Promoters like Re, Pt or Ru are known to improve the reducibility of Co catalysts, which is shown to also improve the dispersion and the activity, leaving the catalyst selectivity unchanged. However, some authors have reported changes in the C_{5+}-selectivity.

Through TPR it was found that the temperature of reduction for both steps (Co_3O_4 to CoO and CoO to Co^0) downshifted to lower temperatures upon addition of Ru and Pt to Co/Al_2O_3 catalysts, however, only the second reduction step was significantly affected in the case of Re promotion. For the promoted Co/TiO_2 catalysts, promotion with Ru and Pt led to decreased temperatures of reduction, while Re did not affect the reduction temperature to a large extent. The addition of promoters to Co/Al_2O_3 enhanced the DoR to the most extent, while the effect of adding promoters to the TiO_2-supported catalysts was rather low. The TiO_2-supported catalysts consisted of larger Co_3O_4 particles, which were easily reduced. The effect of the addition of promoters was therefore low on TiO_2-supported catalysts (compared to Al_2O_3-supported catalysts). All of the promoted catalysts supported on Al_2O_3, except $Co/Pt/Cl/Al_2O_3$, gave a higher dispersion than the unpromoted Co/Al_2O_3 catalyst. For the TiO_2-supported catalysts, the calculated dispersion was low, and showed no significant change upon the addition of promoters, similar to the TPR results. The high cobalt dispersion for the promoted Al_2O_3-supported catalysts gave higher hydrogenation rates of CO, while the Site Time Yield (STY) remained constant. For the promoted Co/TiO_2 catalysts the activity was not significantly affected by the addition of promoters, and the STY remained constant.

For the Al_2O_3-supported catalysts, the addition of Re increased the C_{5+}-selectivity, while the addition of Pt and Ru led to a decrease in C_{5+}. The highest C_{5+}-selectivities were reported for the Co/TiO_2 catalysts, which is explained by the wide pores of TiO_2. For the TiO_2-supported catalysts the promotion with Re and Pt led to a higher C_{5+}-selectivity, while Ru decreased the C_{5+}-selectivity. The Pt-promoted catalysts showed slightly higher selectivities of CO_2 and CH_4, which could suggest WGS activity, but the variations were so small that no conclusion could be drawn. The addition of Pt and Ru led to low olefin/paraffin ratios, meaning that Pt and Ru contributed to hydrogenation. The Re promoted and the unpromoted catalysts, which showed higher olefin/paraffin ratios, were not equally active for hydrogenation.

Sammendrag

I dette arbeidet ble effekten av forskjellige metallpromotorer på katalysatorer med 20 vekt-% kobolt for Fischer-Tropsch Syntesen (FTS) undersøkt. Metallene som ble studert var Ru, Re og Pt på Co/Al_2O_3 og Co/TiO_2 katalysatorer, fremstilt ved våtimpregnering. Atomforholdet mellom promotor og Co var 0.01 for alle de promoterte katalysatorene. Alle de fremstilte katalysatorene ble analysert ved røntgen fluorescens (XRF), røntgen diffraksjon (XRD), temperatur programmert reduksjon (TPR), N_2-fysisorpsjon, og H_2-kjemisorpsjon. Katalysatorenes aktivitet og selektivitet ble testet i en fixed bed reaktor ved 20 bar og 210 ^{o}C (H_2/CO=2.0). Den Pt-promoterte Co/Al_2O_3-katalysatoren ble fremstilt utfra to forskjellige kjemikalier; $Pt(NH_3)_4(NO_3)_2$ og $H_2PtCl_6 \cdot 6\,H_2O$, hvor katalysatoren som inneholdt klor ikke ble analysert i TPR eller FTS-eksperimentet på grunn av den observerte blokkeringen av aktive seter av klor.

FTS er den mest studerte teknologien for produksjon av syntetiske hydrokarboner og drivstoff, men er sterkt avhengig av aktive katalysatorer. Promotorer som Re, Pt eller Ru er kjent for å forbedre reduserbarheten av Co-katalysatorer, som videre forbedrer dispersjonen og aktiviteten, og etterlater katalysatorens selektivitet uendret. Noen forfattere har likevel rapportert om endringer i C_{5+}-selektiviteten.

Fra TPR ble det funnet at temperaturen for begge trinn (Co_3O_4 til CoO og CoO til Co^0) sank til lavere temperaturer ved tilsetning av Ru og Pt til Co/Al_2O_3-katalysatorer, men bare det andre reduksjonstrinnet ble betydelig påvirket ved Re-promotering. For de promoterte Co/TiO_2-katalysatorene førte promotering med Ru og Pt til lavere temperaturer, mens Re ikke påvirket reduksjonstemperaturen i stor grad. Tilsetningen av promotorer til Co/Al_2O_3 forbedret DoR i stor grad, mens effekten av promotorer på de TiO_2-støttede katalysatorene var lav. De TiO_2-støttede katalysatorene bestod av større Co_3O_4-partikler, som var lett reduserbare. Effekten av tilsetningen av promotor var derfor lav på TiO_2-katatlysatorene (sammenlignet med katalysatorene på Al_2O_3). Alle de promoterte katalysatorene på Al_2O_3, unntatt $Co/Pt/Cl/Al_2O_3$, ga høyere dispersjon enn den upromoterte katalysatoren. For katalysatorene på TiO_2 var dispersjonen lav og viste ingen signifikant endring ved tilsetning av promotorer, i likhet med TPR-resultatene. Den høye dispersjonen for de promoterte Co/Al_2O_3 katalysatorene førte til høyere hydrogeneringsrater av CO, mens STY holdt seg konstant. For de promoterte Co/TiO_2-katalysatorene ble aktiviteten ikke påvirket i stor grad ved tilsetning av promotorer, og STY forble konstant.

For katalysatorene på Al_2O_3 økte C_{5+}-selektiviteten ved tilsetningen av Re, mens tilsetningen av Pt og Ru førte til en reduksjon i C_{5+}. De høyeste C_{5+}-selektivitetene ble rapportert på Co/TiO_2-katalysatorene, som kan forklares ved de brede porene til TiO_2. For katalysatorene på TiO_2 førte promoteringen med Re og Pt til en høyere C_{5+}-selektivitet, mens Ru reduserte C_{5+}-selektiviteten. De Pt-promoterte katalysatorene viste litt høyere selektiviteter til CO_2 og CH_4, noe som kunne antyde WGS-aktivitet, men forskjellene var så små at ingen konklusjoner kunne trekkes. Tilsetningen av Pt og Ru førte til lave olefin/parafin-forhold, som betyr at Pt og Ru bidro til hydrogenering. Den Re-promoterte og de upromoterte katalysatorene, som viste høyere olefin/parafin-forhold, ikke var like aktive for hydrogenering.

Contents

List of Figures

List of Tables

1 Introduction

Today, oil and gas are regarded as the most important energy fuels, accounting for more than 60% of the global total primary energy supply. In addition, the global energy demand is expected to increase as the world economy grows larger, and one of the sectors with the highest energy demand is transportation. However, rising CO_2 emissions, climate change, depletion of oil reserves, and a rapidly growing global population underlines the need for alternative, sustainable liquid fuels.[1,2] Fischer-Tropsch Synthesis (FTS) is the most studied technology for the production of synthetic hydrocarbon chemicals and fuels. It is the major step in the transformation of biomass, coal or natural gas into liquid fuels. In theory, all compounds that contain carbon atoms may be converted into a mixture of H_2-, and CO-gas, commonly referred to as synthesis gas, which can be further reacted through the FTS to liquid fuels.[1]

Synthetic fuels have environmental advantages compared to conventional crude-refined fuels since they are practically free of sulphur, nitrogen, and aromatics (if it is refined that way), as well as being blendable and compatible with conventional fuels. This enables synthetic gas to work within the existing vehicle technology and fuel infrastructure.[3,4] Another advantage of FTS is that it allows nations with no natural oil reserves to produce their own liquid fuels for transportation.[2] An example is South-Africa who have used their coal to produce FT fuels which have powered the South-African vehicles for nearly 70 years.[5]

Synthesis gas can be produced from a broad range of biomass resources, including wood, agricultural and animal residues, discarded food, and waste by-products processing residues.[4] Biomass is a natural and renewable carbon resource that is a viable substitute for fossil fuels. The biomass to liquid (BTL) technology comprise of gasification of biomass, synthesis gas cleaning, FTS, and biofuel upgrading.[3] In order to be considered a truly sustainable energy source, biomass feedstocks should be derived from sources which do not compete with agricultural land used for food production, or compromise the environment e.g. through deforestation. Hence, potential feedstocks include oil or cellulosic based materials made from aquatic sources or plants.[2]

An alternative feedstock that might be used in the future is CO_2. In non-fossil applications, H_2 can be produced via electrochemical processes fed by electricity from renewable energy sources. Further, CO_2 can be combined with H_2 or steam to produce synthesis gas through electrochemical or thermochemical catalytically driven processes. The CO_2 can be captured from point sources (industrial exhaust stream) or by Direct Air Capture (DAC). Capturing CO_2 from the atmosphere has created a huge interest in the research community due to the fact that it gives an almost unlimited CO_2 resource regardless of the plant location and reduces the atmospheric CO_2 concentration.[6] An illustration of a sustainable carbon capture and utilization (CCU) cycle using DAC is presented in Figure 1.1.

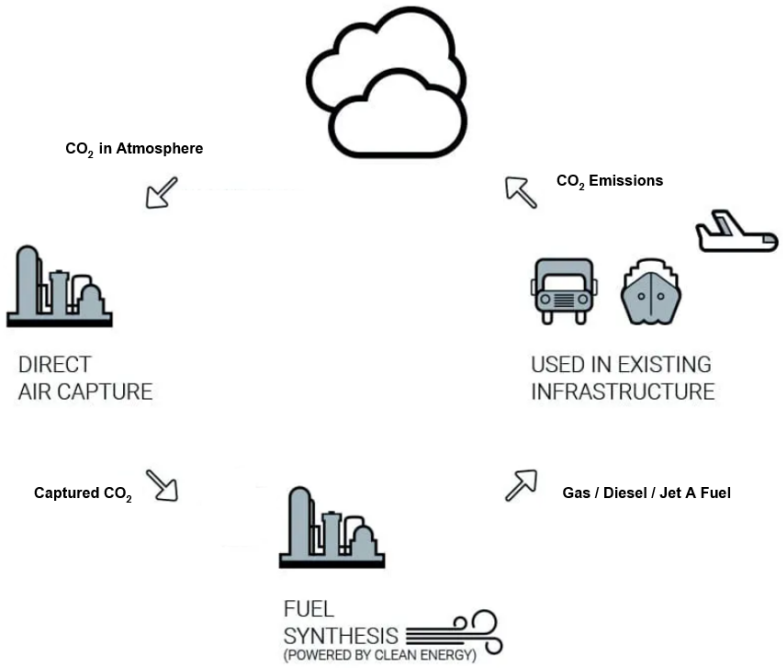

Figure 1.1: Illustration of a carbon capture and utilization cycle using direct air capture, obtained from carbon engineering.[7]

In order to efficiently produce synthetic fuels through FTS, stable, active, and selective catalysts are required. Supported cobalt (Co) catalysts have received great attention in FTS due to their high activity, selectivity for long chain hydrocarbons and low water-gas-shift (WGS) activity.[8] The downside of Co catalysts however, is the inherent difficulty of reducing them to their active metallic state Co^0.[9] This problem can, to a certain extent, be overcome through the addition of promoters.[8]

1.1 Scope of this work

The scope of this work is to investigate the effect of different metal promoters on supported Co catalysts for the Fischer-Tropsch synthesis. The metals which will be studied are ruthenium (Ru), platinum (Pt) and rhenium (Re), on Co/Al_2O_3 and Co/TiO_2 catalysts. Promoters like Re, Pt or Ru are known to improve the reducibility of Co catalysts, and consequently they also improve the dispersion and the activity. This project involves catalyst preparation, characterization and catalyst testing in a FTS experiment.

The obtained results will further be used in comparison with Density-Functional Theory (DFT) calculations, but this will not be part of this work.

2 Theory

2.1 Fischer-Tropsch Synthesis

The first part of the 20th century was a period of triumphs for industrial catalysis. It was a time of great discoveries, for example, the hydrogenation of carbon monoxide and carbon dioxide to methane, and important processes like ammonia and methanol production. It was also at this time that the Fischer-Tropsch (FT) process was discovered. [10]

The FT reaction was discovered by Franz Fischer, Hans Tropsch, and Helmut Pichler in 1923, at the Kaiser Wilhelm Institute in Germany. Synthesis gas (CO and H_2) was reacted over a cobalt catalyst, which resulted in the production of gasoline, diesel, heavy and middle distillate oils. This made it possible for Germany to make fuels from their coal reserves, and in 1938, a total of nine FT plants were in operation. [11,12] Later in the 1950's, the first coal-based Sasol FT plant (Sasol 1) at Sasolburg, South Africa, was constructed. The facility was particularly complex, integrating the two variants of the FT process. [5] A more recent construction is the Gas-to-Liquid (GTL) plant in Qatar, called Pearl, built in 2006. [10]

2.1.1 Chemistry

The FT process transforms synthesis gas to a range of different hydrocarbons, which can be hydrocracked to, mainly, diesel and gasoline of excellent quality. Catalysts utilized are either cobalt or iron, at temperatures ranging from 200-300 ^{o}C, while the pressures varies from 10-60 bar. The reactants adsorb at the catalyst surface and reacts to form a chain initiator. The reaction then goes through a chain propagation, followed by chain termination, and finally a product desorption. This chain reaction is presented in Equation 2.1. [11]

$$2\,\mathrm{nH_2} + \mathrm{nCO} \longrightarrow -(\mathrm{CH_2})-\mathrm{n} + \mathrm{nH_2O} \qquad \Delta \mathrm{H}^0_{250^0\mathrm{C}} = -158{,}5\,\mathrm{kJ/mol}\,(\mathrm{n}=1) \tag{2.1}$$

Additional equations that describe the FT reaction are Equation 2.2 and 2.3, for the production of alkanes and alkenes, respectively. [11]

$$(2\mathrm{n}+1)\,\mathrm{H_2} + \mathrm{nCO} \longrightarrow \mathrm{C}_n\mathrm{H}_{2n+2} + \mathrm{nH_2O} \tag{2.2}$$

$$2\,\mathrm{nH_2} + \mathrm{nCO} \longrightarrow \mathrm{C}_n\mathrm{H}_{2n} + \mathrm{nH_2O} \tag{2.3}$$

All of the reactions above are highly exothermic.

Various side reactions may take place during FTS. One of these side reactions is the water-gas-shift (WGS) reaction (Equation 2.4). Synthesis gas with a low H_2/CO ratio enhances the reaction by being a useful source of hydrogen, on the other hand, higher H_2/CO ratios makes the WGS reaction an unwanted reaction. An additional side reaction is the Boudouard reaction (Equation 2.5) which causes carbon formation that can induce metal carbide or coke formation. The last side reaction is the formation of oxygentates (Equation 2.6), that includes alcohols, but also ketones and aldehydes. [13]

Side reactions:

WGS: $\mathrm{CO + H_2O \longrightarrow CO_2 + H_2}$ (2.4)

Boudouard: $\mathrm{2\,CO \longrightarrow C + CO_2}$ (2.5)

Oxygenates: $\mathrm{nCO + 2\,nH_2 \longrightarrow C_nH_{2n+2}O + (n\text{-}1)\,H_2O}$ (2.6)

2.1.2 Reaction Mechanism

The general surface polymerization reaction in FTS contains the following steps:[13]

1. Reactant adsorption
2. Chain initiation
3. Chain propagation
4. Chain termination
5. Product desorption
6. Re-adsorption and side reactions

Even though the FTS has been known since the 1920's, the exact reaction mechanism is still a broadly discussed topic. However, all of the proposed mechanisms contains a stepwise addition of a single carbon monomer unit from the reactant CO, into a growing chain of hydrocarbons connected to the catalyst surface.[11] Somewhere in the mechanism, the carbon-oxygen bond must be broken, and this is what is considered to be the main difference between all the proposed mechanisms, i.e. at what time, where and how the CO-bond is broken, in addition to different monomers used for each mechanism.

The originally proposed mechanism by Fischer and Tropsch, the carbide mechanism, is the simplest mechanism.[14] It was for a long time the favoured mechanism and was supported by many studies.[15,16] Recent studies show that the alkyl mechanism is the most widely accepted mechanism for FTS, presented in Figure 2.1. However, the mechanism is insufficient to account for the formation of branched hydrocarbons and oxygenates. Additional mechanisms proposed are enol, alkenyl, and CO-insertion mechanisms. All of the FT reaction mechanisms and their corresponding products are presented in Table 2.1.[11] It may be concluded that after 100 years of research on the mechanism, there is still no universal agreement on which mechanism is the correct one.

Table 2.1: Proposed Fischer-Tropsch reaction mechanisms and their products.[11]

Mechanism	Monomer	Chain initiator	Products
Alkyl	=CH2	-CH3	α-olefins, n-paraffins,
Enol	=C(H)OH	=C(CH3)OH	α-olefins, aldehydes, alcohols
Alkenyl	=CH2	-CH=CH2	α-olefins
CO-insertion	=CO	-CH3	α-olefins, n-paraffins, aldehydes, alcohols,

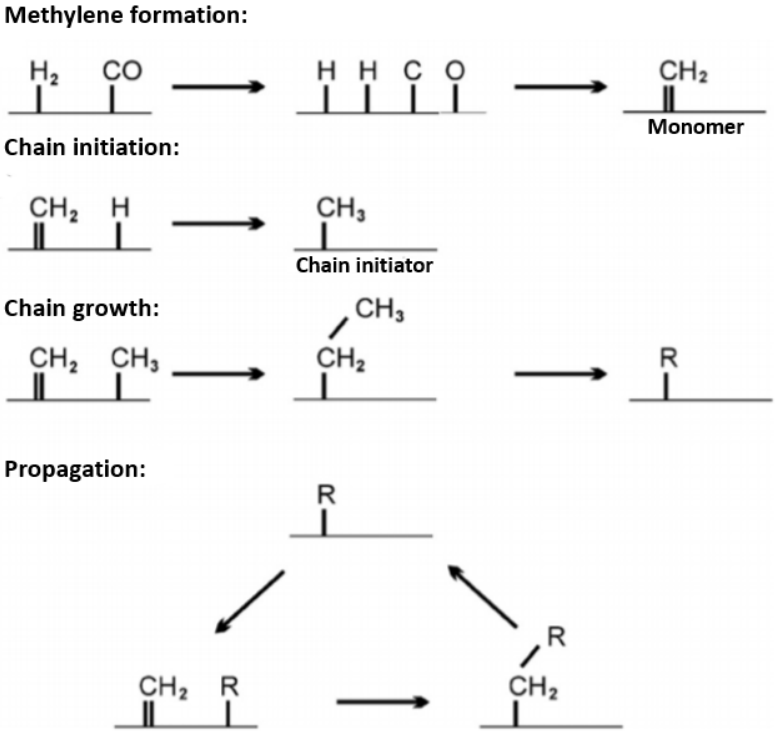

Figure 2.1: Schematic illustration of the alkyl mechanism.[11]

2.1.3 Kinetics

Like reaction mechanisms, the kinetics of the FTS has also been a topic in several research studies. Both empirical power law expressions and Langmuir-Hinshelwood-Hougen-Watson (LHHW) kinetics have been used to describe the kinetics of the FT reactions. A large number of different mechanisms and rate determining steps have been proposed, but none of them are universally accepted. [11]

A power law rate expression of the form, presented in Equation 2.7, can be used to estimate the kinetics of FTS, most of them give a LHHW type of rate equation. [17]

$$-\mathrm{r_{CO}} = \mathrm{k}(\mathrm{P_{H2}})^{x}(\mathrm{P_{CO}})^{y} \tag{2.7}$$

$\mathrm{r_{CO}}$ is the reaction rate of CO, k is the specific rate constant, $\mathrm{P_{H2}}$ is the partial pressure of $\mathrm{H_2}$, and $\mathrm{P_{CO}}$ is the partial pressure of CO. x is the reaction order of $\mathrm{H_2}$ and has been reported to range from 0.5 to 2, while y is the reaction order of CO and can range from +0.65 to -1.0, depending on the reaction conditions. The overall activation energy of the process is approximately 93-103 kJ/mol. [17]

A general LHHW rate equation consists of a kinetic factor, driving force and adsorption term, presented in Equation 2.8. An example of a LHHW rate equation is presented in Equation 2.9, where a, b and c are constants.

$$\mathrm{r} = \frac{[\text{kinetic factor}][\text{driving force}]}{[\text{adsorption term}]^2} \tag{2.8}$$

$$-\mathrm{r_{CO}} = \frac{\mathrm{a}{\mathrm{P_{CO}}}^{0,5}\mathrm{P_{H2}}}{(1 + \mathrm{b}\mathrm{P_{CO}} + \mathrm{c}{\mathrm{P_{H2}}}^{0,5})^2} \tag{2.9}$$

The effect of water on the kinetics

It is known that water influences the activity and selectivity in FTS through mass transfer limitations, which is further discussed in section 2.6.3. However, challenges regarding how water effects FTS kinetics are still being debated. Various studies have reported that water plays a kinetic role in FTS for both Fe and Co catalysts, [18,19,20,21] while others have reported that the role of water in FTS kinetics is negligible. [22,23,24,25,26,27] Hence, additional studies are required in order clarify these questions. [28]

2.1.4 Products

FTS products does not refer to a single product, similarly to conventional crude oil. The FTS can convert synthesis gas into a broad range of hydrocarbons (HC). The variation in products can be altered by choice of catalyst, amount of promoter added, type of reactor utilized, feed gas composition, operating temperatures and pressures used. Independent of the operating conditions, it will always be produced a wide range of HC and oxygenated HC. Methane, which is an undesirable product, is always produced and the selectivity towards methane can vary from 1-100%. Concerning the long chain linear waxes the selectivity varies between 0-70%. [11,29]

The C_{20+} linear hydrocarbons, C_{5+} paraffins and low- and intermediate-molecular weight olefins give rise to the production of fuels and petrochemicals. Obviously, the selectivity of these products should be as large as possible.[11]

The FT product distribution is given by the Anderson-Schultz-Flory (ASF) chain length statistics, presented in Equation 2.10.[30,31,11,32]

$$\frac{W_n}{n} = (1\text{-}\alpha)^2 \alpha^{n-1} \tag{2.10}$$

W_n is the weight fraction of HC linear products with carbon number n, and α is the chain growth probability, it is assumed that α is independent of the chain length.

Figure 2.2 presents how the product distribution varies with the value α.[30] The FT mechanism is anticipated to follow the ASF distribution, although it may be necessary to account for the nature of the catalyst particles, as α is influenced by catalyst properties and operating conditions.[31,13]

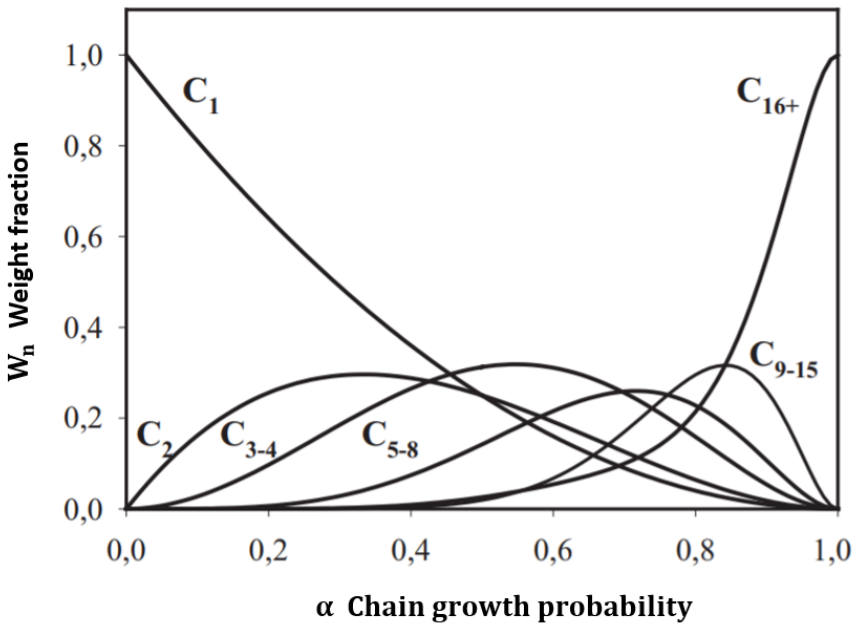

Figure 2.2: Anderson-Schultz-Flory product distribution.[33]

By modifying the catalyst, the distribution of FT products can be adjusted. The modification can be changes in the support or an addition of promoters. In what way various promoters will affect the FTS product distribution will be further discussed in section 2.3. In short, however, it is showed that by adding a promoter, the dispersion and reducibility of the catalyst will increase, leading to an increased catalytic activity, and in certain instances higher selectivity for long chain hydrocarbons.[32]

2.2 Catalysts

An important element in enhanced FT technology is the development of stable and active catalysts with high wax selectivity. A numerous amount of catalysts can be utilized for the FTS, the most widely used are the transition metals iron, cobalt, ruthenium and nickel.[34] However, iron and cobalt are the most commonly used catalysts for commercial purposes.[32] This is because nickel has a tendency to favour production of methane with increasing reaction temperature.[34] And even though ruthenium has a high activity and selectivity towards long chain hydrocarbons, it is too expensive for commercial utilization and thus only used as a promoter or for academic interests.[12]

In contrast to cobalt-based catalysts, iron catalysts are WGS active. This plays a major role when it comes to the stoichiometry of the FT reaction, which is controlled by the ratio of H_2 and CO in the synthesis gas. This makes iron catalysts desirable for CO-rich synthesis gas which is obtained from high temperature coal, or heavy-oil-gasification through partial oxidation. In contrast, cobalt-based catalysts are favourable for H_2-rich synthesis gas, produced from natural gas.[34,11] In the case of synthesis gas obtained from biomass, the composition can be H_2-poor, and consequently require a WGS reactor for cobalt-based FTS.[11]

2.2.1 Cobalt Catalyst

Supported cobalt catalysts have obtained great attention in FTS, and is considered the most favourable metal for production of long chain hydrocarbons, due to its high activity, high selectivity to linear paraffins, and low WGS activity. The catalyst is normally composed of cobalt metal particles dispersed on an oxide support.[35,32,8] The active sites are located on the metallic cobalt phase, and hence, the catalytic activity is a function of both cobalt reducibility and dispersion. In order to obtain a higher dispersion the cobalt metal particles are preferentially dispersed on porous support materials like SiO_2, Al_2O_3 or TiO_2.[36]

2.2.2 Support Materials

Although the active metal is the primary part of the catalyst, their properties are further enhanced by the correct selection of a support. The support provides mechanical strength, and thermal stability,[37] and contributes to a high surface area which stabilizes and disperses the active metal. The metals, cobalt or iron, are commonly used in combination with the supports SiO_2, Al_2O_3, TiO_2 or carbonmaterials.[13] Other supports such as mesoporous materials (SBA-15, MCM-41),[38] niobia (Nb_2O_5),[39] zirconia (ZrO_2),[40] ceria (CeO_2),[41] SiC,[42] and zeolites[43] have also been reported in the literature as supports for FTS.[37] In this paper, the supports Al_2O_3 and TiO_2 are used.

TiO_2 is naturally present in three different crystallographic forms; rutile, anatase, and brookite.[44] The thermodynamically metastable phases, brookite and anatase, can be transformed into the stable rutile phase at high temperatures (600-700 ^oC in pure synthetic TiO_2).[45] Compared with Al_2O_3 and SiO_2 supports, TiO_2-supports generally have relatively low specific surface areas around 60 and 10 m^2/g for the phases anatase and rutile, respectively. Hence, the cobalt loading is limited for these catalysts in order to achieve high metal dispersion. Additionally, TiO_2 is known to display the SMSI effect at high temperatures, which is further explained in section 2.5.2.[37] With respect to se-

lectivity, TiO_2-supported cobalt catalysts were reported by Oh *et al.*[46] to exhibit higher selectivity for long chain hydrocarbons (C_{5+}) compared with their counterparts on Al_2O_3. The fact that TiO_2 has a higher selectivity can be explained by the pore size, since the same effect is observed in Al_2O_3 with very large pores (α-Al_2O_3).[47] Oh *et al.* also found that TiO_2-supported cobalt catalysts showed a four times lower dispersion than the cobalt catalysts supported on Al_2O_3.

Similarly to TiO_2, Al_2O_3 also has different crystallographic forms; γ-Al_2O_3, θ-Al_2O_3, and α-Al_2O_3 derived from boehmite or η-Al_2O_3. γ-Al_2O_3 is the most employed support in FT catalysts, and is transformed from Bohemite under a temperature range of 500-550 ^oC with a departure of structural water.[48] Al_2O_3 gives the catalyst a high surface area, shows good thermal and mechanical stability, is suitable in slurry bubble column reactors, and is therefore the most commonly used support in FTS.[8,37] Al_2O_3-supported cobalt catalysts usually show a dispersion ranging from 2% to a maximum of 10%,[49] where the dispersion is defined as

> *"The ratio of the number of surface Co^0 sites to the total number of metallic Co after reduction of the catalyst"*[49]

Furthermore, Co/Al_2O_3 catalysts show poor reducibility due to the strong interaction between the small cobalt oxide crystallites and Al_2O_3. In order to accomplish maximum Co^0 site density and activity, a high degree of reduction is necessary. This issue can, to a certain extent, be overcome by adding promoters to the catalyst.[8]

2.3 Promotion Effects

Promoters are supplements which improve the effect of a catalyst, like selectivity, activity and catalyst life. They are predominately divided into two different groups; electronic and structural promoters. The electronic promoters improve the catalyst by modifying the surface, while structural promoters give support stabilization.[12,33]

The metals rhenium (Re), platinum (Pt) and ruthenium (Ru) have been extensively studied as promoters for Co-based FTS. Additional metals, like palladium, rhodium, osmium and iridium, have been studied, but not to the same extent.[12] In this section, the documented promotion effects of Ru, Re and Pt are presented.

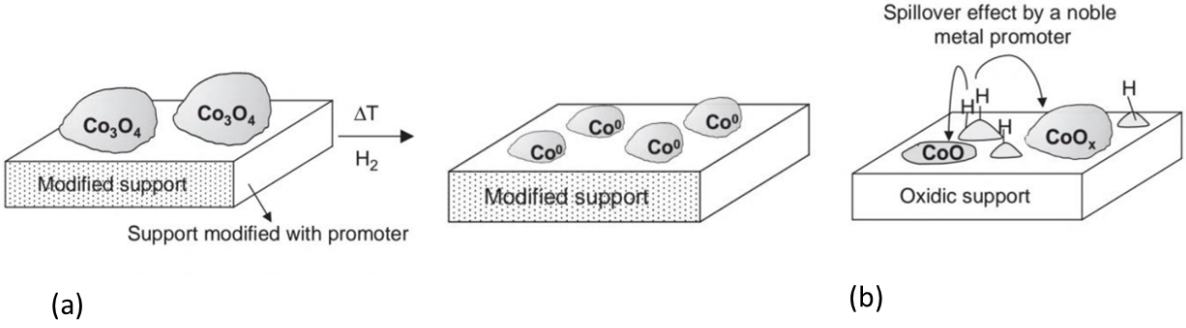

Figure 2.3: (a) structural promoter elements leading to an increased cobalt dispersion and (b) H_2 spillover effect, achieving a higher dispersion of the supported Co particles.[12]

It is reported that the addition of Re, Ru or Pt lead to increased cobalt dispersion.[50,51,9] In the absence of these promoters, large cobalt crystals are formed, while, by adding one of these promoters, smaller cobalt particles are formed. This promotion effect is illustrated

in Figure 2.3 (a). Related to this effect, small metal particles composed of a promoter element can dissociate H_2 to the neighbouring particles. This leads to the formation of atomic hydrogen that may spill over by diffusion to Co, as shown in Figure 2.3 (b). This can result in an enhanced degree of Co reduction and an increase in the number of active sites, and therefore a higher catalyst activity, leaving the catalyst selectivity unchanged.[12] However, some authors have reported changes in the C_{5+} selectivity.[47,52,53]

A defining assumption in H_2 spillover effect is that the promoter is located on the surface of the catalyst. However, Voronov *et al.*[54] showed by XAS and XANES measurements that Re tends to be in the bulk of the cobalt catalyst. Furthermore, EXAFS measurements confirmed that Re is atomically dispersed in the catalyst.[54] In addition, Ruban *et al.*[55] studied the surface segregation energies in transition-metal alloys, that describe the energy cost of transferring an impurity atom from the interior to the surface of a host crystal. They found that Re prefers to migrate to the bulk, as it showed a very strong surface antisegregation energy. On the other hand, Ru showed a moderate antisegregation energy, while Pt showed a strong segregation energy, meaning that Pt migrates to the surface. The latter study was calculated in 1999, hence, it is important to take into account that the accuracy may be poor, and requires more recent calculations. Since Re is not always on the surface, it is uncertain how Re acts as a reduction promoter.

Borg *et al.*[47] studied the effect of Re (0.5 wt%) on the FTS activity and selectivity of γ-Al_2O_3 supported Co (20 wt%) catalysts of different pore sizes in fixed bed reactors. The addition of Re increased the reducibility and the dispersion, and therefore also the activity, which is proportional to the number of available Co particle active sites.[56] Re significantly increased the FTS cobalt-time yield, and the C_{5+}-selectivity (at equal CO conversion 43-44%) when Re was incorporated into the catalyst. The Re promoted catalysts did not modify the site time yield (STY).[47] Similar results were also obtained by Ma *et al.*,[52] who studied the effect of noble metal promoters, on the activity and selectivity of a Co/Al_2O_3 catalyst, at similar CO conversion levels of 50% using a continuously stirred tank reactor (CSTR), at typical FT conditions (220 ^{o}C, 2.2 MPa, H_2/CO=2.1). They found that the reducibility, the dispersion, and the C_{5+}-selectivity increased upon Re addition, while the TOF was not affected. However, Vada *et al.*[50] studied the CO-hydrogenation of Re and Pt-promoted catalysts (8.7 wt% Co/Al_2O_3) at two different conditions, in SSITKA, and found that the selectivity (at approximately equal conversions) did not change as a result of Pt (1 wt%) or Re (1 wt%) addition.

Jermwongratanachai *et al.*[53] compared Pt and Ag-promoted 25%Co/Al_2O_3 catalysts with different loadings of promoters for reducibility, local atomic structure, catalytic activity in FTS, and oxidation–reduction (OR) cycles, in a CSTR at typical FT conditions. The selectivities were compared at approximately 50% conversion for all catalysts. They reported that Pt increased CH_4 and CO_2 selectivities at the expense of C_{5+}. The Pt-promoted catalysts therefore showed lower C_{5+}-selectivities than the unpromoted catalyst. Similar results were obtained by Ma *et al.*[52] who also studied the effect of Pt-promotion. They found that Pt gave higher CH_4 and CO_2 selectivities, and slightly lower C_{5+} selectivity.

Kogelbauer *et al.*[51] investigated the effect of Ru addition on catalyst characteristics and performance in FTS using a series of differently prepared, Ru-promoted Co/Al_2O_3 catalysts. All catalysts contained 20 wt% Co and 0.5 wt% Ru (except one sample that contained 2 wt% Ru). FTS was performed at 220 ^{o}C, 1 atm, and a H_2/CO feed ratio

of 2 in a fixed bed flow reactor under differential conditions. There was little change in product selectivity upon promotion with Ru at steady-state CO hydrogenation. The addition of more than 0.5 wt% Ru improved the catalyst characteristics only marginally. From these results they concluded that Ru acts only as a reduction promoter for Co by increasing the reducibility and dispersion of the cobalt, leaving the selectivity unchanged. Hosseini *et al.*[57] also studied the effect of Ru-addition to 20 wt% Co/Al_2O_3 catalysts in a CSTR at typical FT conditions. The addition of Ru led to improved reducibility and dispersion of Co, while the C_{5+}-selectivity was not improved. Ma *et al.*[52] reported that the addition of Ru decreased CH_4 formation and slightly increased the C_{5+}-selectivity similar as Re.

All of the above studies showed that the reducibility, dispersion, and CO hydrogenation rate increased when adding Re, Ru or Pt to Co/Al_2O_3 catalysts, while the TOF and STY remained constant upon addition of promoters.[47,50,51,52] Regarding the reducibility of Re, Jacobs *et al.*[58] and Vada *et al.*[50] reported that the temperature of reduction of both steps (Co_3O_4 to CoO and CoO to Co^0) moved to lower temperatures in the case of Pt and Ru addition, however, only the second reduction step was significantly affected in the case of Re promotion.[52] A summary of the promotion effects on Al_2O_3-supported cobalt catalysts are presented in Table 2.2

Table 2.2: Summary of the promotion effects on Al_2O_3-supported cobalt catalysts.

Promoter	C_{5+}-selectivity	r_{CO}	STY/TOF	Reference
Re	+ , + , constant	+	constant	[47], [52], [50]
Pt	- , - , constant	+	constant	[53], [52] [50]
Ru	+ , constant , constant	+	constant	[52], [51], [57]

The activity and selectivity of promoted TiO_2-supported cobalt catalysts have not been studied to the same extent as promoted Al_2O_3-supported catalysts. However, some research exists, and the results obtained are presented below and summarized in Table 2.3

Eschemann *et al.*[59] investigated the effects of Ag, Pt, Ru, and Re promotion for Co/TiO_2 FT catalysts. The catalysts contained 7-9 wt% Co and different atomic ratios of promoters. The FTS reaction was performed at typical FT conditions, and at very similar CO conversion levels (25-35%) for the selectivity measurements. The addition of Ag, Re and higher amounts of Ru (0.18 wt%) resulted in higher cobalt time yields (CTY) and C_{5+}, however, the addition of Pt or lower amounts of Ru gave higher CTY, but lower C_{5+}-selectivity. The TPR experiments showed that the addition of noble metals led to decreased reduction temperatures of cobalt oxide, and that the effect was most pronounced for the addition of Ru and Pt, and less pronounced for the addition of Re and Ag.[59]

Mehrbod *et al.*[60] studied the effect of the direct reduction of cobalt nitrate versus the more conventional calcination/reduction treatment for Pt-promoted Co/TiO_2 catalysts (12 wt% Co and 0.5 wt% Pt). The FTS were performed in a CSTR at typical FT conditions. Here, the calcined Pt-promoted Co/TiO_2 catalyst gave slightly higher C_{5+}-selectivity than the unpromoted calcined catalyst at 50 % CO conversion.

Regarding Ru promotion similar results as Eschemann *et al.*[59] were obtained by Bertella *et al.*[61] who studied Ru promotion on 10 wt% Co/TiO_2 in an *in situ* spectroscopic study. The FTS experiments were conducted at typical FT conditions, in a fixed-bed stainless steel reactor. The addition of Ru gave both higher activity per total mass of metal (MTY, metal-time yield) and C_{5+}-selectivity than an equivalent unpromoted catalyst, at equal CO conversion levels (10%).

Li *et al.*[62] investigated the effect of the addition of small amounts of B, Ru and Re on the FT catalyst activity and selectivity of a 10 wt% Co/TiO_2 catalyst in a CSTR (at typical FT conditions). Addition of Re and Ru (atomic ratio between promoter and Co at 0.01) led to higher C_{5+}-selectivities and CO hydrogenation rates.

Table 2.3: Summary of the promotion effects on TiO_2-supported cobalt catalysts.

Promoter	C_{5+}-selectivity	r_{CO}	MTY/CTY	Reference
Re	+ , +	+	+	[59,62]
Pt	- , +			[59,60]
Ru	+ , - , + , +	+	+	[59,59,61,62]

Generally, the activity of FTS increases linearly with the available metallic cobalt surface area, resulting in constant TOFs. However, studies concerning the impact of noble metal promotion on TOF are predominately performed on catalysts supported on Al_2O_3. The support material TiO_2 is an reducible oxide that show strong metal support interactions towards group 8–10 metals, unlike other support materials typically used in FTS. However, TOF has been found to be independent of the support material and noble metals present in the catalyst,[63,64,18] given that the catalysts contain cobalt particles above a critical size of 6 nm. Smaller cobalt particles than 6 nm results in a sharp drop in the TOF.[59]

2.4 Deactivation

Catalyst deactivation mechanisms in FTS has for a long time been an important topic with both academic and industrial interest. There are various mechanisms that may lead to a reduced selectivity and activity, making it a complex problem. Throughout the FTS there are a wide range of intermediates and products produced. Furthermore, high partial pressures of steam are generated throughout the reaction. Accordingly, the chemical environment of the synthesis reactor is surrounded by a large number of interacting species which may negatively affect the catalytic activity. In addition, the FT reaction is a highly exothermic reaction, creating a lot of heat during the reaction. It is therefore possible that local overheating may occur. The correct choice of reactor is therefore of great importance, with respect to the catalysts stability properties.[35]

The mechanisms of catalyst deactivation, proposed by Tsakoumis *et al.*,[35] include sintering, poisoning, surface carbon formation, carbidization, cobalt re-oxidation, cobalt–support mixed compound formation, surface reconstruction and mechanical deactivation through attrition.[35] The catalysts used for FTS are usually highly sensitive to poisoning, hence a purification of the synthesis gas is crucial, particularly for processes using coal or biomass as feedstocks.[65] Synthesis gas from biomass can contain contaminants like COS, H_2S,

HCN, NH_3, HCl, in addition to soot, tars, BTX (benzene, toluene, and xylenes), dust and volatile metals.[66]

Of all the species that may cause poisoning, sulphur is one of the most important ones, with respect to deactivation. Sulphur adsorbs strongly to the active sites, leading to a physical blocking of the sites or electronic modification of neighbouring atoms. For cobalt catalysts it is shown that sulphur appears to be a geometric blockage of sites, more than an electronic modification. Additionally, it is reported that sulphur blocks more than two cobalt atoms on Co/Al_2O_3 catalysts. An example of this is presented in Figure 2.4, which shows a two-dimensional conceptual model of the poisoning by sulphur atoms on a metal surface during ethylene hydrogenation.[67]

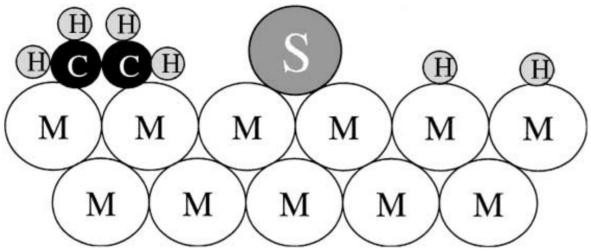

Figure 2.4: Conceptual model regarding the poisoning by sulphur atoms on a metal surface during ethylene hydrogenation. The figure is obtained from Calvin H. Bartholomew.[67]

Throughout FTS the catalyst surface contains a wide range of carbon containing species which may interact differently with the catalyst. Additionally, side reactions like the Boudouard reaction may enhance the carbon formation. The carbon can interact with the metal under reaction conditions and produce inactive species or inhibitors. FTS is classified as a carbon insensitive reaction, meaning that the presence of hydrogen should not allow carbon to accumulate on the surface and deactivate the catalyst. Hence, coke precursors will rapidly react to form hydrocarbons and is therefore considered as reaction intermediates.[35]

FTS is a highly exothermic reaction, hence the potential of sintering is relatively high. It is therefore important to reduce local overheating, since isothermal conditions are essential. Sintering leads to a reduction of active surface and is divided into two main mechanisms. The first is an atomic migration (Ostwald ripening or coarsening), while the second is a crystallite migration (coalescence). Sintering is highly dependent on the support. Al_2O_3 is reported to stabilize cobalt crystallites, and give the catalyst an enhanced resistance to sintering. However, the Hüttig temperature of Co (the temperature at which the atoms at the surface start to exhibit mobility) is not far from the typical FT reaction temperatures. In addition the presence of water may accelerate sintering.[35]

Jacobs *et al.*[68] has reported that the deactivation rate increases with the addition of noble metal promoters to supported cobalt catalysts. However, it is important to keep in mind that catalyst deactivation is a complicated issue depending on reaction conditions. High water partial pressure was found to be connected to more rapid deactivation.[68] In order to determine a promoter's effect on catalyst deactivation, it is important to maintain the same water partial pressure during the testing of the different catalysts. This can be accomplished at equal CO conversion levels (normally 50%) and a constant total reactor pressure.[52]

2.5 Catalyst Characterization

2.5.1 N_2-Physisorption

N_2-physisorption measurements are utilized to determine a range of physical properties related to the pore system of a catalyst. Some of these properties are the pore size, pore size distribution, pore volume, and the surface area. The underlying principle of the method is simple, an inert gas (N_2) is physisorbed to the catalyst and the number of molecules needed to form a complete monolayer is determined. The nitrogen molecule occupies 0.162 nm^2 at 77 K, from this the total surface area can be calculated. Even though the principle sounds straightforward, in practice molecules may adsorb beyond the monolayer and form multilayers. Brunauer, Emmett and Teller (BET) proposed a model regarding multilayer physisorption and derived an equation for calculating the monolayer of adsorbate. The Equation 2.11, called the BET equation, is an extended version of the Langmuir isotherm and describes the volume of gas adsorbed by the catalyst.[33,69]

$$\frac{\mathrm{p}}{\mathrm{V}(\mathrm{p}_0 - \mathrm{p})} = \frac{1}{\mathrm{V}_m \mathrm{c}} + \frac{\mathrm{c}-1}{\mathrm{V}_m \mathrm{c}} \frac{\mathrm{p}}{\mathrm{p}_0} \tag{2.11}$$

p_0 is the saturated vapor pressure of the liquid at the operating temperature, p is the gas pressure, V is the volume of the adsorbed gas, V_m is the volume where an adsorbed monolayer is formed, and c is a constant.

In the order to find the BET surface area the constant c and the monolayer coverage V_m must be determined. By plotting p/[V(p_0-p)] versus p/p_0 a straight line is achieved, and the values V_m and c in Equation 2.11 can then be determined as the intercept and the slope of the line, respectively. The BET surface area can then be calculated from Equation 2.12 by using the additional information of the average area occupied by one adsorbed N_2 molecule. Figure 2.5 illustrates the relationship between the monolayer and the linear region of the adsorption isotherm.[33]

$$\mathrm{S}_{\mathrm{BET}} = \frac{\mathrm{n}_m \mathrm{N}_\mathrm{A} \sigma_{\mathrm{N2}}}{\mathrm{m}} \tag{2.12}$$

n_m is the number of moles of gas in the monolayer, N_A is Avogadro's number, σ_{N2} is the cross-sectional area of one adsorbed nitrogen molecule and m is the sample mass.

For mesoporous materials, the monolayer is first filled up and the isotherm reaches a plateau (V_m in Figure 2.5), at this part the isotherm follows the Langmuir isotherm. At higher pressures, multilayers starts to form until capillary pore condensation sets an end to the adsorption process. Removal of the gas occurs at lower equilibrium pressures than at which it entered, since capillary forces have to be overcome. This will show a hysterisis effect in the isotherm. Figure 2.5 shows a typical Type IV isotherm common for catalysts supported on alumina with specific surface areas of a few hundred m^2/g.[33]

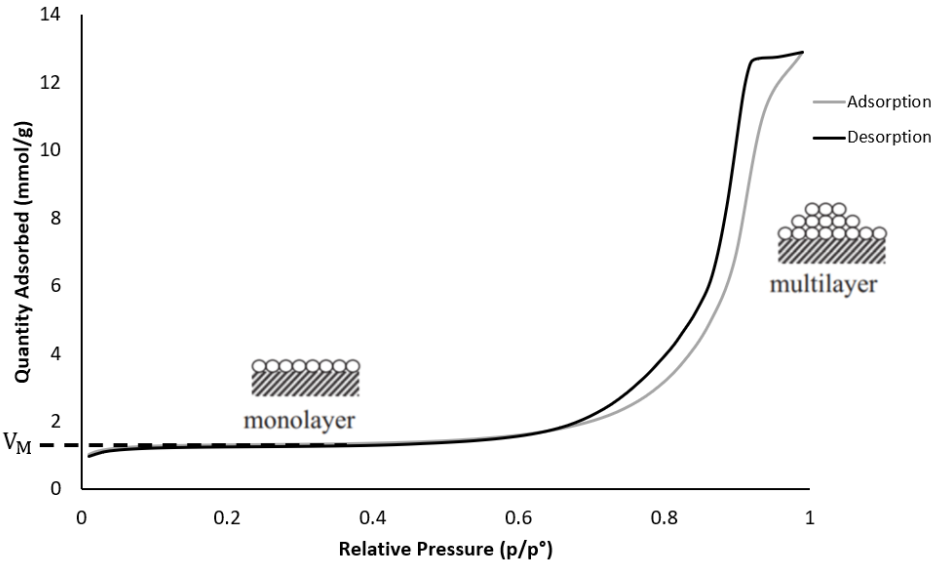

Figure 2.5: Type IV BET isotherm. The isotherm is a result of surface area measurements of the catalyst Co/Al_2O_3.

There are many similarities between the BET and the Langmuir isotherms. The Langmuir isotherm only accounts for monolayer coverage, while the BET isotherm also accounts for multilayer adsorption. The BET isotherm is valid under the following assumptions obtained from *Concepts of Modern Catalysis and Kinetics* (2003)[33]:

- Dynamic equilibrium between adsorptive and adsorbate, i.e. the rate of adsorption and desorption in any layer are equal.
- Molecules adsorb on equivalent adsorption sites in the first layer
- Molecules in the first layer constitute the adsorption sites for molecules in the second layer, and so on for higher layers.
- Adsorbate–adsorbate interactions are ignored.
- The adsorption–desorption conditions are the same for all layers but the first.
- The adsorption energy for molecules in the 2nd and higher layers equals the condensation energy.
- The multilayer grows to infinite thickness at saturation pressure ($P = P_0$)

In addition to mulitlayers, the molecules may condense in small pores. As a matter of fact, the narrower the pores, the easier the N_2 molecules will condense inside them. This phenomenon of capillary pore condensation, is described by the Kelvin equation (Eq.2.13), and can be used to confirm the types of pores and their size distribution inside a system.[33]

$$\ln(\frac{p}{p_0}) = -\frac{2\,\sigma V_m \cos\theta}{rRT} \tag{2.13}$$

In the Kelvin equation (2.13), p is the measured pressure, p_0 is the saturation pressure, σ is the surface tension of liquid N_2, θ is the contact angle, V_m is the molar volume of liquid

nitrogen, r is the radius of the pore, R is the gas constant and T is the temperature.

For a catalyst with one pore series, a unimodal distribution will appear in the pore distribution, while for a catalyst with both large and small pores, a bimodal distribution will arise. This is illustrated in Figure 2.6 where one peak represents a unimodal distribution, while two peaks show a bimodal distribution.[70]

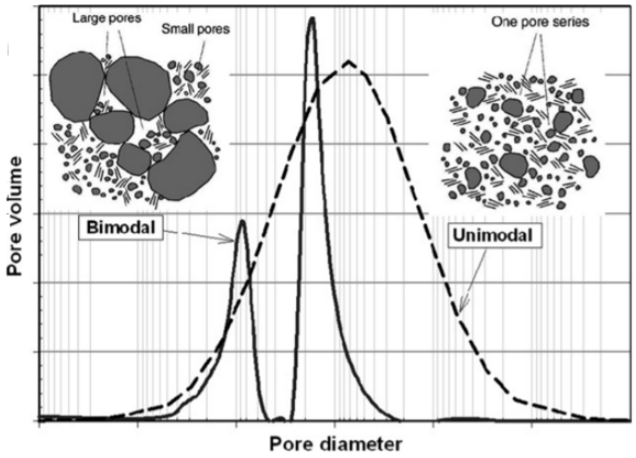

Figure 2.6: Unimodal versus bimodal pore size distribution in soil. The figure is obtained from Alfrendo Satyanaga.[70]

The shape of the physisorption isotherm can give you information about the pore structure of the catalyst. Several unique shapes of hysteresis loops have been reported, however, the main types are presented in Figure 2.7. Types H1, H2(a), H3, and H4 were identified in the original IUPAC classification (1985), which is now extended by more recent findings. All of these characteristic hysteresis loops are closely related to the particular features of the pore structure and the adsorption mechanism of the catalyst. H1 is typical for catalysts with a narrow distribution of mesopores (Figure 2.5). The catalysts showing a H2 isotherm often has a complex pore structure, where network effects appear. The analysis of the desorption loop is often misleading, and is typical for activated carbons. H3 and H4 show no plateau in the isotherm, and therefore has no well-defined mesopore structure, which makes the analysis difficult. H3 is often typical for clays.[71]

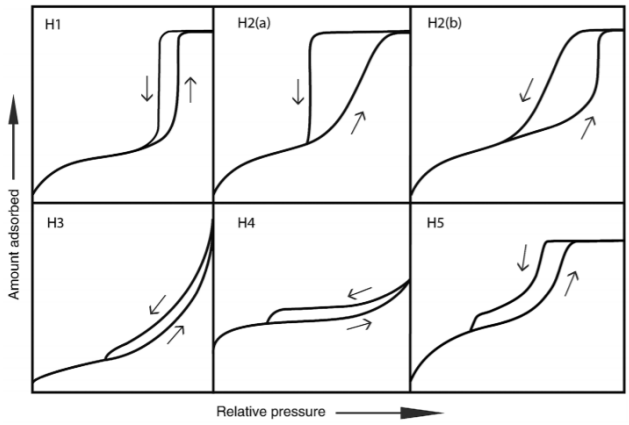

Figure 2.7: The different classified hysteresis loops. The figure is obtained from IUPAC Technical Report.[71]

2.5.2 H_2-Chemisorption

H_2-chemisorption is a method for measuring the dispersion of metal atoms on a catalyst surface. Dispersion is defined as the number of surface atoms in the metal divided by the total number of metal atoms in the catalyst.[72] Hydrogen gas is adsorbed on the catalyst surface at constant temperature and increasing pressures. For cobalt catalysts supported on TiO_2 or Al_2O_3 the dispersion can be determined from an extrapolation of the linear part of the first isotherm to zero pressure (Figure 2.8). Normally, the difference between the two isotherms are used in order to get the chemisorbed species only. However, for catalysts where issues like spillover hydrogen on the support or multilayer adsorption are concerns, it is traditional to only extrapolate the first isotherm.[73]

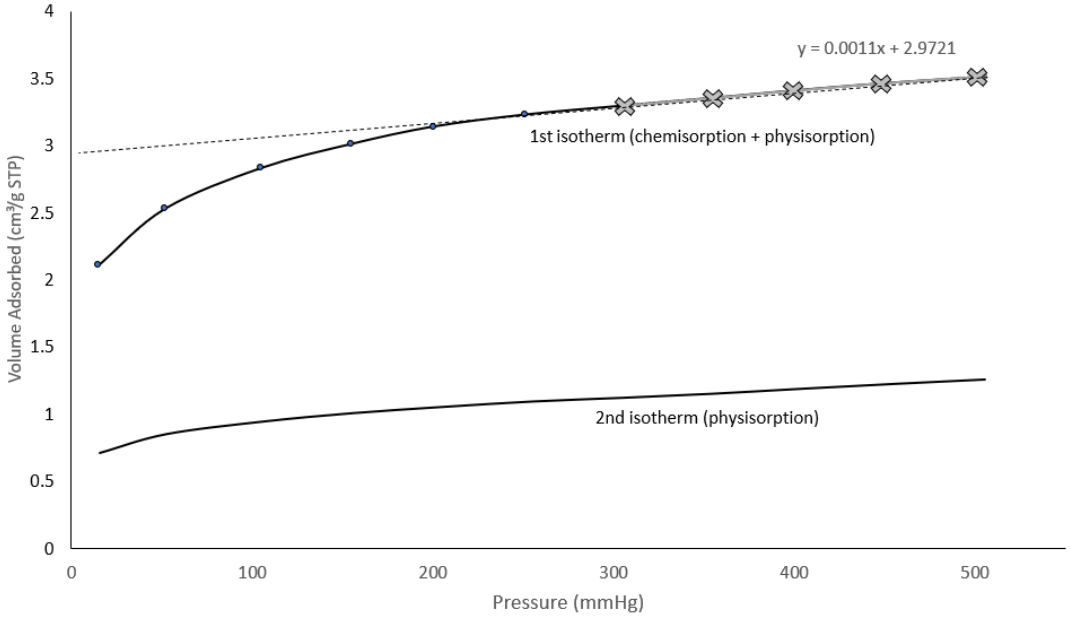

Figure 2.8: An illustration of the extrapolation of an isotherm obtained from chemisorption measurements of $Co/Re/Al_2O_3$. The first isotherm represents the the volume of gas which is chemisorbed and physisorbed. The second isotherm shows the physisorbed gas volume.

The number of adsorbed molecules can be determined by extrapolating back to zero, and the dispersion can be calculated from Equation 2.14.

$$D = \frac{v_{ads}\, M_m\, F}{x_m} \tag{2.14}$$

where v_{ads} [mol/g_{cat}] is the volume of H_2 that is adsorbed (determined from Equation 2.15), M_m is the atomic mass of the metal, F is the adsorption stoichiometry, and x_m is the weight fraction of metal in the catalyst.

$$v_{ads} = \frac{V}{V_m} \tag{2.15}$$

V is the volume absorbed found in the plot after extrapolation and V_m is the volume of one mole of ideal gas at ambient conditions (24 414 cm^3/mol).

H_2 gas generally adsorbs dissociatively (F=2) onto active sites as illustrated in Equation 2.16, where M_s represents a surface metal atom.[69]

$$H_2 + 2\,M_s \longrightarrow 2\,M_s{-}H \tag{2.16}$$

Different effects can alter the well-defined stoichiometry of the H_2 chemisorption, depending on the metal and the support. In addition to hydrogen spillover issues, there is another effect called the the strong metal–support interaction (SMSI) effect[74] first reported by Tauster *et al.* in 1978.[75] It is defined as the encapsulation of metal nanoparticles, usually group VIII metals, by partially reduced oxide supports throughout H_2 treatments at high temperatures (larger than 500 ^{o}C).[76] It is now well accepted that in the case of TiO_2 supported catalysts the partial reduction of TiO_2 induce TiO_x suboxide species (x<2) which migrates over the metal surface covering the metal with a thin reducible oxide layer[77] (Figure 2.9). This effect will cause a decrease in the H_2 uptake, i.e. a lower dispersion.[74]

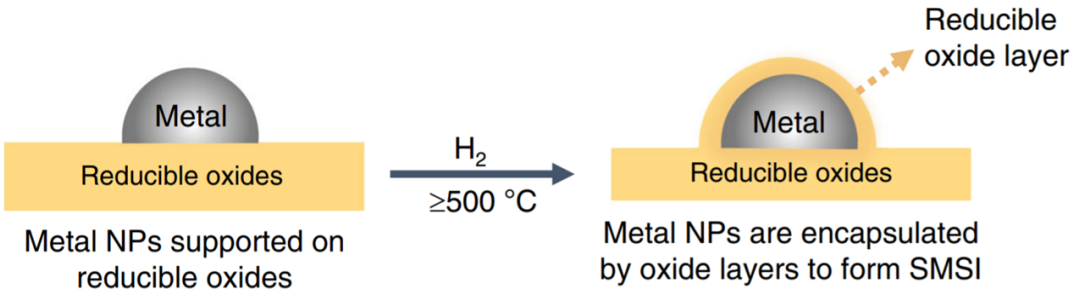

Figure 2.9: The strong metal–support interaction (SMSI) formation process. The catalyst is treated with H_2 at high temperatures creating a thin reducible oxide layer on the metal nanoparticle (NP). The illustration is obtained from Nature Communications.[76]

Another effect that can alter the dispersion is the degree of interaction between the Co atoms and the support. Co has a stronger interaction with Al_2O_3 than it has with TiO_2. The strong bonds between Co and Al_2O_3 results in smaller Co particles which are hard to reduce. The dispersion of unpromoted Co on Al_2O_3 is therefore low. However, by addition of reducing promoters the reduction of small particles is facilitated, and the dispersion increases. The addition of reduction promoters, is therefore much more effective on Al_2O_3 than on TiO_2. Co dispersed on TiO_2 has a weak interaction with the support, i.e. Co forms larger particles which are easily reduced. The effect of the addition of promoters is therefore low on TiO_2.[78]

The presence of contaminants like Cl, S, H_2O, C and metals, from either the catalyst or the gas phase, can also change the gas uptake.[74] It is therefore favourable to avoid using precursors containing any of these impurities.

2.5.3 X-ray Fluorescence

Wavelength Dispersive X-Ray Fluorescence (WDXRF) is a spectroscopic method for material analysis of liquids, bulk solids and powder samples. A Pd-source (X-ray tube) generates X-rays and sends them to the sample where it interacts and produces fluorescent X-rays. The fluorescent X-rays generated are sent to an analyzing crystal, which transfers the X-rays to two different detectors. This allows a quantification of a range of elements from Fluor to Uranium.[79] At an atomic level, X-ray Fluorescence (XRF) can be illustrated in a simple three step process.[80] This process is also summarized in Figure 2.10.

1. The incoming X-ray knocks out an electron from one of the orbitals surrounding the nucleus in an atom.
2. A hole is produced in the orbital. This results in a high energy, unstable configuration for the atom.
3. To reinstate equilibrium, an electron from a higher energy orbital falls into the hole. Since this is a lower energy position, the excess energy is emitted in the form of a fluorescent X-ray.

The difference in energy between the expelled and replacement electrons, i.e. the energy of the fluorescent X-ray, is characteristic for every element and is therefore directly linked to a specific element being analyzed.[80] The resulting plot shows intensity (counts per second) as a function of energy (keV).

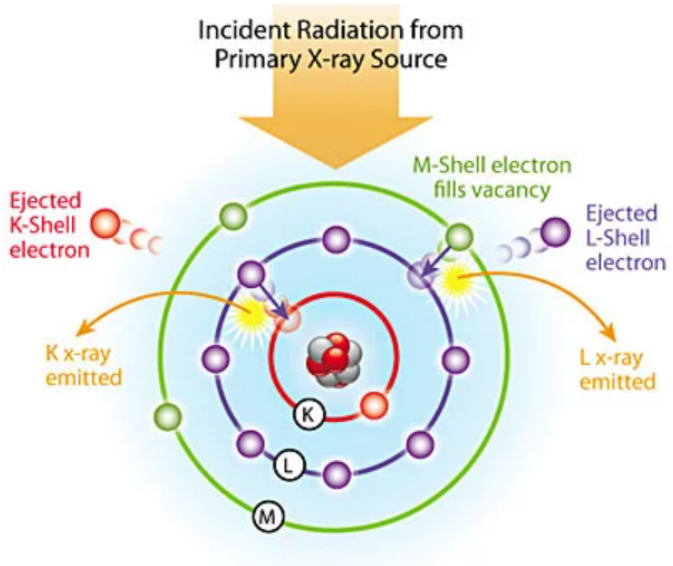

Figure 2.10: X-ray fluorescense excitation model obtained from Thermo Fisher Scientific.[81]

XRF does not give any information about which state, reduced or oxidized, the element exists at. The energy of the fluorescent X-ray for a particular element is therefore not independent of the chemistry of the material, i.e. Co_3O_4 and Co^0 will be in the exact same spectral position.[79,80]

One of the limitations with XRF is that line-overlaps may occur when the line of one element overlaps the line of another element. The overlapping line can come from an

element in the sample, but also from an element in the crystal, tube, or any other component that may appear in the optical path.[82] However, the sample preparation process is the single largest contributor to the overall sources of error in an XRF analysis. The most common sources of error in the preparation process of pressed pellets include the particle size of the sample, dilution ratio, the choice of binder, the amount of pressure applied to the preparation of the pellet, the thickness of the pellet, and cross contamination. The best way to limit these errors require a good method development together with an attention to detail and consistency.[83]

2.5.4 Temperature Programmed Reduction

Temperature programmed reduction (TPR) is a technique based on observing a chemical reduction reaction while the temperature of the system is increased linearly.[84] The experiment consists of two phases, the first phase is a pretreatment stage where the sample is brought to a low pressure and high temperature in order to clean the surface without degrading the sample structure. The second step is an adsorption step where the sample is heated linearly while a flow of diluted hydrogen (typically in nitrogen or argon gas) adsorbs on to the sample. The amount of gas absorbed or reacted can be found from the amount of gas flowing out of the furnace by a quantitative technique (MS, TCD, IR, etc.). Generally, the complete reduction of metal oxides follows the reaction presented in Equation 2.17.[85]

$$\mathrm{M}_x\mathrm{O}_y + \mathrm{yH}_2 \longrightarrow \mathrm{xM} + y\,\mathrm{H}_2\mathrm{O} \tag{2.17}$$

TPR can provide useful information of the reduction temperature for a particular sample, whether the sample is completely reduced in a single step or if multiple steps are required, the effect of promoters, and the degree of reduction.

In order to find the degree of reduction (DoR) of a cobalt catalyst, it is assumed that Co_3O_4 goes through a total reduction to Co^0 (Eq.2.18).

$$\mathrm{Co_3O_4} + 4\,\mathrm{H_2} \longrightarrow 3\,\mathrm{Co^0} + 4\,\mathrm{H_2O} \tag{2.18}$$

If silver oxide is used as the calibration standard, we can assume that silver oxide is completely reduced according to the reaction 2.19.

$$\mathrm{Ag_2O} + \mathrm{H_2} \longrightarrow 2\,\mathrm{Ag} + \mathrm{H_2O} \tag{2.19}$$

A known quantity of silver oxide goes through TPR, and by integrating the area under the TPR curve it will give you a response per mole of H_2 consumed. From this the amount of experimental H_2 consumed in the reduction of Co_3O_4 can be calculated by integrating the TPR curve. With the additional information about the stoichiometry of the reaction, the DoR can be calculated from Equation 2.20.

$$\mathrm{DoR} = \frac{\mathrm{H_2\,consumed}}{\mathrm{Theoretical\,amount\,of\,H_2}} \cdot 100\,\% \tag{2.20}$$

2.5.5 X-ray Diffraction

X-Ray Diffraction (XRD) is a method for characterization of powder samples to identify the crystalline phases and determine the crystallite size using X-rays. The patterns obtained from XRD are measured with a mobile detector and a stationary X-ray source, where the X-ray beam of wavelength λ is diffracted by the sample. The detector measures the intensity of the diffracted beams with respect to the 2θ angle. A schematic illustration of the diffraction of X-rays in a crystalline sample is presented in Figure 2.11. The lattice spacing can be found through Bragg's law (Eq.2.21).[33,86]

$$n\lambda = 2\,d\sin\theta \tag{2.21}$$

In Equation 2.21, n is an integer and gives the order of reflection, λ is the wavelength of the X-rays, d is the spacing between two lattice planes and θ is the angle between the incoming rays and the normal to the reflecting lattice plane.

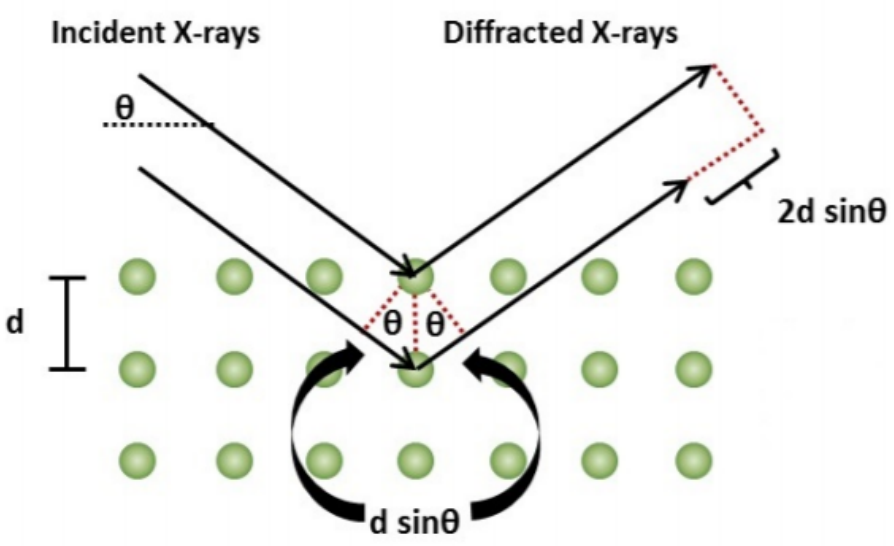

Figure 2.11: Schematic illustration of the diffraction of X-rays in a crystalline sample. The illustration is adapted from Anton Paar.[87]

Since every crystalline mineral have their individual lattice spacings, the mineral measured can be identified by collecting and analyzing the peaks in the diffraction pattern and compare them to a standard reference pattern.[33] The Powder Diffraction File (PDF) administered by the International Centre for Diffraction Data (ICDD), is the reference base most frequently used.[86]

The crystallite size can be found through several methods, but the most exact method is the Pawley method.[88] The Pawley method models each individual intensity peak of the pattern to find the crystallite size of a phase.[89] The only details that must be added are the instrumental details and information from the PDF of the phases present in the sample (space group and the lattice parameters a, b or/and c).

The goodness of the fit (GOF) can be measured in terms of a factor χ^2 given by the equation 2.22.[90]

$$\text{GOF} = \chi^2 = \frac{R_{wp}}{R_{exp}} \tag{2.22}$$

where R_{wp} is the weighted-profile R value and R_{exp} is the statistically expected R value. Ideally, the R_{wp} value should be less than 5, and approach R_{exp}, making χ^2 approach 1. If χ^2 is much larger than 1, the data is over-collected, i.e. errors are no longer dominated by counting statistics. On the other hand, if χ^2 is much smaller than 1 the data have been under-collected, i.e. collected too quickly. Figure 2.12 shows profiles for a perfect fit of a curve (a) (GOF=1) and calculated intensities that are either too high (b) or too low (c).[90]

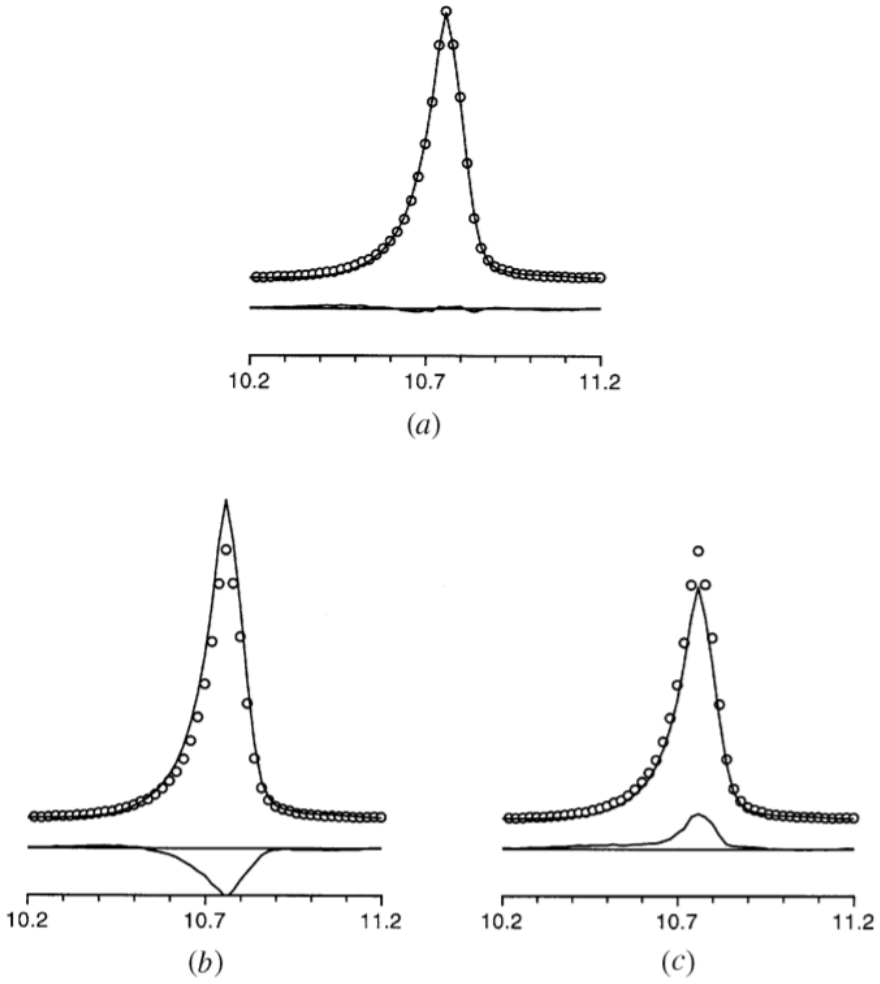

Figure 2.12: The observed (circles), calculated (line) and difference (bottom) profiles for (a) a perfect fit of a peak, (b) a calculated intensity that is too high and (c) a calculated intensity that is too low. The figure is obtained from the Rietveld refinement guidelines by L. B. McCusker.[90]

2.6 Catalyst Performance

2.6.1 Activity

There are several ways of determining the activity of a catalyst in heterogeneous catalysis. The most commonly used terms for describing the activity are Site Time Yield (STY) and Turnover Frequency (TOF).

A definition of STY is

> *"The number of molecules of a specified product made per catalytic site and per unit time"*[91]

If several catalysts are compared, STY distinguishes between a promoter that acts on the geometry, or whether the promoter affects the activity of each cobalt atom on the surface. If all the catalysts show the same STY under otherwise equal conditions, it can be concluded that the promoters have an effect, but only on the available cobalt-metal surface. On the other hand, if the opposite situation occurs where STY show a significant difference, it can be concluded that the catalyst has affected how each cobalt atom behaves in the system.

TOF, on the other hand, is proportional to STY and is defined as

> *"The number of revolutions of the catalytic cycle per unit time"*[91]

In order to compare the intrinsic activity of catalysts, TOF is of great importance. However, a TOF value is not necessarily the most relevant quantity for industrial applications, where the activity per volume of catalyst is of greater interest.[33]

In this paper, the activity measurements will be reflected in terms of CO conversion and STY. The conversion of CO is calculated from Equation 2.23.

$$\eta_{CO} = \frac{F_{0,CO} - F_{1,CO}}{F_{0,CO}} = 1 - \frac{r_{1,CO}}{r_{0,CO}} \tag{2.23}$$

$F_{0,CO}$ is the molar feed flow of CO, $F_{1,CO}$ is the outgoing product flow of CO, $r_{1,CO}$ is the reaction rate of CO in the product flow, and $r_{0,CO}$ is the reaction rate of CO in the feed flow. The reaction rate $r_{0,CO}$ is calculated from Equation 2.24 (similar for $r_{1,CO}$).

$$r_{0,i} = \frac{X_{0,i}}{X_{0,N2}} = K_i \frac{A_{0,i}}{A_{0,N2}} \tag{2.24}$$

$X_{0,i}$ is the mole fraction of component i in the feed flow, $X_{0,N2}$ is the mole fraction of N_2 in the feed flow, K_i is the relative response factor, and A is the Gas Chromatography (GC) area measured by a GC.

In order to calculate STY it is necessary to know the number of cobalt atoms that are present on the catalytic surface, i.e. the number of active sites, if it is assumed that the number of active sites are proportional to the metal area. This can be estimated by H_2-chemisorption or XRD. STY is given by Equation 2.25.

$$\mathrm{STY} = \frac{\mathrm{F_{0,CO}}}{\mathrm{w_{cat.}} \cdot \mathrm{V_m}} \times \frac{\eta_{\mathrm{CO}} \cdot \mathrm{M_{Co}}}{\mathrm{w_m} \cdot \mathrm{D}} \tag{2.25}$$

$\mathrm{F_{0,CO}}$ is the molar feed flow of CO (ml/s), $\mathrm{w_{cat.}}$ is the weight of the catalyst, V_m is the volume of one mole of ideal gas at ambient conditions, η_{CO} is the conversion of CO, M_m is the molar mass of the active metal, w_m is the weight percentage of the active metal, and D is the dispersion.

2.6.2 Selectivity

Selectivity is another term for measuring the performance of a catalyst, and is defined as

"The amount of desired product obtained per amount of consumed reactant"[92]

A value of selectivity without a value of conversion is useless. In FTS, a very active catalyst will give a lot of water in the synthesis gas, since water is one of the main products. It is known that water affects the selectivity by favouring C_{5+} production, rather than methane.[93] If two catalysts are compared, the most active catalyst will give lower methane and higher C_{5+} selectivity than it actually has. It should therefore be a common practice to measure the selectivity at the same conversion for all the catalysts that are compared.

In FTS the selectivity of component j can be calculated from Equation 2.26.

$$\mathrm{S}_j = \frac{\mathrm{n} \cdot (\mathrm{F}_{1,j} - \mathrm{F}_{0,j})}{\mathrm{F_{0,CO}} - \mathrm{F_{1,CO}}} \tag{2.26}$$

In Equation 2.26, n is the carbon number of the component, $\mathrm{F}_{1,j}$ is the product flow of component j, $\mathrm{F}_{0,j}$ is the feed flow of component j, $\mathrm{F_{0,CO}}$ is the feed flow of CO, and $\mathrm{F_{1,CO}}$ is the product flow of CO.

The selectivity of C_{5+} can be calculated from Equation 2.27 after the selectivities of C_1-C_4 and CO_2 are calculated.

$$\mathrm{S_{C5+}} = 100\,\% - \sum_{\mathrm{j}=1}^{4} \mathrm{S}_j - \mathrm{S_{CO2}} \tag{2.27}$$

2.6.3 Mass-and Heat Transfer Limitations

Measuring the activity and the selectivity of a catalyst is not as straightforward as it may seem. The data collected should be under equal conditions of known gas composition and accurate temperature. This may become challenging with fast and strongly exothermic or endothermic reactions. FTS is an exothermic reaction, generating a lot of heat. It is therefore important to avoid local temperature gradients in the reactor. In order to

avoid this, it is essential to have relatively small particles, and dilute the catalyst with an inert, like silicon carbide (SiC).

In addition to heat transfer limitations, mass transfer effects in FTS are also of great importance. Although the reactants are in the gas phase, it is produced water and wax inside the pores, filling the pores with liquid. Diffusion in the liquid phase is nearly three order of magnitude slower than in the gas phase. This makes the reaction mass transfer limited, which influences both the activity and the selectivity.

There are primarily two different types of diffusion limitations; diffusion limited CO arrival and diffusion limited removal of the reactive products. The first type is related to the difference in diffusion rate of CO and H_2. Large particles will have a long diffusion path where the pores are filled with liquid. CO has a lower diffusivity than H_2, meaning that, when the gas reaches the metal particle inside the pore system, the ratio of H_2 and CO can be different from the initial ratio in the gas phase. This effect decreases the selectivity to long-chain hydrocarbons. The second type increases the effect of the primary products in secondary reactions, and can give rise to increased α-olefin re-adsorption or to α-olefin hydrogenation.[14]

In order to avoid mass transfer limitations in catalyst performance measurements, it is recommended to sieve the catalyst to below 50 µm. If larger particles are used, it will affect the selectivity. However, the size 50-90 µm is typically used in order to minimize pressure drops in the reactor. Hilmen *et al.*[94] showed that the reaction rate decreases with 20 % when you go from 50-75 µm to 425-850 µm, similarly, the selectivity decreased from 82.9 % to 64.4 % when particles sieved to 425-850 µm were used. A change to 50-90 µm should therefore not affect the reaction rate and the selectivity to a great extent.

3 Experimental

3.1 Catalyst Preparation

All the catalysts made in this project were prepared by incipient wetness impregnation (IWI). The active material utilized was $Co(NO_2)_3 \cdot 6\,H_2O$ on a support of alumina (Al_2O_3) (g-alumina Puralox SCCa 45 190) or titanium dioxide (TiO_2) (p-25). The noble metal precursors used were $HReO_4$(aq), $Ru(NO)(NO_3)_2$ in dilute nitric acid, $Pt(NH_3)_4(NO_3)_2$, and $H_2PtCl_6 \cdot 6\,H_2O$. The precursor $H_2PtCl_6 \cdot 6\,H_2O$ was only used for the catalyst supported on Al_2O_3 (sample $Co/Pt/Cl/Al_2O_3$). Solvent used for all the impregnations was deionised water.

Initially Al_2O_3 was dried at 500 ^{o}C in a high temperature furnace for 10 hours. TiO_2 was treated in air (calcined) at 700 ^{o}C for 10 hours, in order to push the phase transition from anatase to rutile. Amounts of noble metal precursors, active material and support used in IWI are presented in Appendix A. The amount of cobalt was 20 wt%, and the atomic relation between promoter and cobalt was 1/100, respectively.

After IWI the catalysts were dried in an drying-oven for one hour at 120 ^{o}C with stirring for each 15 minutes. The dried catalysts were then calcined in a calcination setup with flowing air in a 40 mm i.d. tubular quartz reactor for 16 hours at 300 ^{o}C (2 ^{o}C/min). The catalyst samples were sieved to 50-90 µm and stored in tight glass bottles prior to further characterization.

3.2 Catalyst Characterization

3.2.1 N_2-Physisorption

N_2-physisorption was performed using either a Micromeritics Tri Star 3000 Surface Area and Porosity Analyzer, or a Micromeritics Tri Star 3020 Surface Area and Porosity Analyzer, for the purpose of calculating the specific surface area, pore volume, and pore size distribution from adsorption and desorption isotherm branches according to BET-BJH method. Tri Star 3000 was used for the measurements of the catalysts supported on Al_2O_3, while the Tri Star 3020 was used for the catalysts supported on TiO_2 due to the low surface area of TiO_2.

Around 250 mg of the catalysts supported on Al_2O_3, and approximately 1 g for the catalysts supported on TiO_2 was placed in a glass tube. The sample was then degassed overnight in a VacPrep 061 Degasser at 200 ^{o}C before it was placed in the BET instrument for N_2 adsorption measurements.

The method used was BET-BJH with 108 measurement points for Tri Star 3000, and 88 measurement points for Tri Star 3020. The sample was cooled to cryogenic temperature (77 K), and exposed to analysis gas at precisely controlled pressures. The pore volume, average pore size, and pore size distribution was calculated according to the BJH theory. The surface area was found according to the BET theory.

3.2.2 Temperature Programmed Reduction

Temperature Programmed Reduction (TPR) was performed using a Altamira BenchCAT^{TM} Hybrid instrument. The catalyst sample (approximately 0.15 g) was placed in a 4 mm

i.d. quartz u-tube reactor between two wads of quartz wool. In order to desorb water and weakly bound species the sample was heated in 50 mL/min Ar flow to 300 ^{o}C (10 ^{o}C/min) for 30 min. Reduction took place in 50 mL/min reduction gas flow (7% H_2/Ar flow) heating from 50 ^{o}C to 900 ^{o}C (10 ^{o}C/min) and held there for 30 minutes. The effluent gas was then passed over a Drierite^{TM} filled trap to extract moisture before being passed over a thermal conductivity detector (TCD). Calibration was done by reduction of Ag_2O powder at equal conditions.

3.2.3 X-ray Diffraction

The X-ray Diffraction (XRD) analysis was performed using a Bruker D8 Advance DaVinci X-ray diffractometer at ambient conditions. The instrument operated in Bragg-Brentano θ-θ configuration and was equipped with a CuKα X-ray source, LynxEye^{TM} SuperSpeed detector, 2.5 ^{o} primary and secondary soller slits, variable divergence slit and automatic sample changer (Figure 3.1). Due to the toxicity of the samples, the catalysts were placed in kapton foil holders. The prepared holder was then loaded into a magazine. The measurements were performed using a step length of 0.045 ^{o} with a 2θ scanning range of 15-75 ^{o}, and a 0.3 ^{o} fixed divergence slit. The measurement time was 1.35 s/step.

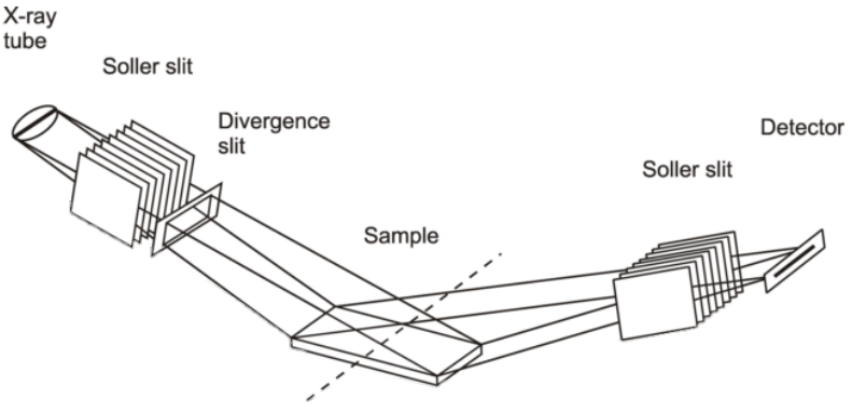

Figure 3.1: Schematic illustration of the components in a X-ray diffractormeter. Obtained from technical reference user manual.

The data was collected using the Bruker Diffrac.Suite EVA software. This software was connected to the PDF-4 database by ICDD[95]. The particle size of Co_3O_4 was calculated using the Pawley method[88] of a full profile analysis in the Bruker Diffrac.Suite Topas 5.0 software[96]. Separate scans of γ-Al_2O_3 and TiO_2 was done to optimise the refinement of the Co_3O_4 scan. Due to their low abundance, visible signals were not obtained for the promoters, and are therefore not reflected in the results. The instrumental details and the phase information added in the Topas software are presented in Appendix D.

The obtained particle sizes of Co_3O_4 were further utilized to calculate the dispersion based on the two equations 3.1 and 3.2.[9,97]

$$d(Co^0) = 0{,}8 \cdot d(Co_3O_4) \tag{3.1}$$

$$D = \frac{96}{d(Co^0)} \qquad [D= \%\ ,d=nm] \tag{3.2}$$

3.2.4 H_2-Chemisorption

The H_2-chemisorption analysis was performed using a micromeritics ASAP 2020C instrument. The adsorptive gas used was H_2, which was assumed to adsorb dissociatively to the catalyst surface. This means that one hydrogen atom adsorbs to one surface Co-atom. The analysis revealed the dispersion of the Co-catalysts.

The catalyst (300 mg) was placed in a 9 mm i.d quartz u-tube reactor between two wads of quartz wool. The sample was then reduced *in situ* at 350 ^{o}C (1 ^{o}C/min) for 16 hours under H_2 flow, followed by cooling under vacuum. The analysis data was gathered at 40 ^{o}C with H_2 pressures ranging from 15-507 mmHg, containing 11 measurement points. The first isotherm of the collected data was used to estimate the dispersion of the catalyst by extrapolation of the linear part back to zero.

3.2.5 X-ray Fluorescence

X-ray Fluorescence (XRF) measurements were done using a Wavelength Dispersive X-Ray Fluorescence (WDXRF) Supermini 200 analyser. XRF was performed to investigate presence of contaminants in the samples, as well as to determine that the calculated amount of Co and promoter agreed with the real amount.

The pellets (40 mm diameter) were prepared using a sample of the prepared catalyst (100 mg) and boric acid (3.0 g) as a binder. This was then crushed in a mortar and mixed for 10 minutes, to achieve a homogeneously dispersed powder. The same mortar was used for all the different catalyst samples to prevent contamination from other samples. The mortar was washed and dried in-between the different catalyst samples. The powder-mix was crushed in a pellet press machine with a load of 10 tonne for 2 minutes. The resulting pellet was then placed in a pellet sample holder covered with polypropylene film (6µm), and submitted for XRF analysis.

Three pellets were prepared of the $Co/Re/Al_2O_3$ sample to investigate the uncertainty in the preparation method. For each of the remaining samples one pellet was prepared. Each pellet was analysed by XRF three times to confirm the certainty of the analysis method.

3.3 Fischer-Tropsch Synthesis

The Fischer-Tropsch experiments were performed in an in-house built laboratory scale setup. The setup contained four separate fixed bed reactor systems. A flow chart of the FT setup is presented in Figure 3.2. Pre-mixed synthesis gas ($H_2/CO/N_2$) with a H_2/CO ratio of 2.0 and 3 vol.% of N_2 was employed for all experiments. The synthesis gas was purified for Fe carbonyl compounds in two PbO traps in series. After cleaning and pressure relief, a side stream could be taken out for analysis of the feed gas. The feed gas was preheated before it was fed to the top of the reactors at a temperature close to the reaction temperature.

The reactor was a 9.4 mm i.d. stainless steel fixed-bed-reactor. The catalyst (1 g for Co/Al_2O_3 catalysts and 2 g for Co/TiO_2 catalysts) was diluted with SiC (20 g for Co/Al_2O_3 catalysts and 19 g for Co/TiO_2 catalysts) in order to minimise temperature gradients, before it was loaded into the reactor between two plugs of quartz wool. The reactor was placed in a cylindrical aluminium block inside an electrically heated, temperature controlled furnace. A 2 mm stainless steel thermowell was placed through the catalyst bed and fitted with a 3-point thermocouple to monitor the process temperature.

The product gas, downstream of the reactor, was passed through a hot condenser, kept at approx. 90 ^oC and a cold condenser at ambient temperature to gather water and heavy FT products. A small amount (approx. 30 NmL/min) of the product stream was split off and analysed by a Gas Chromatograph (GC). The rest was sent through a molsieve type drier and back pressure controller to control the operating pressure.

After the reactor was installed, leak tests were performed by increasing the pressure in the entire apparatus to around 20 bar with a flow of helium (He) (250 mL/min). Final leak check were done by adding a small amount of H_2 and checking with a portable gas detector.

Synthesis gas was delivered in 50 liter bottles at about 200 bar. All bottles connected to the feed-line were analyzed before each experimental series. A feed sequence of 20-30 analyzes was performed to determine the CO/N_2 ratio in the gas. This, together with the H_2/CO ratio (stated by the gas supplier) was the basis for calculating the composition of the product gas. The feed gas analyzes were performed simultaneously with pressure testing and catalyst reduction. The catalyst reduction took place in 250 mL/min H_2 flow at 350 ^oC (1 ^oC/min) for 10 h before being cooled to 170 ^oC. The reactor was then pressurized to operating pressure in 250 mL/min He flow. While 250 mL/min synthesis gas was introduced, the reactor was heated to 200 ^oC (20 ^oC/h), and 208 ^oC (5 ^oC/h) and adjusted to give a reaction temperature of 210 ^oC.

Activity measurements were reported after 24 h ToS. After 24 h ToS, the Gas Hourly Space Velocity (GHSV) was changed to obtain a desired CO conversion level of 50 %, and the selectivity measurements were taken. The containers for hot and cold liquid products were emptied once a day. There were problems adjusting to 50% conversion for the catalysts supported on TiO_2. The conversion reached steady state after 50 h ToS, the period between 24 to 50 h can therefore be ignored. Unfortunately, the catalyst $Co/Ru/TiO_2$ ended up at about 40% conversion, even after several small adjustments of GHSV. However, the low conversion should not affect the interpretation of the data significantly.

Finally, the reactor was flushed with 250 mL/min He for 2-3 h, before cooled to ambient temperature in 125 ml/min He flow. The reactor could be removed when ambient temperatures were reached.

The GC was an HP6890N with a CarboSieve (10 ft packed column) with a TCD and a HP-PLOT Al_2O_3 "M" with a FID. The GC was equipped with a multiposition valve (MPV) which selected which product line being analyzed. The position of the MPV was determined by the analysis method. The activity and selectivity of CH_4 and CO_2 was determined by comparing data from the TCD with calibration data, while the hydrocarbon selectivity was determined by comparing the CH_4 selectivity with the FID data. An example of a GC calculation of selectivity and activity is presented in Appendix C.

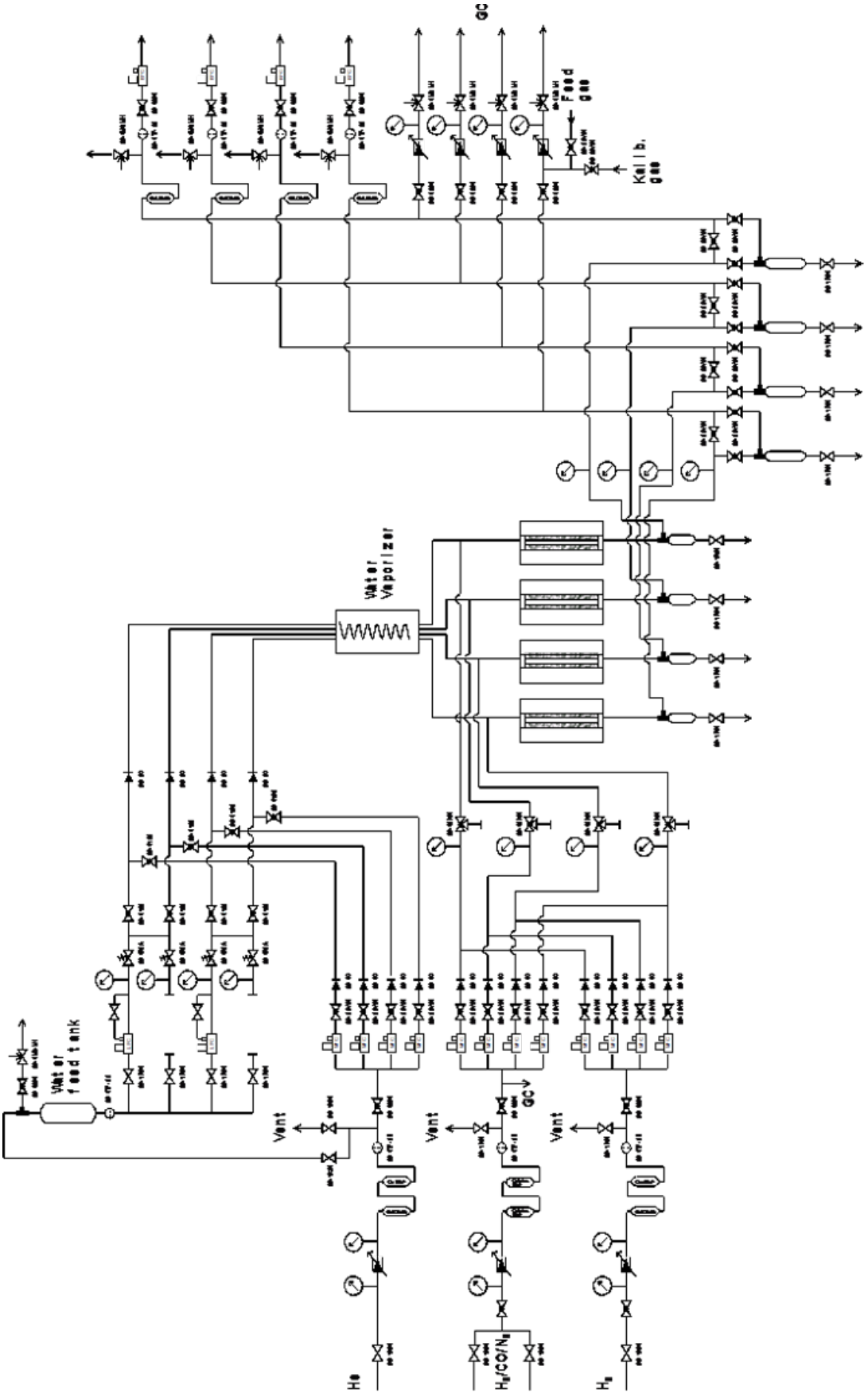

Figure 3.2: Flow chart of the Fischer-Tropsch synthesis setup. The figure is obtained from SINTEF's manual for the FT setup.[98]

4 Results and Discussion

4.1 Catalyst Characterization

4.1.1 Elemental analysis

Every catalyst was analysed by X-ray Fluorescence (XRF) in order to find the weight percentage of Co, the atomic relation between the promoter and Co, and if there were any contaminants in the samples. The primary results from the elemental analysis performed by XRF are presented in Table 4.1, and the remaining results are given in Appendix E. Three pellets were prepared from the $Co/Re/Al_2O_3$ sample to investigate the uncertainty in the preparation method. For each of the remaining samples one pellet was prepared. Each pellet was analysed by XRF three times to confirm the uncertainty of the analysis method.

The XRF-analysis allowed for the calculation of the atomic relation between promoter and Co. The results of this calculation is presented in Table 4.1. According to the nominal values, presented in Table 4.2, the atomic relation should be 1/100, i.e. 0.010.

Table 4.1: XRF results and the calculated atomic relation between promoter and Co for each sample.

Catalyst	Co (wt%)	Al or Ti (wt%)	Promoter (wt%)	Atomic relation (Promoter/Co)
Co/Al_2O_3	24.2 ± 0.3	74.0 ± 0.2	-	-
$Co/Re/Al_2O_3$	29.2 ± 4.1	68.2 ± 4.4	0.86 ± 0.09	0.009
$Co/Ru/Al_2O_3$	24.0 ± 0.4	74.5 ± 0.5	0.35 ± 0.02	0.008
$Co/Pt/Cl/Al_2O_3$	26.3 ± 0.4	70.9 ± 0.4	0.78 ± 0.10	0.009
$Co/Pt/Al_2O_3$	27.7 ± 0.8	69.3 ± 0.6	0.72 ± 0.09	0.008
Co/TiO_2	33.2 ± 0.4	65.8 ± 0.4	-	-
$Co/Re/TiO_2$	31.5 ± 0.4	66.5 ± 0.4	1.22 ± 0.08	0.012
$Co/Ru/TiO_2$	29.2 ± 0.3	69.2 ± 0.3	0.69 ± 0.08	0.014
$Co/Pt/TiO_2$	31.9 ± 0.6	66.1 ± 0.7	1.05 ± 0.03	0.010

Table 4.2: Nominal values for the metal loadings in the catalysts.

	Co	Al	Ti	Re	Ru	Pt
Wt%	20	80	80	0.63	0.34	0.66

The observed Co concentrations are higher than the nominal values of 20 wt%. However, the atomic relation between promoter and Co is approximately the same as the nominal value of 0.01. The results (given in Appendix E) indicated the presence of some minor contaminants in all of the samples.

In three of the catalysts ($Co/Re/Al_2O_3$, $Co/Pt/Al_2O_3$ and $Co/Ru/TiO_2$), 0.1 wt% sulphur was detected, and 1 wt% of potassium was observed in all of the catalysts. If the catalysts contain sulphur, it would greatly reduce the effect of the catalyst due to the highly deactivating properties of sulphur i Co-catalysis. It is reported that sulphur blocks

more than two cobalt atoms on Co/Al_2O_3 catalysts.[67] None of the chemicals used in the preparation of the catalysts contained sulphur or potassium, it is therefore very unlikely that they are present in the samples, and can likely be attributed to residual contaminants in the instrument itself.

The XRF results for the three prepared pellets of the catalyst $Co/Re/Al_2O_3$ showed the highest standard deviation ($\pm 4.1\,\%$) compared to the pellets that were run three times. This underlines the uncertainty connected to the preparation method. As mentioned in Section 2.5.3, the sample preparation process is the single largest contributor to the overall sources of error in an XRF analysis. A smaller particle size (lower than 50 μm), higher amount of pressure (25-35 tonne), and a better mixing method could have reduced the uncertainty of the preparation process.[83]

4.1.2 X-ray Diffraction

Every sample was analysed in X-ray Diffraction (XRD) in order to find the phases present in the catalysts. The XRD results of the catalysts supported on Al_2O_3 and TiO_2 are presented in Figure 4.1 and 4.2, respectively. The observed phases in the catalysts supported on Al_2O_3 are γ-Al_2O_3 and Co_3O_4. For the catalysts supported on TiO_2 the observed phases are the anatase and rutile crystals of TiO_2, and Co_3O_4. Even though TiO_2 was heated to 700 ^{o}C in order to push the phase transition from anatase to rutile, there will always be some anatase. The quantitative amount of each phase and the promoters are not reflected in the results.

The XRD results confirm that there are no other observable cobalt phases than Co_3O_4, but it does not exclude amorphous phases or other phases that can not be detected, e.g. due to low concentration or small particles (smaller than 5 nm).[99]

Due to the toxicity of the samples, kapton foil holders were used to prevent exposure. It is shown that the katpon foil deafens the XRD spectra at low angles, consequently there is background noise in the range 20 to 30 2θ angles.

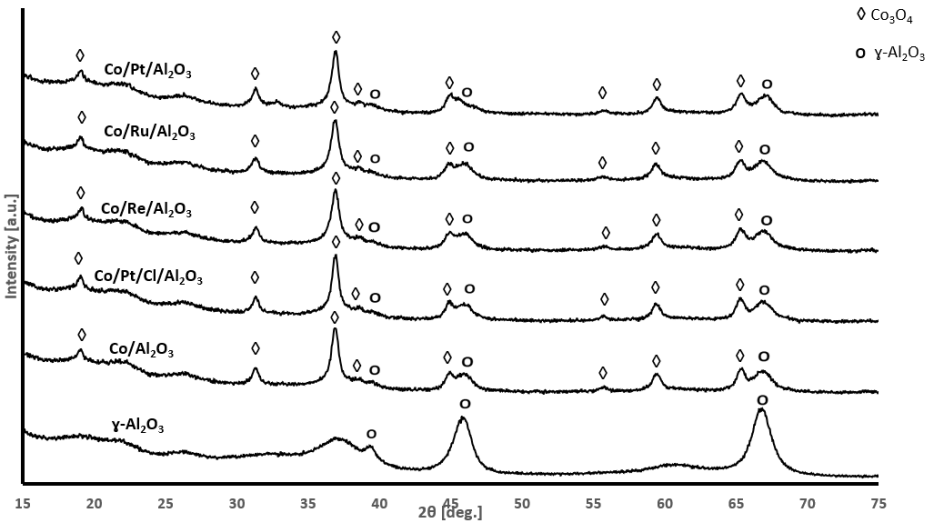

Figure 4.1: X-ray diffraction pattern of the different catalysts supported on γ-Al_2O_3 and the bare support γ-Al_2O_3. The Co_3O_4 and γ-Al_2O_3 peaks correspond to the PDF 00-042-1467 and PDF 00-056-0457, respectively, obtained from the PDF-4 database.[95]

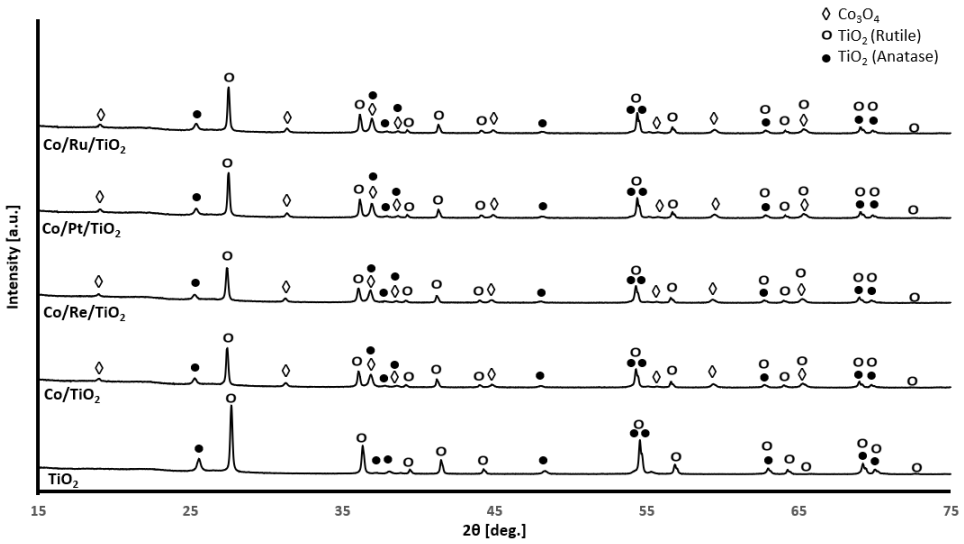

Figure 4.2: X-ray diffraction pattern of the different catalysts supported on TiO_2 and the bare support TiO_2. The Co_3O_4, anatase, and rutile peaks correspond to the PDF 00-042-1467, PDF 00-064-0863, and PDF 04-003-0648, respectively, obtained from the PDF-4 database.[95]

4.1.3 Temperature Programmed Reduction

All the prepared catalysts, except $Co/Pt/Cl/Al_2O_3$, were analysed by Temperature Programmed Reduction (TPR). The results obtained are presented in Figure 4.3 and 4.4, for the catalysts supported on Al_2O_3 and TiO_2, respectively. In between the different TPR experiments, there were several adjustments to the instrument. This may explain discrepancies in the results.

When reducing the Al_2O_3-supported catalysts, the temperature of reduction for both steps (Co_3O_4 to CoO and CoO to Co^0) downshifted to lower temperatures upon addition of Ru and Pt, however, only the second reduction step was significantly affected in the case of Re promotion. The addition of Pt lowered the reduction temperature to the most extent, followed by Ru. This is in good agreement with the literature.[58,50,52] It is well known that Co/Al_2O_3 show poor reducibility due to the strong interaction between the small cobalt oxide crystallites and Al_2O_3, through addition of reduction promoters the reduction temperature is lowered.[8]

There is a small peak around 240 ^{o}C for the catalyst $Co/Pt/Al_2O_3$. This peak can originate from Co-nitrates or promoter oxides. Since, the concentration of promoter oxides was very small, it should not affect the H_2 consumption to a large extent. Furthermore, no nitrates were observed in the XRD. Because the sample was heated to 900 ^{o}C, several reactions may have occured. It is therefore difficult to conclude what this peak originates from.

Eschemann *et al.*[59] showed through TPR experiments that the addition of noble metals to Co/TiO_2 catalysts led to decreased reduction temperatures of cobalt oxide. The effect was most pronounced for the addition of Ru and Pt, and less pronounced for the addition of Re and Ag. This is in good agreement with the results presented in Figure 4.4, for the promoted Co/TiO_2 catalysts. Ru and Pt led to decreased temperatures, while Re did not affect the reduction temperature to a large extent. However, it is difficult to determine where the first and second peaks start for the catalysts supported on TiO_2, since there

is no baseline separation, but the curves should principally contain both reduction steps from Co_3O_4 to Co^0.

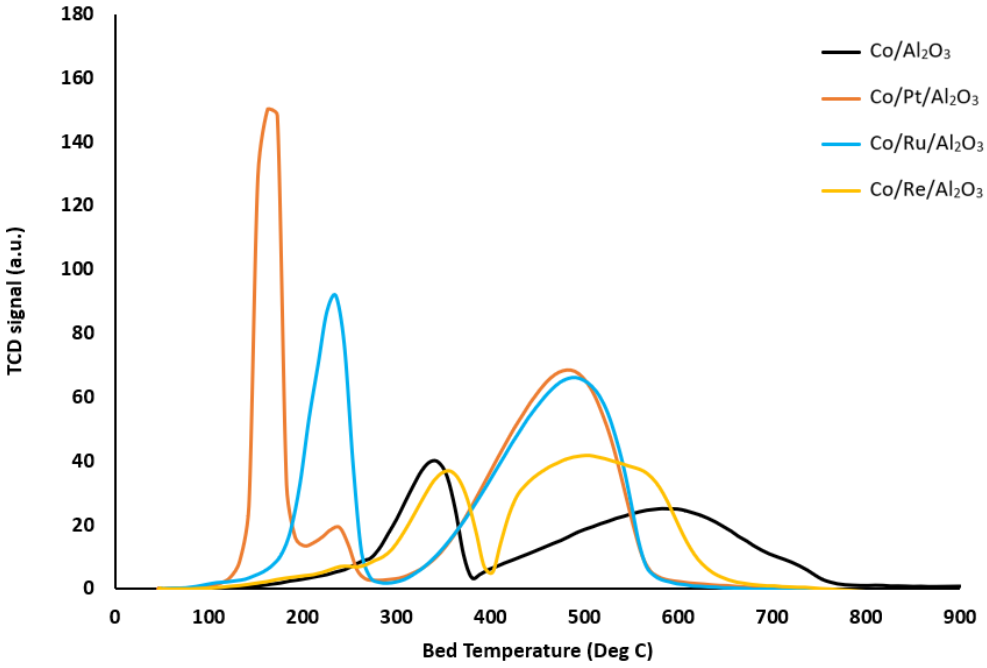

Figure 4.3: Temperature Programmed Reduction results for the catalysts supported on γ-Al_2O_3.

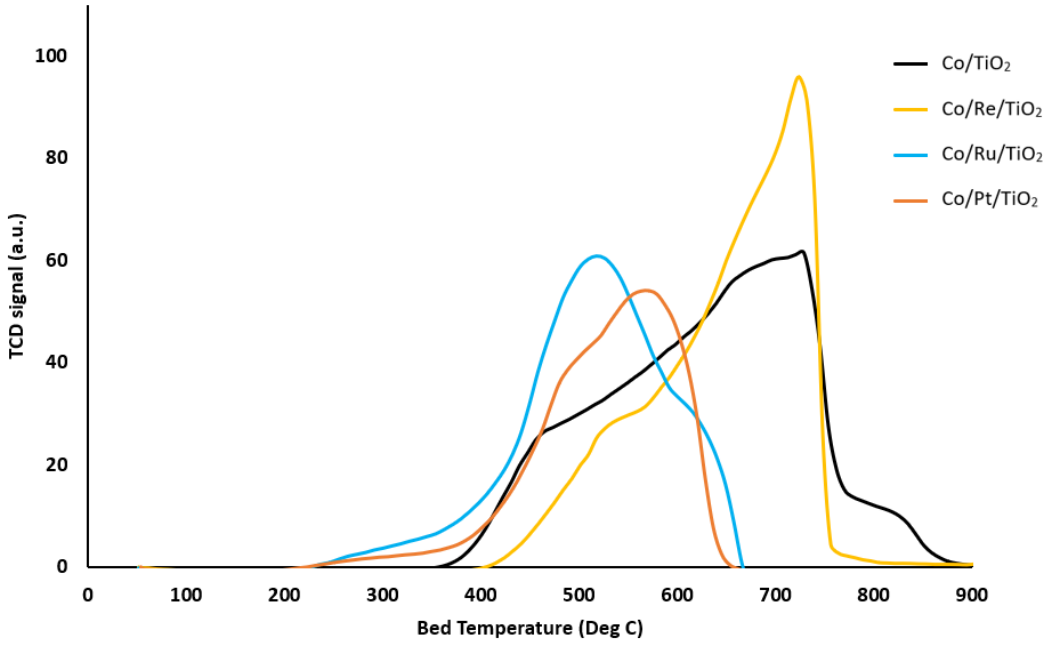

Figure 4.4: Temperature Programmed Reduction results for the catalysts supported on TiO_2.

For a perfect two step reduction of Co_3O_4 to Co^0, the ratio between the area of two peaks in TPR should be 1:3, i.e. 0.33. The calculated ratio of each catalyst is presented in Table 4.3 together with the calculated Degree of Reduction (DoR). The ratio of the TiO_2-supported catalysts are not calculated due to the difficulty of defining the area below the first and second peak. The DoR calculations are given in Appendix B. The DoR is calculated based on the assumption that the catalyst contains 20 wt% Co, and on the basis of the XRF results. In the calculation of DoR it is assumed a total reduction of Co_3O_4 to Co^0, any reduction of Co-nitrates or promoter oxides are not taken into account.

Table 4.3: Degree of reduction based on the assumption of 20 wt% of Co in the catalyst, degree of reduction based on XRF results, and the ratio between the hydrogen consumption for reduction of Co_3O_4 to CoO and the hydrogen consumption for reduction of CoO to Co^0.

Catalyst	Degree of Reduction (%)		Ratio
	20 wt%	XRF	
Co/Al_2O_3	78	64	0.56
$Co/Pt/Al_2O_3$	69	104	0.63
$Co/Ru/Al_2O_3$	125	104	0.53
$Co/Re/Al_2O_3$	78	54	0.47
Co/TiO_2	127	76	-
$Co/Pt/TiO_2$	76	48	-
$Co/Ru/TiO_2$	87	60	-
$Co/Re/TiO_2$	119	76	-

Based on these results, it can be seen that the accuracy of the weight percentage of Co when calculating the DoR is crucial. Only 7.7 wt% difference gave drastic changes as shown for the sample $Co/Pt/Al_2O_3$, which gives a DoR of 69 % when 20 wt% Co is assumed, and a DoR of 104 % when 27.7 % is assumed. Despite uncertainties connected to the XRF results, there are no clear trends for 20 wt% Co in the DoR. It therefore implies that the assumption of 20 wt% Co in all samples is not in agreement with reality.

Some of the samples showed a DoR above 100%. For TiO_2-supported catalysts, this can be explained by the SMSI effect, which is observed when the reduction temperature is above 500 ^{o}C.[76] If the support is reduced to form a suboxide (TiO_x), the H_2 consumption will increase, higher than the theoretical value, causing an observed reduction over 100 %.

The DoR reflects the extent of metal-support interaction.[100] Jacobs *et al.*[64] found the metal-support interaction to be in the order γ-Al_2O_3 > TiO_2 > SiO_2. The extent of the metal-support interaction for TiO_2 is strongly dependent on its phase, where rutile shows weaker interaction than anatase.[100] The TiO_2-supported catalysts prepared should contain mostly rutile. Hence, it is expected that the Al_2O_3-supported catalysts should be the most affected by the addition of reduction promoters, giving a higher DoR when adding promoters, while TiO_2-supported catalysts should not be affected to the same extent. Based on DoR calculated from XRF results, this agrees quite well, with the exception of $Co/Re/Al_2O_3$ which showed a lower DoR than expected. Hilmen[101] found through O_2-titration that the addition of Re to a 17 wt% Co/Al_2O_3 catalyst increased

the DoR with 16%. Similar results were obtained by Storsæter[100] who, through TPR and O_2-titration experiments, found that the addition of Re to a 12 wt% Co/Al_2O_3 catalyst, increased the DoR with 25% in TPR and 8% in O_2-titration. The cobalt-loading is of great importance when comparing DoR results, since there will always be a proportion of cobalt that is non-reducible. The proportion of unreduced cobalt will be greater for the catalysts with 12 wt%. Fredriksen[102] found that the proportion of non-reducible cobolt is 1 wt%, below this loading it is not possible to produce an active Fischer-Tropsch catalyst. In addition, it is reported that $\sim 3\%$ cobalt-aluminate is formed during realistic FTS conditions.[103]

An element that can affect the reducibility of cobalt is water produced in the reduction. Water may influence the metal-support-interaction and the reducibility of γ-Al_2O_3 and TiO_2 supported catalysts. For Co/TiO_2 catalysts, the produced water results in a rather large decrease in reducibility, indicating formation of non-reducible "Co-titanate". This effect is even larger on γ-Al_2O_3 cobalt catalysts, since it results in an increased Co-aluminate interaction and/or formation of non-reducible cobalt compounds.[100] However, the amount of water produced depends on how much cobalt is reduced, but the concentration of water over the catalyst depends on the gas velocity. A high gas velocity drives away the water faster, resulting in a smaller effect. The gas flow utilized was quite high and the experiments were done equally for all the catalysts, which indicates that this effect should not be pronounced to a great extent.

The ratios between the hydrogen consumption for the two peaks, for the catalysts supported on Al_2O_3, are quite high compared to 1:3 for a perfect reduction. This can indicate that the second reduction step (Co^{2+} to Co^0) was not complete. γ-Al_2O_3 has a spinel structure containing holes that ions can migrate into. Migration of cobalt ions into the tetrahedral sites of Al_2O_3 can form nonreducible cobalt aluminates. In the case of $CoAl_2O_4$, Co^{2+} ions can easily fit into the spinel structure. The term "non-reducible" is applied because the cobalt aluminates can only be reduced above 800–900 ^{o}C.[104] It is therefore reasonable to assume that the second reduction step is not complete, and that some cobalt-aluminate has been formed. However, the total hydrogen consumption for the catalyst $Co/Ru/Al_2O_3$ and $Co/Pt/Al_2O_3$, based on XRF results, corresponds to a complete reduction of Co_3O_4 to Co^0. Hence, it may seem like the calculated DoR (over 100%) is over-estimated.

The main conclusion from the TPR and DoR results is that the addition of promoters have a larger effect on the reduction of cobalt on Al_2O_3, and less effect on TiO_2-supported cobalt. Discrepancies in the results can be connected to the adjustments of the instrument. The catalyst Co/Al_2O_3 was analysed three times in TPR to investigate if the results were reproducible. The resulting TPR plot is presented in Appendix B.2. The curves changes both positions and intensities when analysed several times, and underlines the uncertainties related to the results, due to problems and adjustments of the instrument. The curve used in the results, given above, is used due to the fact that it fits better with the literature of how the peaks of Re-promoted Co/Al_2O_3 catalysts behaves.[58,50]

4.1.4 N_2-Physisorption

All the catalysts were analysed by N_2-physisorption measurements for the purpose of calculating the specific surface area, pore volume, and average pore size from adsorption and desorption isotherm branches according to BET-BJH method. The N_2-physisorption results are presented in Table 4.4. The isotherm plots, from the N_2-physisorption measurements, are given in Appendix E.1.

Table 4.4: N_2-physisorption results

Catalyst	Surface area (m^2/g)	Pore volume (cm^3/g)	Average Pore size (nm)
γ-Al_2O_3	148	0.62	16.3
Co/Al_2O_3	119	0.45	16.4
$Co/Pt/Al_2O_3$	96	0.42	19.5
$Co/Pt/Cl/Al_2O_3$	115	0.44	16.8
$Co/Re/Al_2O_3$	117	0.43	16.9
$Co/Ru/Al_2O_3$	121	0.46	17.1
TiO_2	21	0.02	4.5
Co/TiO_2	18	0.02	4.7
$Co/Pt/TiO_2$	22	0.03	4.6
$Co/Re/TiO_2$	21	0.02	4.5
$Co/Ru/TiO_2$	21	0.02	4.5

The support Al_2O_3 had a high surface area (148 m^2/g) and relatively small pores, which was as expected.[8,37] The Co/Al_2O_3 catalysts all had a surface area of 118 ± 3 m^2/g, with the exception of $Co/Pt/Al_2O_3$ which had a surface area of 96 m^2/g (measured twice). The smallest pores contribute a lot to the surface area, so if these become plugged, it is expected that the surface area decreases considerably. This may indicate that the smallest pores have been plugged for the Co/Al_2O_3 catalysts, and to the most extent for $Co/Pt/Al_2O_3$, since there was a loss of surface area. This agrees well with the fact that $Co/Pt/Al_2O_3$ showed the largest average pore size. The other catalyst containing Pt ($Co/Pt/Cl/Al_2O_3$) behaved similarly to the other catalysts, this implies the plugging of pores is not connected to Pt, but the precursor used.

The support TiO_2 and the Co/TiO_2 catalysts all showed a surface area of 20 ± 2 m^2/g. Compared with Al_2O_3 and SiO_2 supports, TiO_2-supports generally has relatively low specific surface areas around 60 and 10 m^2/g for the phases anatase and rutile, respectively.[37] A surface area of 20 ± 2 m^2/g is therefore in good agreement with the literature,[37,78,100] knowing that the catalysts consists of mostly rutile and some anatase. However, the results show that TiO_2 has small average pore sizes, this is inconsistent with the literature which states that TiO_2 should have a higher average pore size, due to the presence of wider pores.[78,100] This can be explained by the fact that a nitrogen desorption isotherm is used for calculation of pores with pore radius in the range of 1 - 30 nm.[100] Larger pores than 30 nm will therefore not be detected.

Storsæter[100] reported an average pore size of 770 nm for a Co/TiO_2 catalyst prepared with the same precursors and conditions as the catalysts in this project. However, the measurement used was mercury intrusion. Mercury intrusion is used for calculation of pores with pore radius in the range of 5 nm - 55 μm. Hence, the catalysts supported on TiO_2 should have been measured by mercury intrusion in addition to N_2-physisorption. It is therefore reasonable to assume that the catalysts supported on TiO_2 have larger average pore sizes than those shown here. The assumption that the pores are larger than reported is reinforced by the fact that the selectivity data in section 4.2.3 agree well with the literature, which states that TiO_2 catalysts give higher selectivity due to larger pores.[46,47] This does not exclude the presence of any mesopores (2-50 nm) in the catalyst. The N_2-physisorption results indicate the presence of mesopores, however, it is not likely that these dominate the overall pore distribution when macropores are added to the distribution.

The total pore volume of the catalyst can be calculated, based on bulk and crystal densities. The bulk density is found through weighing the support (TiO_2) in a known volume, and the crystal density is found in the literature for a mixture of rutile and anatase. The densities were found to be 4.23 g/cm^3, and 3.78 g/cm^3 for rutile and anatase, respectively.[105] For a mixture of rutile and anatase a crystal density of 4.00 g/cm^3 was assumed. The bulk density was found to be 0.32 g/cm^3. The total pore volume is given by Equation 4.1, and the fraction of mesopores is given in Equation 4.2.

$$\text{Total pore volume} = \frac{1}{0{,}32\text{g/cm}^3} - \frac{1}{4{,}00\text{g/cm}^3} = 2{,}84\,\text{cm}^3/\text{g} \tag{4.1}$$

$$\text{Fraction of mesopores} = \frac{0{,}02\text{cm}^3/\text{g}}{2{,}84\text{cm}^3/\text{g}} \cdot 100\,\% = 0{,}7\,\% \tag{4.2}$$

Only 0.7% of the total pore volume is represented in the results from N_2-physisorption. This shows that 99.3% of the total pore volume are macropores (> 50 nm) and the volume of the empty space between the particles. It is therefore reasonable to assume that the average pore size of the TiO_2-supported catalysts should be similar to what Storsæter[100] obtained for her catalysts, around 770 nm.

All of the catalysts showed a H1 type of isotherm, while two of the catalysts supported on TiO_2 ($Co/Re/TiO_2$ and $Co/Pt/TiO_2$) showed a type H3 or H4 isotherm. The isotherms for the two catalysts are presented in Figure 4.5. These two catalysts were run one more time, but continued to give the same result. H3 and H4 show no plateau in the isotherm, and therefore has no well-defined mesopore structure, which makes the analysis difficult.[71]

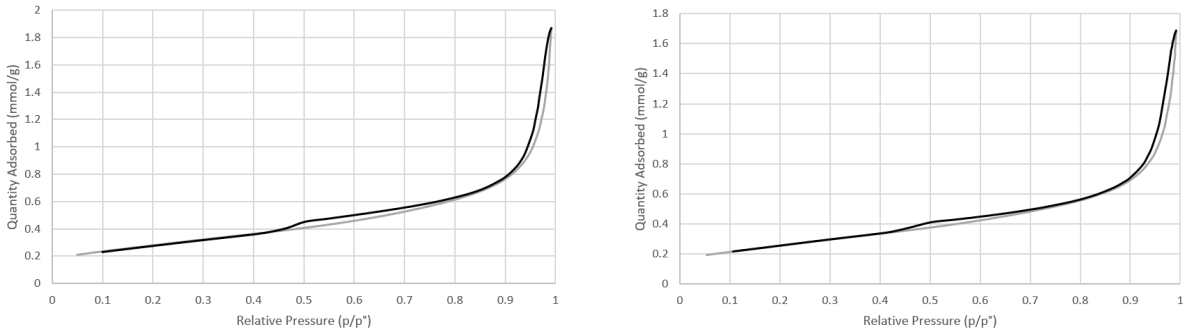

(a) Co/Pt/TiO_2 **(b)** Co/Re/TiO_2

Figure 4.5: Adsorption (grey)/desorption (black) curves for the catalysts Co/Pt/TiO_2 and Co/Re/TiO_2, obtained from N_2-physisorption.

Pore size distributions

The pore size distributions of the catalysts supported on Al_2O_3 and TiO_2 are presented in the Figure 4.6 and 4.7, respectively.

The pore size distribution of the catalysts supported on Al_2O_3 and the bare support show a unimodal distribution, where one pore series dominates. The pore size distribution of the support Al_2O_3 is larger than the distribution of the Co/Al_2O_3 catalysts. This can be explained by plugging of pores when adding cobalt. Promoters have no major effect on the pore size distribution, except for the case of Co/Pt/Al_2O_3 which has a distribution that starts at a higher pore width than the other catalysts, due to plugging of the smallest pores.

The mesopores detected on the TiO_2-supported catalysts, showed a unimodal distribution in the case of the bare support TiO_2, while a bimodal distribution was observed when cobalt was added (Figure 4.7). The height of the second peak depends on the promoter added, and is ranked in the order, from highest to lowest, Pt > Re > Ru > unpromoted. The curves continually rise, indicating the presence of larger pores. Storsæter[100] got somewhat similar peaks, but these were in a completely different order of magnitude (100-8000 nm). She found that the promoted catalyst (promoted with Re) had a clear bimodal distribution and a larger fraction of both the smallest pores (100 nm) and the largest pores (8000 nm), compared to the unpromoted catalyst which primarily consisted of the average pores (around 700 nm).

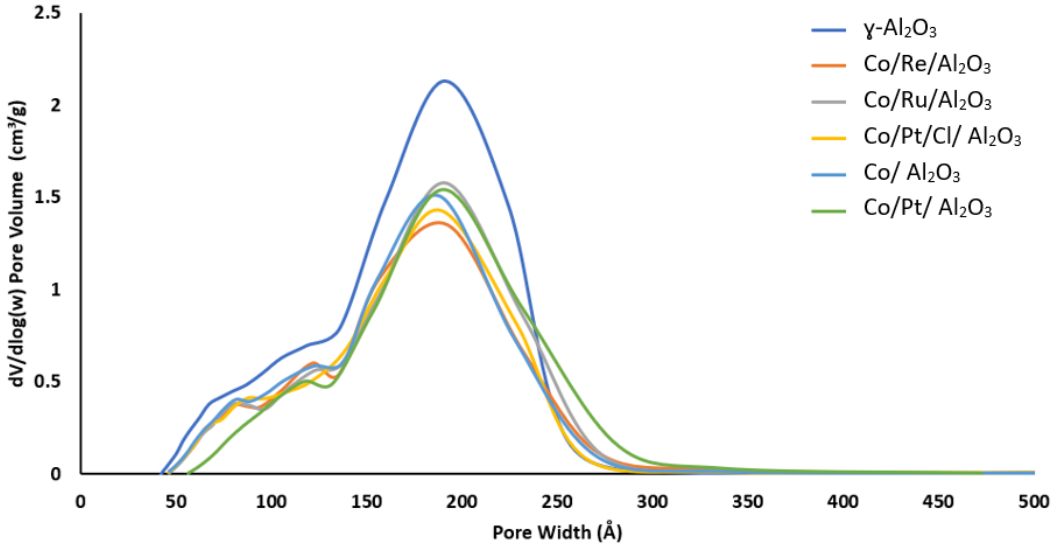

Figure 4.6: Pore size distributions of the catalysts supported on Al_2O_3 and the bare support γ-Al_2O_3.

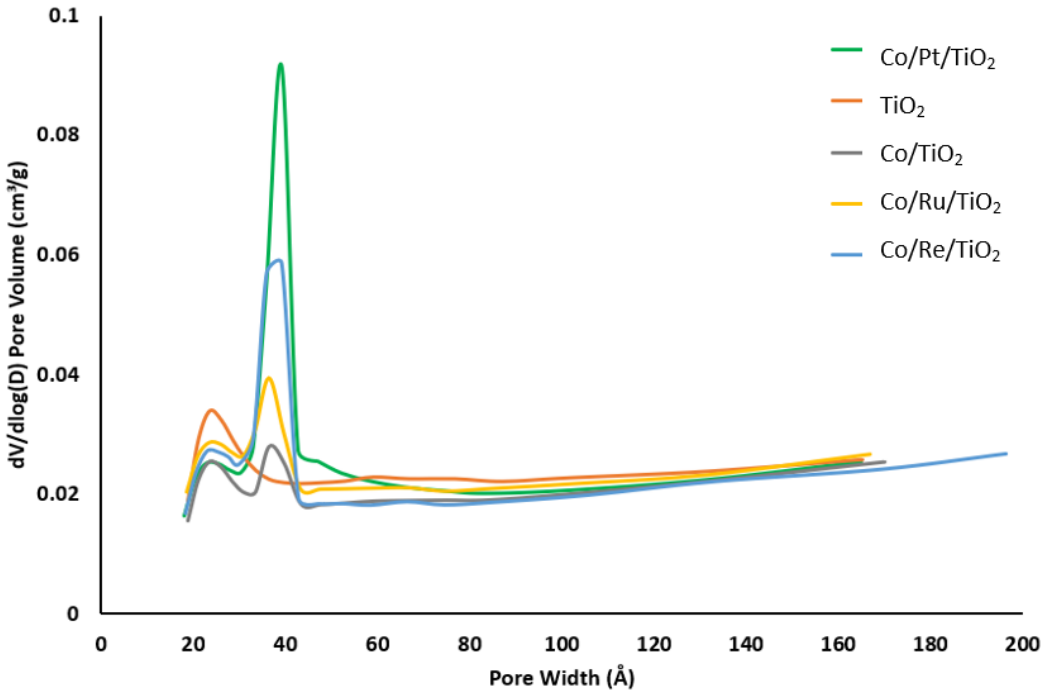

Figure 4.7: Pore size distributions of the catalysts supported on TiO_2 and the bare support TiO_2.

Due to the fact that the bare support of TiO_2 showed a different pore size distribution, unlike the cobalt catalysts supported on TiO_2, a hypothesis was tested. Did the pore size distribution change due to the acidic environment of the cobalt precursor ($Co(NO_2)_3 \cdot 6\,H_2O$), or because of addition of cobalt particles? The cobalt solution added in all the impregnations had a pH of 1.83. It was therefore made a solution with the same pH (1.90), containing water and nitric acid. The resulting pore distributions of TiO_2 (pH=7.00) and TiO_2 (pH=1.90) are presented in Figure 4.8. The surface area, pore volume and average pore size is given in Table 4.5.

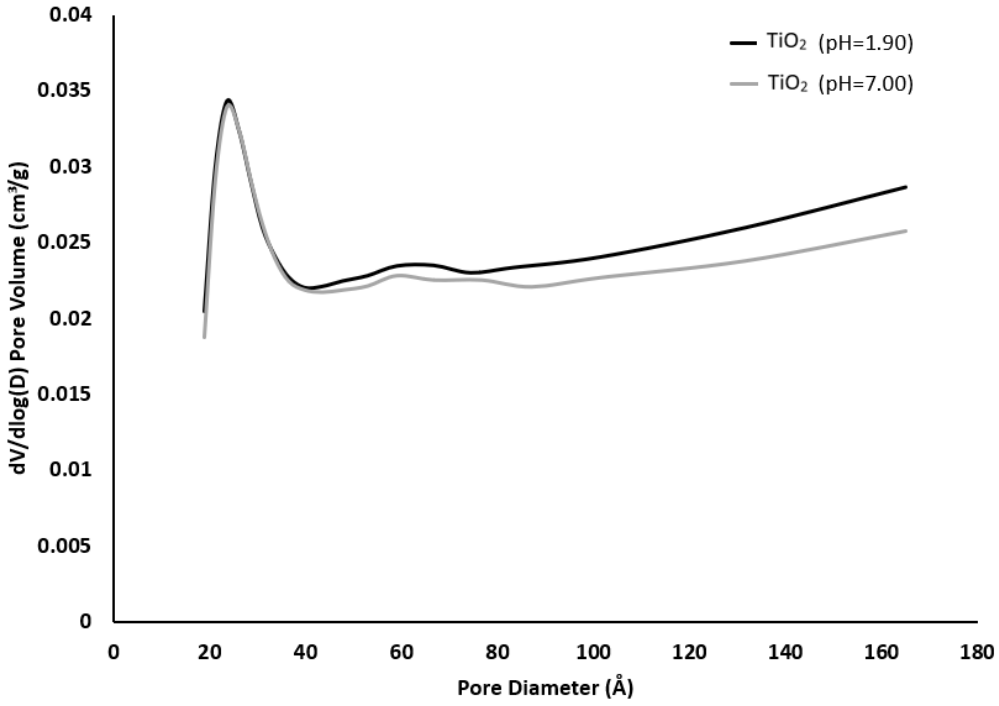

Figure 4.8: Comparison of pore size distributions of the support TiO_2 with a pH=7.00 (grey), and TiO_2 with a pH=1.90 (black).

Table 4.5: N_2-physisorption results of TiO_2 with a pH=7.00, and TiO_2 with a pH of 1.90

Sample	Surface area (m^2/g)	Pore volume (cm^3/g)	Average Pore size (nm)
TiO_2 (pH=7.00)	21	0.02	4.5
TiO_2 (pH=1.90)	21	0.03	4.6

The pore size distribution of TiO_2 (pH=7.00) and TiO_2 (pH=1.90) did not change due to the acidic environment, the only change that could be seen was a slightly increase in the average pore size and pore volume. It is therefore concluded that the addition of cobalt particles to the support TiO_2 caused the change of the pore size distribution from a unimodal distribution to a bimodal distribution.

4.1.5 Dispersion

Dispersion was found both by H_2-chemisorption experiments and by calculating it based on particle size obtained from X-ray Diffraction (XRD).

The crystallite size of Co_3O_4 was found through the Pawley method by employing the Bruker Diffrac.Topas 5.0 software, based on the XRD results (Fig. 4.1 and Fig. 4.2). The resulting diameters of the Co_3O_4 crystallites are presented in Table 4.6 together with the corresponding dispersions calculated by Equation 3.1 and 3.2. The goodness of the XRD results are also given in the table, where R_{wp} is the weighted-profile R value and GOF is the goodness of fit. R_{wp} should ideally be less than 5 and GOF should be 1 in order to have a good fit (Section 2.5.5).

The dispersions gathered from H_2-chemisorption are also presented in Table 4.6, and were found through extrapolation of the linear part of the first isotherm back to zero pressure. It was assumed that H_2 gas adsorbed dissociatively onto the active sites, i.e. H:Co=1. The isotherm plots, for the H_2-chemisorption, are given in Appendix E.2.

Table 4.6: Characterization results from XRD and H_2-chemisorption.

	D (%)		Particle size (d)[b] (nm)		Goodness of XRD results	
Catalyst	H2[a]	XRD	Co_3O_4	Co^0	R_{wp}	GOF
Co/Al_2O_3	4.0	11.5	10.4	8.3	3.5	1.5
$Co/Re/Al_2O_3$	7.2	13.4	9.0	7.2	3.3	1.4
$Co/Pt/Cl/Al_2O_3$	4.8	11.1	10.8	8.6	3.4	1.5
$Co/Pt/Al_2O_3$	8.1	11.9	10.1	8.1	4.4	1.8
$Co/Ru/Al_2O_3$	8.4	13.2	9.1	7.3	3.4	1.5
Co/TiO_2	2.8	4.2	28.7	23.0	4.5	1.5
$Co/Re/TiO_2$	3.0	4.0	30.2	24.2	4.4	1.5
$Co/Pt/TiO_2$	2.9	4.0	30.1	24.1	4.5	1.6
$Co/Ru/TiO_2$	2.7	3.9	31.0	24.8	4.6	1.6

[a]Measured by H_2-chemisorption. [b] Measured by XRD

All of the promoted catalysts supported on Al_2O_3, except $Co/Pt/Cl/Al_2O_3$, gave a higher dispersion than the unpromoted Co/Al_2O_3 catalyst according to the results obtained by both H_2-chemisorption and XRD. Based on XRD, the dispersion is ranked in the order Pt < Ru < Re, while on H_2-chemisorption it increases in the order Re < Pt < Ru. For the Ru-promoted catalyst the H_2 dispersion doubled compared to the unpromoted catalyst, the same was observed for the catalyst promoted by Pt. All of this agrees with the theory that the addition of Ru, Re or Pt lead to increased cobalt dispersion on Co/Al_2O_3 catalysts.[50,51,9,47,52,57]

The catalyst $Co/Pt/Cl/Al_2O_3$ did not improve the dispersion in H_2-chemisorption. The presence of Cl changed the gas uptake and lowered the dispersion, due to Cl-blocking of sites.[74] The isotherm is as expected, and the result is confirmed by the XRD measurement, which gave a lower dispersion than the unpromoted catalyst. The promoter precursor $H_2PtCl_6 \cdot 6\,H_2O$, is therefore not ideal to use if a high degree of dispersion is desired. The catalyst $Co/Pt/Cl/Al_2O_3$ was therefore not further used in TPR and catalyst performance measurements.

The difference in dispersions measured by XRD and H_2-chemisorption can be due to several reasons. Cobalt is in its reduced state during H_2- chemisorption, while XRD measurements are performed on the oxidized state, hence perfect agreement is not expected. In addition, XRD does not exclude amorphous phases or other phases that can not be detected, e.g.due to low concentration or smaller particles than 5 nm.[99] Furthermore, some of the surface of the particle may not be available for adsorption from the gas phase, because it is oriented towards the support surface or incorporated in the support.

For the TiO_2-supported catalysts, the calculated dispersion is low, and show no large effect upon the addition of promoters. This is in good agreement with literature, and is mainly due to the weak metal-support interaction of TiO_2.[78,100] The TiO_2-supported catalysts consist of larger Co_3O_4 particles (30 nm), which are easily reduced. The effect of the addition of promoters is therefore low on TiO_2-supported catalysts. The XRD measurements of the TiO_2-supported catalysts agree well with the dispersions measured by H_2-chemisorption.

The Pawley method was used to determine the particle size based on the XRD results. All samples showed a R_{wp}-value lower than 5, and GOF close to 1. The slightly high GOF values can be explained by the background noice observed in all of the samples, due to the kapton foil, making the difference profile oscillating in the 2θ angles between 20 and 30. The observed, calculated, and difference profiles for all of the catalysts are given in Appendix E.3. An example is presented in Figure 4.9 of the catalyst Co/Al_2O_3. As seen from the figure, the difference profile oscillates in the 2θ angles between 20 and 30, due to the kapton foil. The small variations between the calculated and observed profiles should not affect the results to a large extent.

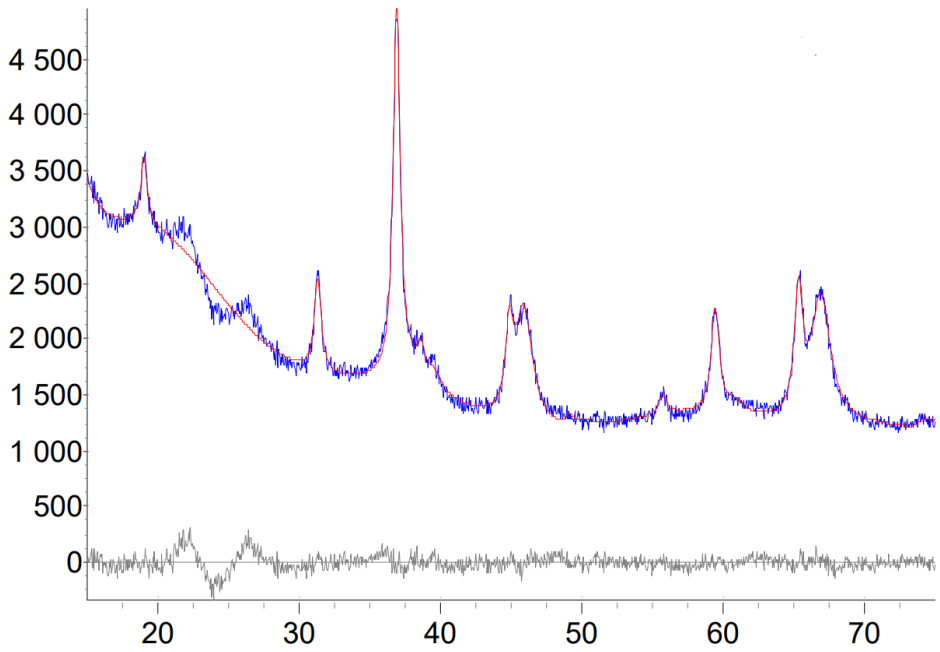

Figure 4.9: The observed (blue), calculated (red) and difference (grey) profiles for the unpromoted catalyst Co/Al_2O_3.

4.2 Catalyst Performance

Catalyst performance measurements were performed in a FTS setup for all of the prepared catalysts, except $Co/Pt/Cl/Al_2O_3$, due to blocking of its active sites by chloride. All of the results from the Fischer-Tropsch experiments are given in Appendix F and G, for the catalysts supported on Al_2O_3 and TiO_2, respectively.

4.2.1 Activity Measurements

The activity of the catalysts are reported as CO conversion, hydrogenation rate of CO (r_{CO}), and Site Time Yield (STY). The obtained results are given in Table 4.7. The calculation of STY can be found in Appendix C.

Table 4.7: CO Conversion, hydrogenation rate of CO (r_{CO}) and calculated STY after 23 hours ToS.

Sample	CO Conversion (%)	r_{CO} ($mol/g \cdot h$)	STY (s^{-1})
Co/Al_2O_3	6.3	0.0136	0.028
$Co/Re/Al_2O_3$	23.3	0.0504	0.057
$Co/Pt/Al_2O_3$	17.9	0.0387	0.039
$Co/Ru/Al_2O_3$	16.9	0.0365	0.036
Co/TiO_2	15.3	0.0165	0.048
$Co/Re/TiO_2$	20.3	0.0219	0.060
$Co/Pt/TiO_2$	18.4	0.0199	0.056
$Co/Ru/TiO_2$	11.5	0.0124	0.038

The CO conversion increased for all the promoted catalysts, except for $Co/Ru/TiO_2$. Most results found in the literature show that the addition of Ru, Re or Pt to Co/Al_2O_3 catalysts increases the dispersion and the reducibility of cobalt, which further leads to higher activities.[50,51,9,12] The CO conversion of Co/Al_2O_3 was much lower than expected. It may have happened something in the preparation or in the activity measurement of this catalyst. The promoter Re enhanced the CO-conversion and the hydrogenation rate to the most extent on both of the supports. This, despite that the DoR of $Co/Re/Al_2O_3$ was rather low, while the dispersion was as expected. Due to the high dispersion, a high activity is also expected. It is important to keep in mind that the reduction achieved through TPR is not comparable to the reduction in the activity measurements. In an activity measurement the temperatures are lower, and the gas is not diluted in an inert. This might cause less cobalt to be reduced in a TPR experiment than in a normal reduction in FTS. A better method of measuring DoR could have been to analyse, by TPR, the reduced sample after a normal reduction in the FT setup, in order to determine the amount of unreduced cobalt remaining in the sample.

The hydrogenation rate of CO increased when promoters were added to both Al_2O_3 and TiO_2 supported catalysts, except for $Co/Ru/TiO_2$, which decreased the hydrogenation rate. The increase was most pronounced for the catalysts supported on Al_2O_3, which is in good agreement with literature, which states that the hydrogenation rate increases

upon the promotion with Re, Pt and Ru on Co/Al_2O_3.[50,51,52] Co/TiO_2 catalysts were not studied to the same extent as Co/Al_2O_3 catalysts in the literature, and as so there are uncertainties regarding how a TiO_2 support affects the hydrogenation rate. However, cobalt dispersed on TiO_2 has a weak interaction with the support, meaning that cobalt forms larger particles which are easily reduced. The effect of the addition of promoters is therefore low on TiO_2[78], and it is therefore reasonable to assume that the hydrogenation rate should not increase to a large extent. In addition, the SMSI effect could have decorated the cobalt particles to some extent, giving a lower dispersion for the TiO_2-supported catalysts. The reduction does not occur at temperatures as high as 500 ^oC, however some part of the catalyst could still be decorated with a reducible oxide layer. The measured CO conversions on the TiO_2-supported catalysts range between 15 ± 5 %. Some of the difference may be due to uncertainties connected to the activity measurement. The low activity of $Co/Ru/TiO_2$ is maybe due to some of these mentioned factors, or because the promoter has a negative effect on the activity. If the promoter has a negative effect on the activity, this would be inconsistent with studies by Eschemann *et al.*[59] and Bertella *et al.*[61], who found that the activity increased upon Ru-addition.

Results from the literature indicate that the intrinsic activity (TOF and STY) remains constant upon addition of the promoters Ru, Re and Pt to Co/Al_2O_3 catalysts.[47,50,51,52] Studies concerning the impact of noble metal promotion on TOF and STY are predominately performed on catalysts supported on Al_2O_3. However, TOF/STY has been found to be independent of the support material and noble metals present in the catalyst,[63,64,18] given that the catalysts contain cobalt particles above a critical size of 6 nm. Smaller cobalt particles than 6 nm experience a sharp drop in the TOF.[59] The particle size of the catalysts supported on TiO_2 and Al_2O_3 was found through XRD to be around 30 nm, and 8 nm, respectively, and should therefore not be a problem.

All the catalysts had a STY inside the range of ± 0.015 s^{-1}. Due to intrinsic uncertainties in the data used for the calculations, the STY can be said to be constant, with a median value of 0.040 s^{-1} and 0.051 s^{-1} for the catalysts supported on Al_2O_3 and TiO_2, respectively. The range of uncertainty is allowed to be as high as it is due to accumulated uncertainties connected to the preparation, the cobalt loading, the reduction, the method used for dispersion measurements, and the activity measurements. The samples $Co/Re/Al_2O_3$ and Co/Al_2O_3 experienced a doubling of STY upon addition of Re, which is a significant difference. It may seem that Re has a greater effect since it showed higher activities on both supports, however the literature agree that the STY should not be affected upon Re-promotion.[47,50,52] Which argues that the difference is not linked to Re as a promoter, and rather is due to the various uncertainties. Since all the catalysts showed similar STY within the 0.015 s^{-1} range, under otherwise equal conditions, it can be concluded that the promoters have an effect, but only on the available cobalt-metal surface, i.e. the promoter acts on the geometry.

4.2.2 Selectivity Measurements

All the catalysts were tested in a FTS setup in order to measure their selectivites. The total selectivities of CH_4, C_2-C_4, CO_2 and C_{5+} were measured at equal CO conversions up to 50%. The results of these measurments are presented in Table 4.8. The catalyst $Co/Ru/TiO_2$ did not achieve a conversion greater than 40%, even after several small adjustments of GHSV. However, the low conversion should not affect the interpretation of the data significantly.

Table 4.8: Total selectivities of CH_4, C_2-C_4, CO_2 and C_{5+} after 70 hours ToS, and CO conversion at 47.2-52.4% (*CO-conversion at 39.8%).

Sample	Total selectivities (%)								
	CH_4	C_2=	C_2-	C_3=	C_3-	1-C_4=	n-C_4-	CO_2	C_{5+}
Co/Al_2O_3	7.65	0.10	0.90	2.79	1.09	2.29	1.42	0.58	83.01
$Co/Re/Al_2O_3$	7.98	0.08	0.68	2.30	0.90	2.08	1.37	0.33	84.07
$Co/Pt/Al_2O_3$	8.96	0.08	0.94	2.89	1.38	2.45	1.98	0.40	80.62
$Co/Ru/Al_2O_3$	9.74	0.08	0.81	2.56	1.13	2.33	1.72	0.35	81.04
Co/TiO_2	5.81	0.06	0.53	1.27	0.52	0.98	0.68	0.20	89.84
$Co/Re/TiO_2$	5.11	0.07	0.37	1.05	0.35	0.90	0.48	0.20	91.39
$Co/Pt/TiO_2$	5.49	0.06	0.42	0.97	0.41	0.79	0.55	0.54	90.68
$Co/Ru/TiO_2$*	8.16	0.07	0.47	1.23	0.66	1.25	1.03	0.26	86.75

The CO conversion and C_{5+}-selectivity as a function of ToS (h) is presented in Figure 4.10 for the catalysts supported on Al_2O_3, and in Figure 4.11 for the catalysts supported on TiO_2. There were problems adjusting to 50% conversion for the catalysts supported on TiO_2. The conversion reached steady state after 50 h ToS, the period between 24 to 50 h is therefore ignored.

CO_2-selectivities and WGS

There are two routes to CO_2 production in FTS, the first is the water-gas-shift (WGS) reaction, and the other route is CO disproportionation (Reaction 4.3).[106] The latter reaction leads to coke formation on the surface, i.e. deactivation. As seen from Figure 4.10 and 4.11, it does not seem like there are any particular deactivation. It is therefore, most likely, that the CO_2 produced originates from the WGS reaction in this case.

$$2\,CO \longrightarrow C_{surface} + CO_2 \tag{4.3}$$

WGS is often neglected in Co-based FTS catalysts because of its low extent. However, three of the catalysts tested exhibited slightly different WGS rates during FTS. The CO_2 selectivity remained nearly unchanged (0.2-0.3%) for the unpromoted Co/TiO_2, Re and Ru promoted catalysts. However, it was higher (0.4-0.6%) for the catalysts containing Pt promoters and the unpromoted Co/Al_2O_3 catalyst. Pt promoters have been reported to show slightly higher WGS activity, which may further contribute to higher CH_4-selectivity because of the additional H_2 available. For the Re and Ru promoters,

the metals themselves have been observed to have CO hydrogenation activity.[52,53] The Pt promoted catalysts showed a high selectivity of CH_4, but the highest measured CH_4-selectivity was on the catalysts promoted by Ru. On the other hand, the Ru promoted catalysts did not show such high selectivities for CO_2 like Pt did. The high selectivity for CH_4 for Co-Ru is therefore, most likely, not due to high CO_2-selectivities, i.e. WGS activity.

Since the changes in CO_2-selectivity were so small, it is not likely that it would affect the amount of hydrogen to a large extent. Additionally, there are also differences in conversion, which may affect the amount of hydrogen available. The methane selectivity can therefore be a function of other factors as well. The higher selectivity of CO_2 and CH_4 for Pt can suggest WGS activity, but the variations are so small that no conclusion can be drawn.

Selectivities of the promoted Co/Al_2O_3 catalysts

For the Al_2O_3-supported catalysts, the addition of Re increased the C_{5+}-selectivity, while the addition of Pt and Ru led to a decrease in C_{5+}. The selectivity of C_2 olefins ($C_{2=}$) was slightly higher for Co/Al_2O_3, but remained constant independent of the promoter used. For the C_2 paraffins (C_{2-}) and C_3 olefins, the selectivities decreased in the order Pt > unpromoted > Ru > Re, where Re had the lowest selectivity. The order changed slightly for C_{3-}, 1-$C_{4=}$ and n-C_{4-}, and decreased in the order Pt > Ru > unpromoted > Re. The CO_2-selectivity decreased in the order unpromoted > Pt > Ru > Re. As seen from the latter orders, Re showed the lowest selectivity to C_2-C_4, and CO_2, while Pt exhibited the highest selectivities to C_2-C_4.

The fact that Pt showed the lowest C_{5+}-selectivity is in good agreement with the studies from Jermwongratanachai *et al.*[53] and Ma *et al.*[52]. They found that the addition of Pt led to lower C_{5+}, and that CH_4 and CO_2 selectivities increased. This is partly in good agreement with the results, where the CH_4-selectivity increased, while the CO_2-selectivity decreased when Pt was added, compared to the unpromoted catalyst. The low C_{5+}-selectivity is more likely to be connected to the high production of C_3-C_4.

The addition of Re gave a higher C_{5+}-selectivity, which agreed well with the results obtained by Borg *et al.*[47] and Ma *et al.*[52]. Re obtained a high C_{5+}-selectivity at the expense of paraffins and olefins (C_2-C_4), and CO_2.

Promotion with Ru led to a decrease in the C_{5+}-selectivity. There is not much of a consensus on how Ru affects the C_{5+} production. Kogelbauer *et al.*[51] found that the C_{5+} remained constant when adding Ru, and Hosseini *et al.*[57] reported that the C_{5+} was not improved. Ma *et al.*[52] reported that the addition of Ru led to lower CH_4 and higher C_{5+} selectivities. The results are not in good agreement with the study by Ma *et al.*, the addition of Ru led to the highest measured CH_4 selectivity and the C_{5+} decreased, due to more production of C_{3-}, 1-$C_{4=}$ and n-C_{4-}. Ma *et al.* analysed their catalysts in a CSTR reactor, which has a slightly different reactor configuration than a fixed bed reactor. In addition, Kogelbauer *et al.* performed their measurements with a reaction pressure of 1 bar. This may explain some of the differences in the results.

Selectivities of the promoted Co/TiO_2 catalysts

The highest C_{5+}-selectivities were reported on the Co/TiO_2 catalysts. This is in good agreement with the studies by Oh *et al.*[46], who found that TiO_2-supported catalysts exhibit higher selectivities for long chain hydrocarbons (C_{5+}) compared to their counterparts on Al_2O_3. The fact that TiO_2 has a higher selectivity is explained by the pore size, since the same effect is observed in Al_2O_3 with very large pores (α-Al_2O_3).[47]

The promotion with Re and Pt led to a higher C_{5+}-selectivity, while Ru decreased the C_{5+}-selectivity. The highest measured selectivity of C_{5+} was reported for the promotion with Re, due to the higher selectivities of CO_2 for $Co/Pt/TiO_2$. The CO_2-selectivity was doubled when Pt was used as a promoter, indicating higher WGS activity. For the olefin and paraffin selectivities, similarly as Al_2O_3, the selectivity to $C_{2=}$ was low and remained constant upon promotion. Ru and the unpromoted catalyst showed the highest selectivities to C_2-C_4 hydrocarbons, where the unpromoted catalyst showed a slightly higher selectivity to C_{2-} and $C_{3=}$, while Ru showed a slightly higher selectivity to C_{3-}, 1-$C_{4=}$, and n-C_{4-}. Pt and Re showed the lowest selectivities to C_2-C_4 hydrocarbons, where Pt showed a slightly higher selectivity to paraffins than Re, while Re showed a slightly higher selectivity to olefins than Pt did.

Equally for the Re-addition to Co/Al_2O_3, the addition of Re to Co/TiO_2 resulted in a higher C_{5+}-selectivity. The obtained results agree well with the results obtained by Eschemann *et al.*[59] and Li *et al.*[62]. Re obtained a high C_{5+}-selectivity at the expense of C_2-C_4 paraffins.

Eschemann *et al.*[59], also studied the effect of Pt promotion and found that the C_{5+}-selectivity decreased, while Mehrbod *et al.*[60] reported slightly higher C_{5+}-selectivities with Pt. The addition of Pt led to a slight increase in C_{5+}-selectivity, which is in good agreement with Mehrbod *et al.*[60]. The main differences between the study by Eschemann *et al.*[59] and Mehrbod *et al.*[60]is that the cobalt loading was different (7-9wt% and 12 wt%, respectively), and the conversion levels, at which the selectivity measurements were done, was around 25-35% for Eschemann *et al.*[59], and 50% for Mehrbod *et al.*[60].

The Ru promotion of Co/TiO_2 resulted in a lower C_{5+} selectivity. Most of the mentioned studies[59,61,62] have reported an increase in C_{5+}, when Ru is added. However, Eschemann *et al.*[59] reported that the addition of 0.05wt% Ru (atomic ratio of 0.0035) led to lower C_{5+}, while an addition of 0.18 wt% (atomic ratio of 0.0140) gave higher C_{5+}. Here, the atomic ratio between cobalt and promoter was 0.01, it was therefore expected, based on the atomic ratio, that the C_{5+}-selectivity of $Co/Ru/TiO_2$ should have been higher. However the studies mentioned are different from this study due to *in situ* experiments (Bertella *et al.*), and low conversion levels (10 % for Bertella *et al.* and 25-35% for Eschemann *et al.*) for selectivity measurements. On the other hand, the catalyst $Co/Ru/TiO_2$ showed some similarities to the Ru-promoted Co/Al_2O_3 catalyst, both showed a low C_{5+}-selectivity and higher C_{3-}, n-$C_{4=}$ and n-C_{4-} selectivities. It should also be mentioned that the challenges with adjustment of conversion of $Co/Ru/TiO_2$ can have led to some degree of deactivation which influenced the results. However, from the Figure 4.11(b) it does not seem like any deactivation has occured, since the CO-conversion remains constant after the adjustments of GHSV.

One suggested interpretation, connected to the problems of adjusting the conversion to 50% for the catalysts supported on TiO_2, is that it is because of a positive kinetic effect

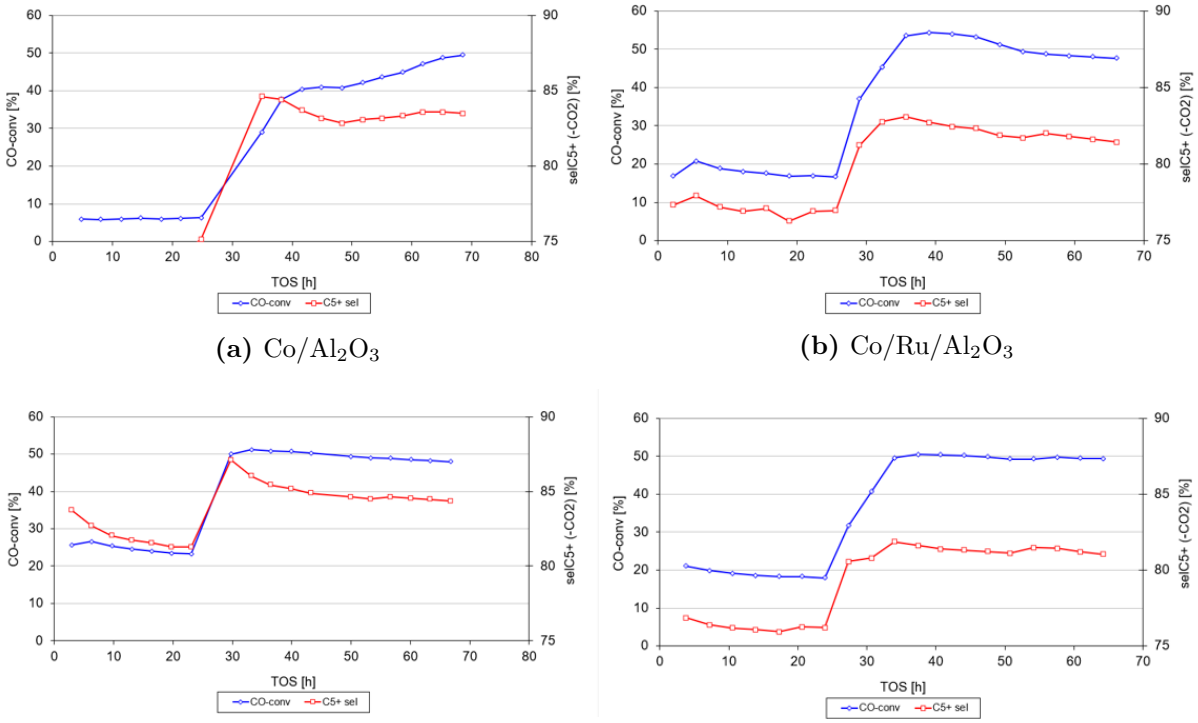

(a) Co/Al_2O_3 **(b)** $Co/Ru/Al_2O_3$

(c) $Co/Re/Al_2O_3$ **(d)** $Co/Pt/Al_2O_3$

Figure 4.10: CO conversion and C_{5+}-selectivity as a function of ToS (h) for the catalysts supported on Al_2O_3. Steady state is obtained at 40-70 h

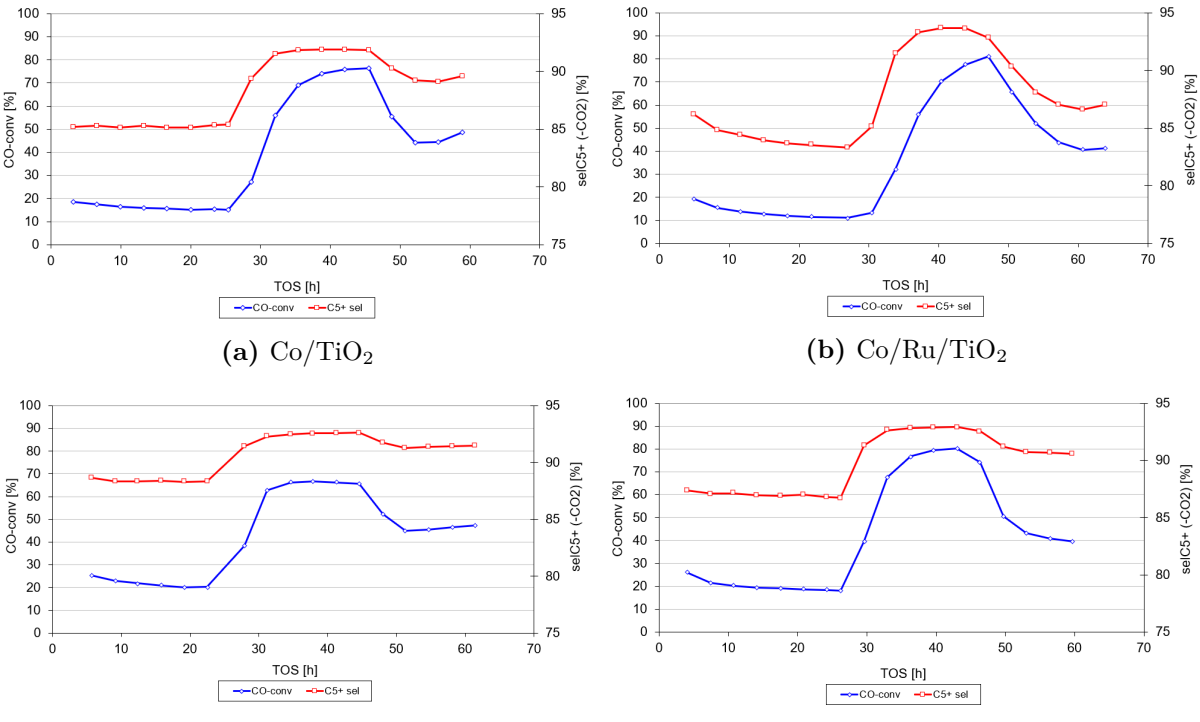

(a) Co/TiO_2 **(b)** $Co/Ru/TiO_2$

(c) $Co/Re/TiO_2$ **(d)** $Co/Pt/TiO_2$

Figure 4.11: CO conversion and C_{5+}-selectivity as a function of ToS (h) for the catalysts supported on TiO_2. Steady state is obtained at 50-60 h ToS.

of water associated with the wide pores of the TiO_2 support. The method used for adjusting the conversion is an experience-based method that is primarily used on traditional cobalt catalysts, which are mainly mesoporous. The method is based on an halvation of the GHSV, which leads to a doubled conversion. For all the catalysts supported on TiO_2, the conversion kept on increasing after reached 50% when halving the GHSV. Due to high conversions a lot of water is also produced, increasing the partial pressure of water.

Storsæter[100], studied the effect of water on FTS over supported cobalt catalysts. She reported that when water ($\sim$ 20%) is added, the partial pressure of water increases, and it shows a positive effect on the reaction rate and on deactivation. The positive kinetic effect of adding water was reversed when the water co-feeding stopped. The main part of deactivation took place during the second water period ($\sim$ 33% water) and appeared to be permanent.

Whether the reaction rate increases at higher partial pressures of water is much discussed in the literature.[18–27] There is a lot of disagreement about this, and it is therefore not certain whether this effect applies to all systems.

4.2.3 Olefin/Paraffin Ratios

The olefin/paraffin ratio for each catalyst is presented in Table 4.9. The olefin/paraffin ratios are quite similar for all the catalysts. However, the olefin/paraffin ratios (C_3 and C_4) decrease in the order Re $\sim$ unpromoted > Pt $\sim$ Ru for both the Al_2O_3-supported and the TiO_2-supported catalysts. Since the olefin/paraffin ratios for C_2 are small, there are more uncertainties connected to these ratios, it is therefore reasonable to assume that the C_2 ratios are quite similar for all the catalysts. Ma *et al.*[52], who studied Co/Al_2O_3 promoted catalysts, found that the olefin/paraffin ratios decreased in the order Re $\sim$ Ru $\sim$ unpromoted > Pt > Pd. In this experiment, $Co/Pt/Al_2O_3$ showed the lowest olefin/paraffin ratios, which agrees well with the results obtained by Ma *et al.*[52]. The olefin/paraffin ratio is first and foremost an indicator of how the catalyst behaves, i.e. how active it is to hydrogenate. The addition of Pt and Ru led to low olefin/paraffin ratios, which means that Pt and Ru contribute to hydrogenation. While, the Re promoted and the unpromoted catalysts, which showed higher olefin/paraffin ratios, are not equally active for hydrogenation.

Table 4.9: Olefin/paraffin ratios after 70 hours ToS and CO conversion at 47.2-52.4% (*CO-conversion at 39.8%).

Sample	Olefin/paraffin		
	$C_2{=}/C_2{-}$	$C_3{=}/C_3{-}$	$C_4{=}/C_4{-}$
Co/Al_2O_3	0.11	2.56	1.61
$Co/Re/Al_2O_3$	0.12	2.56	1.52
$Co/Pt/Al_2O_3$	0.09	2.09	1.24
$Co/Ru/Al_2O_3$	0.10	2.27	1.35
Co/TiO_2	0.11	2.44	1.44
$Co/Re/TiO_2$	0.19	3.00	1.88
$Co/Pt/TiO_2$	0.14	2.37	1.44
$Co/Ru/TiO_2$*	0.15	1.86	1.21

5 Conclusions and Future Work

5.1 Conclusions

In this work, the effect of different metal promoters on supported Co catalysts for the Fischer-Tropsch Synthesis (FTS) was investigated. The metal promoters studied were Ru, Pt and Re, on Co/Al_2O_3 and Co/TiO_2 catalysts. The atomic ratio between the promoter and cobalt was 0.01, and it was aimed for a cobalt loading of 20 wt%. The project involved catalyst preparation, characterization, and catalyst testing in a FTS setup. The characterization methods performed were X-Ray Fluorescence (XRF), X-Ray Diffraction (XRD), Temperature Programmed Reduction (TPR), N_2-physisorption, and H_2-chemisorption.

Nine different catalysts were successfully prepared by incipient wetness impregnation. There were two different Pt-promoted catalysts on Al_2O_3, prepared from the precursor $Pt(NH_3)_4(NO_3)_2$,and the other prepared from $H_2PtCl_6 \cdot 6\,H_2O$. The Pt-promoted catalyst containing chloride was not used in TPR and in the FTS setup, due to the observed blocking of active sites by chloride.

The XRF measurements showed that the Co concentrations were higher than the nominal values of 20 wt%. However, XRF also showed that the atomic relation between promoter and Co was approximately the same as the nominal value of 0.01. The XRD experiments confirmed that the observable phases in the catalysts supported on Al_2O_3 were γ-Al_2O_3 and Co_3O_4. For the catalysts supported on TiO_2 the observable phases were the anatase and rutile crystals of TiO_2, and Co_3O_4. The quantitative amount of each phase was not determined in the results.

Through TPR it was found that the temperature of reduction for both steps (Co_3O_4 to CoO and CoO to Co^0) downshifted to lower temperatures upon addition of Ru and Pt to Co/Al_2O_3 catalysts, however, only the second reduction step was significantly affected in the case of Re promotion. For the promoted Co/TiO_2 catalysts, promotion with Ru and Pt led to decreased temperatures of reduction, while Re did not affect the reduction temperature to a large extent. The results on both supports agrees well with the literature.

The degree of reduction (DoR) reflects the metal-support interaction between cobalt and the support, where Al_2O_3 showed the strongest interaction with cobalt. The addition of promoters to Co/Al_2O_3 enhanced the DoR to the most extent, while the effect of adding promoters to the TiO_2-supported catalysts was rather low. $Co/Re/Al_2O_3$ showed a lower DoR than expected, lower than the unpromoted catalyst on Al_2O_3. Most of the results in the literature indicate that the promotion with Re increases the DoR. Discrepancies in the results can be attributed to the adjustments of the instrument.

The ratio between the hydrogen consumption for the reduction of Co_3O_4 to CoO and the hydrogen consumption for reduction of CoO to Co^0, was found to be quite high compared to the ideal ratio of 1:3 for a perfect reduction. The high ratio indicates that the second reduction step (Co^{2+} to Co^0) was not completed, likely due to the formation of non-reducible cobalt-aluminates in the γ-Al_2O_3 spinel structure.

N_2-physisorption measurements showed that the Al_2O_3-supported catalysts had a large surface area (118 ± 3 m^2/g) with relatively small pores. The TiO_2-supported catalysts

showed a low surface area (20 ± 2 m^2/g) with both macro- and mesopores. The N_2-physisiorption is used for the calculation of pores with pore radius in the range of 1-30 nm, and hence, only the mesopores in the catalysts were observed. It was calculated that only 0.7% of the total pore volume in the catalyst was mesopores. It is therefore reasonable to assume that the pore distribution contains macropores in addition to the mesopores.

Dispersion was found both by H_2-chemisorption experiments and by calculating it based on the particle size obtained from XRD. All of the promoted catalysts supported on Al_2O_3, except $Co/Pt/Cl/Al_2O_3$, gave a higher dispersion than the unpromoted Co/Al_2O_3 catalyst. This is in good agreement with the literature. For the TiO_2-supported catalysts, the calculated dispersion was low, and showed no significant change upon the addition of promoters. This is also in good agreement with literature, and is mainly due to the weak metal-support interaction of TiO_2.

The high cobalt dispersions for the promoted Al_2O_3-supported catalysts resulted in higher hydrogenation rates of CO, while the STY remained constant, which is in good agreement with the literature. For the catalysts supported on TiO_2 the hydrogenation rate of CO was not affected in the same way, as those on Al_2O_3. However, the Pt and Re promoted Co/TiO_2 catalysts showed slightly higher hydrogenation rates than the unpromoted, while $Co/Ru/TiO_2$ decreased the hydrogenation rate. Co/TiO_2 catalysts are not studied to the same extent as Co/Al_2O_3 catalysts in the literature, and as so there are uncertainties regarding how a TiO_2 support affects the hydrogenation rate. However, based on the measured dispersion it was not expected that the activity would be significantly affected upon the addition of promoters. The STY of the TiO_2-supported catalysts also remained constant when adding promoters. Since all the catalysts showed similar STY within the 0.015 s^{-1} range, under otherwise equal conditions, it could be concluded that the promoters had an effect, but only on the available cobalt-metal surface, i.e. the promoter acted on the geometry.

For the Al_2O_3-supported catalysts, the addition of Re increased the C_{5+}-selectivity, while the addition of Pt and Ru led to a decrease in C_{5+}. The results for Re and Pt promotion agreed well with the literature, while the effect of Ru is debated in literature. The highest C_{5+}-selectivities were reported on the Co/TiO_2 catalysts. This was in good agreement with the literature, which explained the high selectivity by the pore size, since the same effect is observed in Al_2O_3 with very large pores (α-Al_2O_3). For the TiO_2-supported catalysts, the promotion with Re and Pt led to a higher C_{5+}-selectivity, while Ru decreased the C_{5+}-selectivity. The results for Re agreed well with the literature. However, the effect of Ru and Pt promotion on TiO_2-supported Co catalysts has seen varying results in published studies and is a topic of debate. The higher selectivity of CO_2 and CH_4 for Pt could suggest WGS activity, but the variations were so small that no conclusion can be drawn.

The addition of Pt and Ru led to low olefin/paraffin ratios, meaning that Pt and Ru contributed to hydrogenation. While, the Re promoted and the unpromoted catalysts, which showed higher olefin/paraffin ratios, were not equally active for hydrogenation.

5.2 Suggestions for Future Work

The background for this work was to obtain experimental data on the effect of metal promoters in Co-based FTS, in order to compare it to Density Functional Theory (DFT) calculations. DFT investigations will further contribute to precisely explain the promotional effect that Re, Ru and Pt imposes on Co.

Other suggested future work is to make promoted cobalt catalysts with other supports like silica, carbonmaterials or α-Al_2O_3, in order to see if the support have an effect on the promotion. Furthermore, mercury intrusion measurements would have given a more realistic picture of the pore size distribution of the TiO_2-supported catalysts, as mercury intrusion is used for calculation of pores with pore radius in the range 5 nm-55 µm.

Additional characterization techniques that could be interesting to perform is Transmission Electron Microscopy (TEM), Steady-State Isotopic Transient Kinetic Analysis (SSITKA) and X-ray Photoelectron Spectroscopy (XPS). TEM would give useful information about the surface of the catalyst and how it looks like. XPS and SSITKA would provide a detailed study on the way in which the promoter affects the residence time on the surface and the composition.

References

[1] F. Pardo-Tarifa, S. Cabrera, M. Sanchez-Dominguez, and M. Boutonnet. Ce-promoted Co/Al_2O_3 catalysts for Fischer–Tropsch synthesis. *International journal of hydrogen energy*, 42(15):9754–9765, 2017.

[2] H. Jahangiri, J. Bennett, P. Mahjoubi, K. Wilson, and S. Gu. A review of advanced catalyst development for Fischer-Tropsch synthesis of hydrocarbons from biomass derived syn-gas. *Catalysis science & technology*, 4(8):221–2229, 2014.

[3] R. Rauch, A. Kiennemann, and A. Sauciuc. *The Role of Catalysis for the Sustainable Production of Bio-fuels and Bio-chemicals*. Elsevier, Amsterdam, 2013.

[4] R. Luque, A.R. de la Osa, J.M. Campelo, A.A. Romero, J.L. Valverde, and P. Sanchez. Design and development of catalysts for Biomass-To-Liquid-Fischer–Tropsch (BTL-FT) processes for biofuels production. *Energy Environ. Sci.*, 5:5186–5202, 2012.

[5] D. Leckel. Diesel production from Fischer-Tropsch: The Past, the Present, and New Concepts. *Energy & Fuels*, 23(5):2342–2358, 2009.

[6] M. Marchese, G. Buffo, M. Santarelli, and A. Lanzini. CO_2 from direct air capture as carbon feedstock for Fischer-Tropsch chemicals and fuels: Energy and economic analysis. *Journal of CO_2 Utilization*, 46:101487, 2021.

[7] Carbonengineering. Air to fuels. http://carbonengineering.com/, 2021. [Online; accessed May 21, 2021].

[8] J. Barrientos, V. Garcilaso, B. Venezia, A. Aho, J.A. Odriozola, M. Boutonnet, and S. Järås. Fischer–Tropsch Synthesis Over Zr-Promoted Co/γ-Al_2O_3 Catalysts. *Topics in Catalysis*, 60(17):1285–1298, 2017.

[9] D. Schanke, S. Vada, E.A. Blekkan, A-M Hilmen, A. Hoff, and A. Holmen. Study of Pt-Promoted Cobalt CO Hydrogenation Catalysts. *Journal of catalysis*, 156(1):85–95, 1995.

[10] J.L. Casci, C.M. Lok, and M.D. Shannon. Fischer–Tropsch catalysis: The basis for an emerging industry with origins in the early 20th Century. *Catalysis today*, 145(1):38–44, 2009.

[11] S.S. Ail and S. Dasappa. Biomass to liquid transportation fuel via Fischer Tropsch synthesis – Technology review and current scenario. *Renewable & sustainable energy reviews*, 58:267–286, 2016.

[12] F. Morales and B.M. Weckhuysen. Promotion Effects in Co-based Fischer–Tropsch Catalysis. In *Catalysis*, volume 19, pages 1–40. The Royal Society of Chemistry, 2006.

[13] E. Ø. Pedersen. *Mn promotion effects in Co based Fischer-Tropsch production of light olefins*, volume 2018:180 of *Doctoral theses at NTNU*. Norwegian University of Science and Technology, Faculty of Natural Sciences and Technology, Department of Chemical Engineering, Trondheim, 2018.

[14] Ø. Borg. *Role of alumina support in cobalt Fischer-Tropsch synthesis*, volume 2007:56 of *Doctoral theses at NTNU*. Norwegian University of Science and Technology, Faculty of Natural Sciences and Technology, Department of Chemical Engineering, Trondheim, 2007.

[15] J.T. Kummer, H.H. Podgurski, W.B. Spencer, and P.H. Emmett. Mechanism Studies of the Fischer—Tropsch Synthesis.The Addition of Radioactive Alcohol. *Journal of the American Chemical Society*, 73(2):564–569, 1951.

[16] J.T. Kummer and P.H. Emmett. Fischer-Tropsch Synthesis Mechanism Studies. The Addition of Radioactive Alcohols to the Synthesis Gas. *Journal of the American Chemical Society*, 75:5177–5183, 1953.

[17] K. Keyvanloo, S.J. Lanham, and W.C. Hecker. Kinetics of Fischer-Tropsch synthesis on supported cobalt: Effect of temperature on CO and H_2 partial pressure dependencies. *Catalysis today*, 270:9–18, 2016.

[18] E. Iglesia. Design, synthesis, and use of cobalt-based Fischer-Tropsch synthesis catalysts. *Applied Catalysis A: General*, 161(1):59–78, 1997.

[19] T.K. Das, X. Zhan, J. Li, G. Jacobs, M.E. Dry, and B.H. Davis. Fischer-Tropsch Synthesis: Kinetics and Effect of Water for a Co/Al_2O_3 Catalyst. In B.H. Davis and M.L. Occelli, editors, *Fischer-Tropsch Synthesis, Catalyst and Catalysis*, volume 163 of *Studies in Surface Science and Catalysis*, pages 289–314. Elsevier, 2007.

[20] E. van Steen and H. Schulz. Polymerisation kinetics of the Fischer–Tropsch CO hydrogenation using iron and cobalt based catalysts. *Applied Catalysis A: General*, 186(1):309–320, 1999.

[21] W. Ma, G. Jacobs, D.E. Sparks, M.K. Gnanamani, V.R.R. Pendyala, C.H. Yen, J.L.S. Klettlinger, T.M. Tomsik, and B.H. Davis. Fischer–Tropsch synthesis: Support and cobalt cluster size effects on kinetics over Co/Al_2O_3 and Co/SiO_2 catalysts. *Fuel*, 90(2):756–765, 2011.

[22] G. Botes. Influences of Water and Syngas Partial Pressure on the Kinetics of a Commercial Alumina-Supported Cobalt Fischer-Tropsch Catalyst. *Industrial & engineering chemistry research*, 48(4):1859–1865, 2009.

[23] R. Zennaro, M. Tagliabue, and C.H. Bartholomew. Kinetics of Fischer–Tropsch synthesis on titania-supported cobalt. *Catalysis Today*, 58(4):309–319, 2000.

[24] B. Sarup and B.W. Wojciechowski. Studies of the Fischer-Tropsch synthesis on a cobalt catalyst II. Kinetics of carbon monoxide conversion to methane and to higher hydrocarbons. *The Canadian Journal of Chemical Engineering*, 67(1):62–74, 1989.

[25] B.W. Wojciechowski. The kinetics of the Fischer-Tropsch Synthesis. *Catalysis Reviews*, 30(4):629–702, 1988.

[26] I.C. Yates and C.N. Satterfield. Intrinsic kinetics of the Fischer-Tropsch synthesis on a cobalt catalyst. *Energy & Fuels*, 5(1):168–173, 1991.

[27] A. Outi, I. Rautavuoma, and H.S. van der Baan. Kinetics and mechanism of the fischer tropsch hydrocarbon synthesis on a cobalt on alumina catalyst. *Applied Catalysis*, 1(5):247–272, 1981.

[28] W. Ma, G. Jacobs, D.E. Sparks, R.L. Spicer, B.H. Davis, J.L.S. Klettlinger, and C.H. Yen. Fischer-Tropsch synthesis: Kinetics and water effect study over 25%Co/Al_2O_3 catalysts. *Catalysis today*, 228:158–166, 2014.

[29] M.E. Dry. Chapter 3 - Chemical concepts used for engineering purposes. In A. Steynberg and M.E. Dry, editors, *Fischer-Tropsch Technology*, volume 152 of *Studies in Surface Science and Catalysis*, pages 196 – 257. Elsevier, 2004.

[30] R.W. Dorner, D.R. Hardy, F.W. Williams, and H.D. Willauer. Heterogeneous catalytic CO_2 conversion to value-added hydrocarbons. *Energy Environ. Sci.*, 3:884–890, 2010.

[31] M.J. Overett, R.O. Hill, and J.R. Moss. Organometallic chemistry and surface science: mechanistic models for the Fischer–Tropsch synthesis. *Coordination Chemistry Reviews*, 206-207:581 – 605, 2000.

[32] J.S. Albuquerque, F.O. Costa, and B.V.S. Barbosa. Fischer–Tropsch Synthesis: Analysis of Products by Anderson–Schulz–Flory Distribution Using Promoted Cobalt Catalyst. *Catalysis letters*, 149(3):831–839, 2019.

[33] I. Chorkendorff and J. W. Niemantsverdriet. *Concepts of Modern Catalysis and Kinetics*. Wiley-VCH, Weinheim Germany, 2003.

[34] H. Schulz. Short history and present trends of Fischer–Tropsch synthesis. *Applied Catalysis A: General*, 186(1):3 – 12, 1999.

[35] N.E. Tsakoumis, M. Rønning, Ø. Borg, E. Rytter, and A. Holmen. Deactivation of cobalt based Fischer–Tropsch catalysts: A review. *Catalysis today*, 154(3):162–182, 2010.

[36] M.L. Davis, B.H.and Occelli. *Fischer-Tropsch synthesis, catalysts, and catalysis : advances and applications*, volume 142 of *Chemical industries*. CRC Press, Boca Raton, 2016.

[37] R. Munirathinam, D. Pham Minh, and A. Nzihou. Effect of the Support and Its Surface Modifications in Cobalt-Based Fischer–Tropsch Synthesis. *Industrial & engineering chemistry research*, 57(48):16137–16161, 2018.

[38] A.Y. Khodakov, V.L. Zholobenko, R. Bechara, and D. Durand. Impact of aqueous impregnation on the long-range ordering and mesoporous structure of cobalt containing MCM-41 and SBA-15 materials. *Microporous and mesoporous materials*, 79(1):29–39, 2005.

[39] J.H. Den Otter and K.P. De Jong. Highly Selective and Active Niobia-Supported Cobalt Catalysts for Fischer-Tropsch Synthesis. *Topics in catalysis*, 57(6-9):445–450, 2014.

[40] D.I. Enache, M. Roy-Auberger, and R. Revel. Differences in the Characteristics and Catalytic Properties of Cobalt-Based Fischer–Tropsch Catalysts Supported on Zirconia and Alumina. *Applied catalysis. A, General*, 268(1):51–60, 2004.

[41] L. Spadaro, F. Arena, M.L. Granados, M. Ojeda, J.L.G. Fierro, and F. Frusteri. Metal-support interactions and reactivity of Co/CeO_2 catalysts in the Fischer-Tropsch synthesis reaction. *Journal of catalysis*, 234(2):451–462, 2005.

[42] M. Lacroix, L. Dreibine, B. de Tymowski, F. Vigneron, D. Edouard, D. Bégin, P. Nguyen, C. Pham, S. Savin-Poncet, F. Luck, M-J Ledoux, and C. Pham-Huu. Silicon carbide foam composite containing cobalt as a highly selective and re-usable Fischer–Tropsch synthesis catalyst. *Applied catalysis. A, General*, 397(1):62–72, 2011.

[43] S. Bessell. Investigation of Bifunctional Zeolite Supported Cobalt Fischer-Tropsch Catalysts. *Applied catalysis. A, General*, 126(2):235–244, 1995.

[44] S.D. Mo and W.Y. Ching. Electronic and optical properties of three phases of titanium dioxide: Rutile, anatase, and brookite. *Physical review. B, Condensed matter*, 51(19):13023–13032, 1995.

[45] C. Byrne, L. Moran, D. Hermosilla, N. Merayo, Á. Blanco, S. Rhatigan, S. Hinder, P. Ganguly, M. Nolan, and S.C. Pillai. Effect of Cu doping on the anatase-to-rutile phase transition in TiO_2 photocatalysts: Theory and experiments. *Applied Catalysis B: Environmental*, 246:266–276, 2019.

[46] J-H Oh, J.W. Bae, S-J Park, P.K. Khanna, and K-W Jun. Slurry-Phase Fischer–Tropsch Synthesis Using $Co/\gamma\text{-}Al_2O_3$, Co/SiO_2 and Co/TiO_2: Effect of Support on Catalyst Aggregation. *Catalysis letters*, 130(3-4):403–409, 2009.

[47] Ø. Borg, N. Hammer, S. Eri, O.A. Lindvåg, R. Myrstad, E.A. Blekkan, M. Rønning, E. Rytter, and A. Holmen. Fischer-Tropsch synthesis over un-promoted and Re-promoted $\gamma\text{-}Al_2O_3$ supported cobalt catalysts with different pore sizes. *Catalysis today*, 142(1-2):70–77, 2009.

[48] S. Lamouri, M. Hamidouche, N. Bouaouadja, H. Belhouchet, V. Garnier, G. Fantozzi, and J.F. Trelkat. Control of the γ-alumina to α-alumina phase transformation for an optimized alumina densification. *Boletín de la Sociedad Española de Cerámica y Vidrio*, 56(2):47–54, 2017.

[49] H. Romar, E. Rivoire, P. Tynjälä, and U. Lassi. Effect of Calcination Conditions on the Dispersion of Cobalt over Re, Ru and Rh Promoted $Co/\gamma\text{-}Al_2O_3$ Catalysts. *Topics in catalysis*, 60(17):1408–1414, 2017.

[50] S. Vada, A. Hoff, E. Ådnanes, D. Schanke, and A. Holmen. Fischer-Tropsch synthesis on supported cobalt catalysts promoted by platinum and rhenium. *Topics in catalysis*, 2(1-4):155–162, 1995.

[51] A. Kogelbauer, J.G. Goodwin Jr, and R. Oukaci. Ruthenium promotion of Co/Al_2O_3 Fischer-Tropsch catalysts. *Journal of catalysis*, 160(1):125–133, 1996.

[52] W. Ma, G. Jacobs, R.A. Keogh, D.B. Bukur, and B.H. Davis. Fischer–Tropsch synthesis: Effect of Pd, Pt, Re, and Ru noble metal promoters on the activity and selectivity of a 25%Co/Al_2O_3 catalyst. *Applied catalysis. A, General*, 437-438:1–9, 2012.

[53] T. Jermwongratanachai, G. Jacobs, W. Ma, W. D. Shafer, M.K. Gnanamani, P. Gao, B. Kitiyanan, B.H. Davis, J.L.S. Klettlinger, C.H. Yen, D.C. Cronauer, A.J. Kropf, and C.L. Marshall. Fischer-Tropsch synthesis: Comparisons between Pt and Ag promoted Co/Al_2O_3 catalysts for reducibility, local atomic structure, catalytic activity, and oxidation–reduction (OR) cycles. *Applied Catalysis A: General*, 464-465:165–180, 2013.

[54] A. Voronov, N.E. Tsakoumis, N. Hammer, W. van Beek, H. Emerich, and M. Rønning. The state and location of Re in Co–Re/Al_2O_3 catalysts during Fischer–Tropsch synthesis: Exploring high-energy XAFS for *in situ* catalysts characterisation. *Catalysis Today*, 229:23–33, 2014.

[55] A.V. Ruban, H.L. Skriver, and J.K. Nørskov. Surface segregation energies in transition-metal alloys. *Phys. Rev. B*, 59:15990–16000, 1999.

[56] J-I Yang and C.H. Ko. Effect of cobalt metal loading on Fischer–Tropsch synthesis activities over Co/γ-Al_2O_3 catalysts: CO conversion, C_{5+} productivity, and α value. *Research on chemical intermediates*, 45(9):4417–4429, 2019.

[57] S.A. Hosseini, A. Taeb, F. Feyzi, and F. Yaripour. Fischer–Tropsch synthesis over Ru promoted Co/γ-Al_2O_3 catalysts in a CSTR. *Catalysis communications*, 5(3):137–143, 2004.

[58] G. Jacobs, J.A. Chaney, P.M. Patterson, T.K. Das, and B.H. Davis. Fischer–Tropsch synthesis: study of the promotion of Re on the reduction property of Co/Al_2O_3 catalysts by in situ EXAFS/XANES of Co K and Re LIII edges and XPS. *Applied Catalysis A: General*, 264(2):203–212, 2004.

[59] T.O. Eschemann, J. Oenema, and K.P. de Jong. Effects of noble metal promotion for Co/TiO_2 Fischer-Tropsch catalysts. *Catalysis today*, 261:60–66, 2016.

[60] M. Mehrbod, M. Martinelli, A.G. Martino, D.C. Cronauer, A. Jeremy Kropf, C.L. Marshall, and G. Jacobs. Fischer-Tropsch synthesis: Direct cobalt nitrate reduction of promoted Co/TiO_2 catalysts. *Fuel*, 245:488–504, 2019.

[61] F. Bertella, C.W. Lopes, A.C. Foucher, G. Agostini, P. Concepcion, E.A. Stach, and A. Martinez. Insights into the Promotion with Ru of Co/TiO_2 Fischer–Tropsch Catalysts: An *in situ* Spectroscopic Study. *ACS catalysis*, 10(11):6042–6057, 2020.

[62] J.L. Li, G. Jacobs, Y.Q. Zhang, T.K. Das, and B.H. Davis. Fischer-Tropsch synthesis: effect of small amounts of boron, ruthenium and rhenium on Co/TiO_2 catalysts. *Applied catalysis. A, General*, 223(1-2):195–203, 2002.

[63] F. Diehl and A.Y. Khodakov. Promotion of Cobalt Fischer-Tropsch Catalysts with Noble Metals: a Review. *Oil & gas science and technology*, 64(1):11–24, 2009.

[64] G. Jacobs, T.K. Das, Y. Zhang, J. Li, G. Racoillet, and B.H. Davis. Fischer–Tropsch synthesis: support, loading, and promoter effects on the reducibility of cobalt catalysts. *Applied Catalysis A: General*, 233(1):263–281, 2002.

[65] E. van Steen and M. Claeys. Fischer-Tropsch Catalysts for the Biomass-to-Liquid (BTL)-Process. *Chemical Engineering & Technology*, 31(5):655–666, 2008.

[66] C.N. Hamelinck, A.P.C. Faaij, H. den Uil, and H. Boerrigter. Production of FT transportation fuels from biomass; technical options, process analysis and optimisation, and development potential. *Energy*, 29(11):1743 – 1771, 2004.

[67] C.H. Bartholomew. Mechanisms of catalyst deactivation. *Applied Catalysis A: General*, 212(1):17 – 60, 2001.

[68] G. Jacobs, P.M. Patterson, Y. Zhang, T.K. Das, J. Li, and B.H. Davis. Fischer–Tropsch synthesis: deactivation of noble metal-promoted Co/Al_2O_3 catalysts. *Applied Catalysis A: General*, 233(1):215–226, 2002.

[69] M.A. Vannice and W.H. Joyce. *Kinetics of Catalytic Reactions*. Springer, Boston, 2005.

[70] A. Satyanaga, H. Rahardjo, E.C. Leong, and J.Y. Wang. Water characteristic curve of soil with bimodal grain-size distribution. *Computers and Geotechnics*, 48:51–61, 2013.

[71] M. Thommes, K. Kaneko, A.V. Neimark, J.P. Olivier, F. Rodriguez-Reinoso, J. Rouquerol, and K.S.W. Sing. Physisorption of gases, with special reference to the evaluation of surface area and pore size distribution (IUPAC Technical Report). *Pure and Applied Chemistry*, 87(9-10):1051–1069, 2015.

[72] A. Holmen. Heterogen katalyse. Institutt for kjemisk prosessteknologi, NTNU, 2002.

[73] S.L. Soled, A. Malek, S. Miseo, J. Baumgartner, C. Kliewer, M. Afeworki, and P.A. Stevens. *Scientific Bases for the Preparation of Heterogeneous Catalysts*, volume 162 of *Studies in Surface Science and Catalysis*, pages 103–110. Elsevier, 2006.

[74] G. Bergeret and P. Gallezot. *Particle Size and Dispersion Measurements*. In Handbook of Heterogeneous Catalysis (eds G. Ertl, H. Knözinger, F. Schüth and J. Weitkamp). 2008.

[75] S.J. Tauster, S.C. Fung, and R.L. Garten. Strong metal-support interactions. Group 8 noble metals supported on titanium dioxide. *Journal of the American Chemical Society*, 100(1):170–175, 1978.

[76] P. Wu, S. Tan, J. Moon, Z. Yan, V. Fung, N. Li, S. Yang, Y. Cheng, C.W. Abney, Z. Wu, A. Savara, A.M. Momen, D. Jiang, D. Su, H. Li, W. Zhu, S. Dai, and H. Zhu. Harnessing strong metal–support interactions via a reverse route. *Nature communications*, 11(1):3042–3042, 2020.

[77] V.P. O'Shea, M.C.Á. Galván, A.P. Prats, J. M. Campos-Martin, and J.L.G. Fierro. Direct evidence of the SMSI decoration effect: the case of Co/TiO_2 catalyst. *Chemical communications (Cambridge, England)*, 47(25):7131–7133, 2011.

[78] S. Lögdberg, J. Yang, M. Lualdi, J.C. Walmsley, S. Järås, M. Boutonnet, E.A Blekkan, E. Rytter, and A. Holmen. Further insights into methane and higher hydrocarbons formation over cobalt-based catalysts with γ-Al_2O_3, α-Al_2O_3 and TiO_2 as support materials. *Journal of catalysis*, 352:515–531, 2017.

[79] C. Ledesma. XRF Procedure. Department of Chemical Engineering at NTNU. 2015.

[80] Horiba. What is X-ray Fluorescence Spectroscopy. https://www.horiba.com/en_en/x-ray-fluorescence-spectroscopy-xrf/. [Online; accessed March 18, 2021].

[81] Thermo Fisher Scientific – Handheld Elemental & Radiation Detection. Energy Dispersive X-Ray Fluorescence, EDXRF, for Material Analysis and Sample Identification Using Niton Handheld XRF Analysers. https://www.azom.com/article.aspx?ArticleID=5251, 2010. [Online;accessed March 18, 2021].

[82] P. Brouwer. Theory of XRF. *Almelo, Netherlands: PANalytical BV*, 2006.

[83] I. Campbell D. Coler, L. Bruzenak. The Common Sources of Error in Sample Preparation for XRF Analysis and the Capabilities of Standalone Automation. (FLSmidth). Bethlehem , PA, USA. https://cdn2.hubspot.net/hubfs/494827/AAACaseStoryPDF/Common_sources_of_error_in_sample_preparation_for_XRF_Analysis_and_the_Capabilities_of_Standalone_Automation.pdf , [Online;accessed March 18, 2021].

[84] A. Gervasini. *Calorimetry and Thermal Methods in Catalysis*. Springer Berlin Heidelberg, Berlin, Heidelberg, 2013.

[85] A. Mekki-Berrada and A. Auroux. *Characterization of Solid Materials and Heterogeneous Catalysts*, pages 747–852. Wiley-VCH Verlag GmbH & Co. KGaA, Weinheim, Germany, 2012.

[86] G. Bergeret. Structure and Morphology. In Handbook of Heterogeneous Catalysis (eds G. Ertl, H. Knözinger, F. Schüth and J. Weitkamp). 2008.

[87] A. Paar. X-Ray Diffraction (XRD). https://wiki.anton-paar.com/en/x-ray-diffraction-xrd/, 2013. [Online; accessed March 11, 2021].

[88] G.S. Pawley. Unit-cell refinement from powder diffraction scans. *Journal of applied crystallography*, 14(6):357–361, 1981.

[89] G.V.P. Bhagath Singh and K.V.L. Subramaniam. Direct decomposition X-ray diffraction method for amorphous phase quantification and glassy phase determination in binary blends of siliceous fly ash and hydrated cement. *Journal of Sustainable Cement-Based Materials*, 6(2):111–125, 2017.

[90] L.B. McCusker, R.B. Von Dreele, D.E. Cox, D. Louër, and P. Scardi. Rietveld refinement guidelines. *Journal of applied crystallography*, 32(1):36–50, 1999.

[91] M. Boudart. Turnover Rates in Heterogeneous Catalysis. *Chemical reviews*, 95(3):661–666, 1995.

[92] M. Boudart. Principles of Heterogeneous Catalysis. In Handbook of Heterogeneous Catalysis (eds G. Ertl, H. Knözinger, F. Schüth and J. Weitkamp). 2008.

[93] A-M Hilmen, O.A. Lindvåg, E. Bergene, D. Schanke, S. Eri, and A. Holmen. Selectivity and activity changes upon water addition during Fischer-Tropsch synthesis. In *Natural Gas Conversion VI*, volume 136 of *Studies in Surface Science and Catalysis*, pages 295–300. Elsevier, 2001.

[94] A-M Hilmen, E. Bergene, O.A. Lindvåg, D. Schanke, S. Eri, and A. Holmen. *Fischer-Tropsch synthesis using monolithic catalysts*, volume 130 of *12th International Congress on Catalysis, Proceedings of the 12th ICC*. Elsevier„ [Amsterdam ; New York] :, 2000.

[95] ICDD. PDF-4+2010 (database). International Centre for Diffraction Data, Newtown Square, PA, USA, 2010.

[96] Bruker AXS. TOPAS V4: General profile and structure analysis software for powder diffraction data, 2008.

[97] N.E. Tsakoumis, J.C. Walmsley, M. Rønning, W. van Beek, E. Rytter, and A. Holmen. Evaluation of Reoxidation Thresholds for γ-Al_2O_3-Supported Cobalt Catalysts under Fischer–Tropsch Synthesis Conditions. *Journal of the American Chemical Society*, 139(10):3706–3715, 2017.

[98] R. Myrstad. Rigg: Apparatur og prosedyrer for 4-reaktors fixed bed rigg, 2009.

[99] J. Niemantsverdriet. *Spectroscopy in Catalysis: An introduction*. John Wiley & Sons, Ltd, 2000.

[100] S. Storsæter. *Fischer-Tropsch synthesis over cobalt supported catalysts*, volume 2005:134 of *Doctoral theses at NTNU*. Norwegian University of Science and Technology, Faculty of Natural Sciences and Technology, Department of Chemical Engineering, Trondheim, 2005.

[101] A-M Hilmen. *Reduction and reoxidation of cobalt Fischer-Tropsch catalysts*, volume 1996:66 of *Doctoral theses at NTNU*. Norwegian University of Science and Technology, Faculty of Natural Sciences and Technology, Department of Industrial Chemistry, Trondheim, 1996.

[102] G.R. Fredriksen. *Hydrogenation of CO on supported cobalt catalysts studied by in situ FTIR spectroscopy*, volume 1993:113 of *Doktor ingeniøravhandling*. Universitetet i Trondheim, Norges tekniske høgskole, Institutt for industriell kjemi, Trondheim, 1993.

[103] G. Jacobs, W. Ma, and B.H. Davis. Influence of Reduction Promoters on Stability of Cobalt/g-Alumina Fischer-Tropsch Synthesis Catalysts. *Catalysts*, 4(1):49–76, 2014.

[104] J-S Jung, J-S Lee, G. Choi, S. Ramesh, and D.J. Moon. The characterization of micro-structure of cobalt on γ-Al_2O_3 for FTS: Effects of pretreatment on Ru–Co/γ-Al_2O_3. *Fuel*, 149:118–129, 2015.

[105] A. Blackman. *Aylward and Findlay's SI Chemical Data.* John Wiley & Sons, Milton, 7th ed. edition, 2014.

[106] C. Cabet, A.C. Roger, A. Kiennemann, S. Läkamp, and G. Pourroy. Synthesis of New Fe-Co Based Metal/Oxide Composite Materials: Application to the Fischer–Tropsch Synthesis. *Journal of Catalysis*, 173(1):64–73, 1998.

Trondheim, June 13, 2021

A Catalyst Synthesis Calculations

A.1 Mass Calculations

In this project it was produced 9 different samples; Co/Al_2O_3, $Co/Re/Al_2O_3$, $Co/Ru/Al_2O_3$, $Co/Pt/Cl/Al_2O_3$, $Co/Pt/Al_2O_3$, Co/TiO_2, $Co/Re/TiO_2$, $Co/Ru/TiO_2$ and $Co/Pt/TiO_2$.

The total mass of each sample was 10 g, and the atomic relation between promoter and cobalt was 1/100, respectively (Eq.A.1). The amount of cobalt in each sample was 20 wt%. Thus, the mass of Co was 2 g in each sample and 8 g of the support (Al_2O_3 or TiO_2).

$$\mathrm{n_{promoter}} = \frac{\mathrm{n_{Co}}}{100} \tag{A.1}$$

The mass of $Co(NO_3)_2 \cdot 6\,H_2O$ and the different promoters were calculated using Equation A.2 and A.3, respectively. The results of calculated masses are presented in Table A.1. While, the calculated weight percentages for each of the metal promoters are presented in Table A.2.

$$\mathrm{m_{Co(NO3)2{\cdot}6H2O}} = n_{Co} \cdot M_{m,Co} \tag{A.2}$$

$$\mathrm{m_{promoter}} = \mathrm{n_{promoter}} \cdot \mathrm{M_{m,promoter}} \tag{A.3}$$

Table A.1: Masses of active material and promoters used in IWI

Active material and support	Molar mass [g/mol]	Mass [g]
$Co(NO_3)_2 \cdot 6\,H_2O$	182.94	9.88
Al_2O_3		8.0
TiO_2		8.0
Promoter	**Molar mass [g/mol]**	**Mass [g]**
$H_2PtCl_6 \cdot 6\,H_2O$	517.91	0.1758
$Pt(NH_3)_4(NO_3)_2$	387.10	0.1314
$HReO_4$ (solution)	251.21	0.0853
$Ru(NO)(NO_3)_2$ (solution)	318.10	0.1080

Table A.2: Calculated wt% of each promoter

Promoter	Molar mass [g/mol]	Wt%
Pt	195.08	0.66
Re	186.23	0.63
Ru	101.07	0.34

A.2 Concentration Calculations

After IWI method it was found that for 5.0 g Al_2O_3 it was necessary with 7.1 mL water to reach the IW point. For 8 g of Al_2O_3 it was therefore required 11.3 mL water. The calculation is showed in Equation A.4.

$$V_{water} = \frac{7{,}1\,mL}{5{,}0\,g} \cdot 8{,}0\,g = 11{,}3mL \tag{A.4}$$

To be certain that the IW point was reached when making the catalyst, it was made a bit more solution of catalyst and promoter to be sure. The calculations for this is presented in the next subsections.

A.2.1 Unpromoted Co-catalyst

Since the cobalt-salt contains water, this needs to be removed to know how much water must be added when making the cobalt solution for impregnation. The calculation is showed in Equation A.5.

$$V_{H2OinCo-salt} = \frac{n_{Co} \cdot M_{m,H2O}}{\rho_{H2O}} = 3{,}7\,mL \tag{A.5}$$

The water that must be added is then found by subtracting 11.3 mL by 3.7, which gives 7.6 mL of water. For making a solution of 10 mL of water, the mass of $Co(NO_3)_2 \cdot 6\,H_2O$ is calculated in Equation A.6.

$$m_{Co(NO3)2*6H2O} = \frac{9{,}88\,g}{7{,}6\,mL} \cdot 10\,mL = 12{,}97\,g \tag{A.6}$$

The solution made for this impregnation contained 12.97 g $Co(NO_3)_2 \cdot 6\,H_2O$ and 10 mL deionized water.

A.2.2 Co-catalyst containing Pt-promoter with chlorine

The cobalt-salt and the Pt-salt contains water. This must be removed to know how much water must be added when making the catalyst solution for impregnation. The amount of water in the Pt-salt is presented in Equation A.7.

$$V_{H2OinPt-salt} \frac{6 \cdot n_{promoter} \cdot M_{m,H2O}}{\rho_{H2O}} = 0{,}04\,mL \tag{A.7}$$

The amount of water in the promoter is small, we can therefore neglect this when calculating the amount of water that should be added. The amount of water that should be added is thus the same as for the Co-catalyst without promoter (7.6 mL). For making a solution with 15 mL of water the calculated masses are presented in Equation A.8 and A.9.

$$m_{Co(NO3)2*6H2O} = \frac{9{,}88\,g}{7{,}6\,mL} \cdot 15\,mL = 19{,}56\,g \tag{A.8}$$

$$m_{H2PtCl6*6H2O} = \frac{0{,}1758\,g}{7{,}6\,mL} \cdot 15\,mL = 0{,}35\,g \tag{A.9}$$

The solution made for this impregnation contained 19.56 g $Co(NO_3)_2 \cdot 6\,H_2O$, 0.35 g $H_2PtCl_6 \cdot 6\,H_2O$ and 15 mL deionized water.

A.2.3 Co-catalyst containing Pt-promoter without chlorine

The amount of Co-salt and water to be added was calculated with the exact same procedure as for the Pt-promoter with chlorine. The mass of $Pt(NH_3)_4(NO_3)_2$ for a solution containing 15 mL water is calculated in Equation A.10.

$$m_{Pt(NH3)4(NO3)2} = \frac{0{,}1314\,g}{7{,}6\,mL} \cdot 15\,mL = 0{,}26\,g \tag{A.10}$$

The solution made for this impregnation contained 19.56 g $Co(NO_3)_2 \cdot 6\,H_2O$, 0.26 g $Pt(NH_3)_4(NO_3)_2$ and 15 mL deionized water.

A.2.4 Co-catalyst containing Re-promoter

The $HReO_4$-solution contains 65-70% $HReO_4$. The mass of the solution that should be taken out is given in Equation A.11

$$m_{solution} = \frac{m_{HReO_4}}{wt\%(HReO_4)} = \frac{0{,}0853\,g}{0{,}675\,wt/wt} = 0{,}1264\,g \tag{A.11}$$

Calculations for making a solution with 15 mL of water is given in Equation A.12 and A.13.

$$m_{Co(NO3)2*6H2O} = \frac{9{,}88\,g}{7{,}6\,mL} \cdot 15\,mL = 19{,}56\,g \tag{A.12}$$

$$m_{solution} = \frac{0{,}1264\,g}{7{,}6\,mL} \cdot 15\,mL = 0{,}249\,g \tag{A.13}$$

The solution made for this impregnation contained 19.56 g $Co(NO_3)_2 \cdot 6\,H_2O$, 0.25 g $HReO_4$ and 15 mL deionized water.

A.2.5 Co-catalyst containing Ru-promoter

The Ru-solution contained 5-11 wt% HNO_3, 1-2 wt% Ru, and the rest was water. The amount of water, Co-salt and Ru-solution to be added is calculated in Equation A.14 and A.15.

$$m_{solution} = \frac{m_{Ru}}{wt\%Ru} = \frac{0{,}1080\,g}{0{,}015\,wt/wt} = 7{,}2\,g \tag{A.14}$$

$$m_{H2OinRu-solution} = m_{solution} \cdot 0{,}905 = 6{,}52\,g \tag{A.15}$$

Subtract amount of water in Co-salt and Ru-solution gives 1.1 mL of water to be added.

The solution made for this impregnation contained 9.88 g $Co(NO_3)_2 \cdot 6\,H_2O$, 7.2 g $Ru(NO)(NO_3)_2$ solution and 1.1 g deionized water.

B Degree of Reduction Calculations

In order to find the degree of reduction (DoR) of a cobalt catalyst, the area under the TPR curves must be found. A known quantity of silver oxide (Ag_2O) goes through TPR, and by integrating the area under the TPR curve (section B.1) it will give you a response per mole of H_2 consumed (calibration factor). From this the amount of experimental H_2 consumed in the reduction of Co_3O_4 can be calculated by integrating the TPR curve. With the additional information about the stoichiometry of the reaction, the DoR can be calculated.

Since the TPR curves are rather complex a paper with the curves were printed and each peak of the TPR peaks were weighed. The sample mass used in TPR, and the weights of the peaks are presented in Table B.1. Since the first and second peak of the catalysts supported on TiO_2 overlapped, they were not weighed separately.

Table B.1: The sample mass used in TPR and the weights of the peaks

Sample	Sample mass used in TPR (g)	Weight of both peaks (g)	Weight of peak 1 (g)	Weight of peak 2 (g)
Ag_2O	0.1617	0.0688	-	-
Co/Al_2O_3	0.1557	0.0542	0.0194	0.0348
$Co/Pt/Al_2O_3$	0.1498	0.0965	0.0372	0.0593
$Co/Ru/Al_2O_3$	0.1547	0.0864	0.0298	0.0566
$Co/Re/Al_2O_3$	0.1782	0.0623	0.0200	0.0423
Co/TiO_2	0.1591	0.0901	-	-
$Co/Pt/TiO_2$	0.1528	0.0521	-	-
$Co/Ru/TiO_2$	0.1600	0.0623	-	-
$Co/Re/TiO_2$	0.1526	0.0810	-	-

It is assumed that Ag_2O goes through a total reduction, presented in Equation B.1.

$$Ag_2O + H_2 \longrightarrow 2\,Ag + H_2O \tag{B.1}$$

The mass of Ag_2O used in TPR was 0.1617 g, from this the amount of H_2 consumed can be calculated from Equation B.2, knowing that the molar mass of Ag_2O is 231.735 g/mol.

$$n_{H2} = n_{Ag2O} = \frac{0{,}1617\text{g}}{231{,}735\text{g/mol}} = 6{,}9778 \cdot 10^{-4} \tag{B.2}$$

With the additional information that the weight of the Ag_2O peak is 0.0688 g, the calibration factor can be calculated from Equation B.3.

$$\text{Calibration factor} = \frac{\text{weight of } Ag_2O \text{ peak}}{n_{H2}} = \frac{0{,}0688\text{g}}{6{,}9778 \cdot 10^{-4}} = 98{,}5984\,\text{g/mol} \tag{B.3}$$

Degree of reduction of the catalyst Co/Al_2O_3

As an example the DoR of Co/Al_2O_3 is calculated. The amount of H_2 consumed is calculated from Equation B.4, based on the total weight of the Co/Al_2O_3 peaks and the calibration factor.

$$H_2\,\text{consumed} = \frac{\text{weight of } Co/Al_2O_3 \text{ peaks}}{\text{Calibration factor}} = \frac{0{,}0542\,\text{g}}{98{,}5984\,\text{g/mol}} = 5{,}497 \cdot 10^{-4}\,\text{mol} \quad \text{(B.4)}$$

Assuming that the sample contains 20 wt% Co, the mass of Co in the sample can be calculated from Equation B.5, and with the additional information of the molar mass of Co (58.93 g/mol), the amount of Co on a molar basis (n_{Co})can be calculated from Equation B.6.

$$m_{Co} = 0{,}1557\,\text{g} \cdot 0{,}20 = 0{,}0311\,\text{g} \quad \text{(B.5)}$$

$$n_{Co} = \frac{m_{Co}}{M_{m,Co}} = \frac{0{,}0311\text{g}}{58{,}93\text{g/mol}} = 5{,}2842 \cdot 10^{-4}\,\text{mol} \quad \text{(B.6)}$$

Assuming that Co_3O_4 is completely reduced to Co^0 (Equation B.7), the theoretical amount of H_2 used in the reduction can be calculated from Equation B.8.

$$Co_3O_4 + 4\,H_2 \longrightarrow 3\,Co^0 + 4\,H_2O \quad \text{(B.7)}$$

$$\text{Theoretical amount of } H_2 = \frac{4}{3} \cdot n_{Co} = 7{,}0456 \cdot 10^{-4}\,\text{mol} \quad \text{(B.8)}$$

Finally, the DoR can then be calculated according to Equation B.9

$$\text{DoR} = \frac{H_2\,\text{consumed}}{\text{Theoretical amount of } H_2} \cdot 100\,\% = \frac{5{,}4970 \cdot 10^{-4}}{7{,}0456 \cdot 10^{-4}} \cdot 100\,\% = 78\% \quad \text{(B.9)}$$

If XRF results are used instead of an assumption that the catalyst contain 20wt% of Co, the Equation B.5 changes to:

$$m_{Co} = 0{,}1557\,\text{g} \cdot 0{,}242 = 0{,}0377\,\text{g} \quad \text{(B.10)}$$

Using the same equations as above (B.6-B.8), the DoR is then given by Equation B.11

$$\text{DoR} = \frac{H_2\,\text{consumed}}{\text{Theoretical amountof } H_2} \cdot 100\,\% = \frac{5{,}4970 \cdot 10^{-4}}{8{,}5252 \cdot 10^{-4}} \cdot 100\,\% = 64\% \quad \text{(B.11)}$$

The calculated DoR and ratio between the hydrogen consumption for reduction of Co_3O_4 to CoO and the hydrogen consumption for reduction of CoO to Co^0, for all the catalysts are presented in section 4.1.3 in the main report.

B.1 TPR curve of Ag_2O

The TPR results from the sample Ag_2O, used for calibration, is presented in Figure B.1.

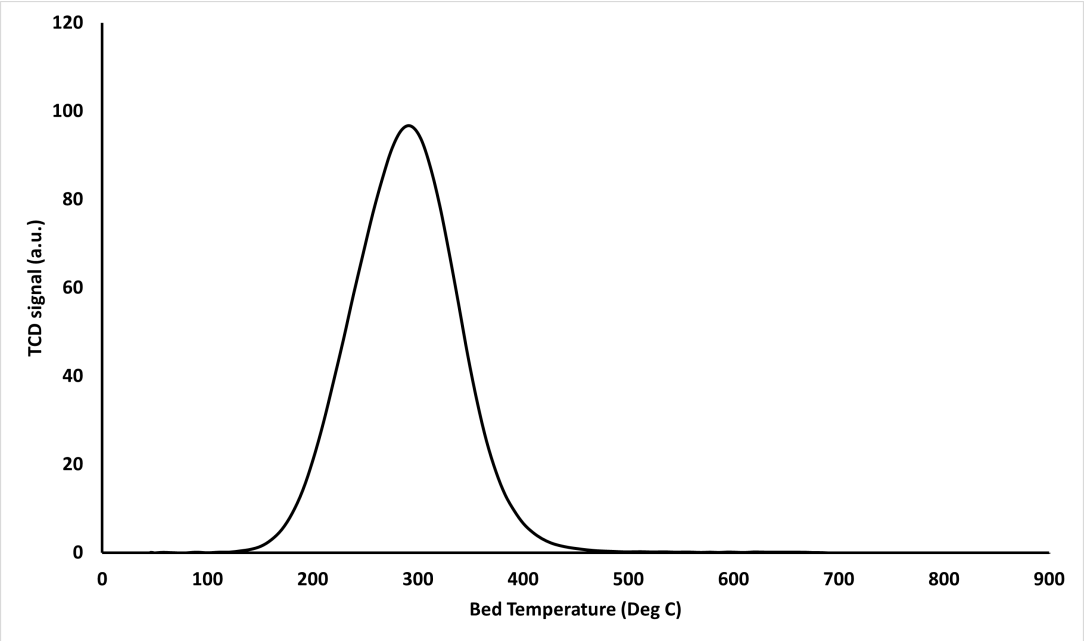

Figure B.1: TPR results for the sample Ag_2O

B.2 Reproducibility of the TPR results

The catalyst Co/Al_2O_3 was analysed three times in TPR to investigate if the results were reproducible. The resulting TPR plot is presented in Figure B.2. The curves changes both positions and intensities when analysed several times. This underlines the uncertainties related to the results, due to problems and adjustments of the instrument.

It is uncertain how much the adjustments of the instrument affected the results, or if the discrepancies are related to the packing of the reactor. The placement of the sample was not always the exact same, and the amount of quartz wool varied. The first curve (black) was used in the results, due to the fact that it fits better with the literature of how the peaks of Re-promoted Co/Al_2O_3 catalysts behaves. [50,58]

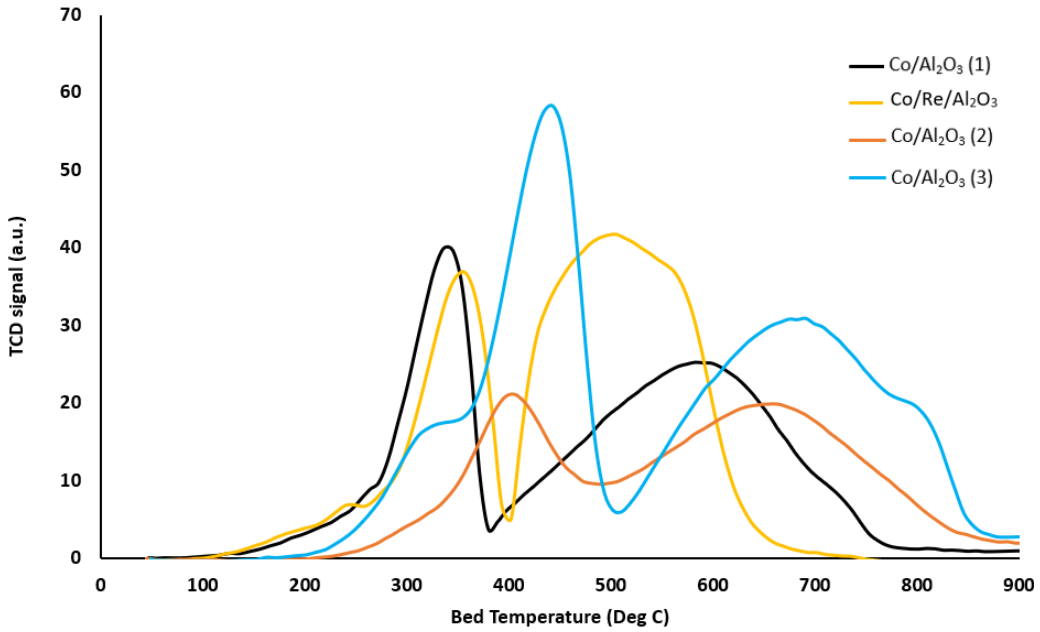

Figure B.2: TPR results for the catalyst Co/Al_2O_3 analysed three times, and the catalyst $Co/Re/Al_2O_3$

C GC Calculations - Activity and Selectivity

The GC-results for the $Co/Re/Al_2O_3$ sample, after 23 hours of running, are here used to show an example of how the conversion of CO and the selectivity are calculated. Figure C.1 is a simplified flowsheet of the FT process and shows the feed stream, the outgoing product gas stream, the known values of the incoming total volumetric flow ($V_{0,tot}$), mole fractions (X) of each component, temperature, pressure, weight of the reduced catalyst ($w_{cat.}$), and the H_2/CO ratio.

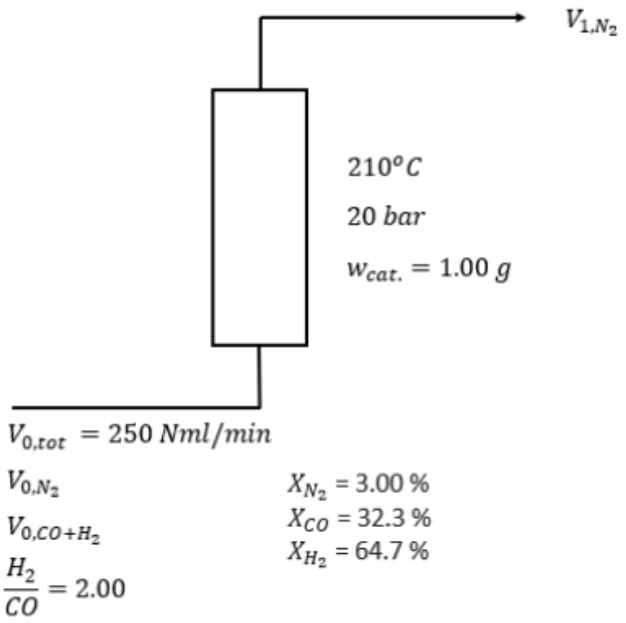

Figure C.1: Simplified flowsheet

Knowing the amount of feedgas and that it consists of 3,00% N_2, the outgoing flow of N_2 and the feed flow of $CO+H_2$ can be calculated using equations C.1 - C.2.

$$\mathrm{V_{1,N2}} = \mathrm{V_{0,N2}} = = 250\,\mathrm{Nml/min} \cdot 0{,}03 = 7{,}5\,\mathrm{Nml/min} \tag{C.1}$$

$$\mathrm{V_{0,CO+H2}} = 250\,\mathrm{Nml/min} - 7{,}5\,\mathrm{Nml/min} = 242{,}5\,\mathrm{Nml/min} \tag{C.2}$$

The results from the GC-analysis are presented in Table C.1 and C.2. Table C.1 shows the GC-analysis results of the feed stream, while Table C.2 presents the results of the outgoing product stream. The product stream consists of C_{2+} hydrocarbons, which are detected by a Flame Ionization Detector (FID).The remaining components are measured by a Thermal Conductivity Detector (TCD). From Equation C.3 the relative response factor, K_i, is calculated, where i represents the components measured by TCD. The area A and A′ in the Tables C.1 and C.2 are the GC area, and j represents the components measured by FID in Table C.2(b).

$$\mathrm{K}_i = \frac{\mathrm{X}_i/\mathrm{A}_i}{\mathrm{X_{N2}}/\mathrm{A_{N2}}} \tag{C.3}$$

Table C.1: GC results obtained from the feed stream, analyzed by TCD

Component	$A_{0,i}$	K_i
N_2	1395.75098	1.0
H_2	1289.39246	23.35
CO	$1.43134 \cdot 10^4$	1.05
CH_4	0.00001	1.45
CO_2	0.00001	0.95

Table C.2: GC results obtained from the outgoing product stream, analyzed by TCD (a) and FID (b)

(a) TCD

Component	$A_{1,i}$	K_i
N_2	1780.53748	1.0
H_2	1217.83936	23.35
CO	$1.40127 \cdot 10^4$	1.05
CH_4	303.27209	1.45
CO_2	26.28142	0.95

(b) FID

C-number	Component	$A'_{1,j}$
1	CH4	566.44128
2	C2-	41.57736
	C2=	7.70236
3	C3-	50.39691
	C3=	158.36417
4	C4-	80.56915
	C4=	152.40488
5	i-C5-	2.00502
	n-C5-	82.70982
	i-C5=	1.06935
	1-C5=	133.59717
6	n-C6-	83.52695
	1-C6=	87.06399
7	n-C7-	53.55657
	1-C7=	16.05857

Conversion

The conversion of CO (η_{CO}) can be calculated from the reaction rates given in the equations C.4 and C.5.

$$r_{0,CO} = \frac{X_{0,CO}}{X_{0,N2}} = K_{CO} \cdot \frac{A_{0,CO}}{A_{0,N2}} = 1{,}05 \cdot \frac{1{,}43134 \cdot 10^4}{1395{,}75098} = 10{,}76773022 \tag{C.4}$$

$$r_{1,CO} = \frac{X_{1,CO}}{X_{1,N2}} = K_{CO} \cdot \frac{A_{1,CO}}{A_{1,N2}} = 1{,}05 \cdot \frac{1{,}40127 \cdot 10^4}{1780{,}53748} = 8{,}263423357 \tag{C.5}$$

The conversion of CO is then given by Equation C.6.

$$\eta_{CO} = \frac{F_{0,CO} - F_{1,CO}}{F_{0,CO}} = 1\text{-}\frac{r_{1,CO}}{r_{0,CO}} = 1 - \frac{8{,}263423357}{10{,}76773022} = 0{,}2326 = 23{,}26\,\% \tag{C.6}$$

The obtained conversion fits well with the results given in Table F.7 in Appendix F.

Selectivity

In order to calculate the selectivities, the flows F_1 and F_0 must be calculated for each component. This is done by multiplying the reaction rates (r) of the component (i or j) with the inert feed flow ($F_{0,N2}$). The reaction rates are calculated according to the equations C.7 and C.8, where n is the carbon number, and the resulting values are presented in Table C.3.

$$r_{0,i} = \frac{X_{0,i}}{X_{0,N2}} = K_i \frac{A_{0,i}}{A_{0,N2}} \tag{C.7}$$

$$r_{0,j} = \frac{X_{0,j}}{X_{0,N2}} = \frac{A'_{0,j}}{A'_{0,CH4} \cdot n} \cdot r_{1,CH4} \tag{C.8}$$

Table C.3: Calculated reaction rates of the feed flow (r_0) and product flow (r_1), for the components i and j. For simplicity only the reaction rates of the hydrocarbons C1-C4 is calculated.

Component	$r_{0,i}$	$r_{0,j}$	$r_{1,i}$	$r_{1,j}$
H_2	21.5707		15.9708	
CO	10.7677		8.2634	
CO_2	$6.81 \cdot 10^{-9}$		0.0140	
CH_4	$1.04 \cdot 10^{-8}$		0.2470	0.2470
C2-				$9.06 \cdot 10^{-3}$
C2=				$1.68 \cdot 10^{-3}$
C3-				$7.32 \cdot 10^{-3}$
C3=				0.0230
C4-				$8.78 \cdot 10^{-3}$
C4=				0.0166
		$\sum r_0 = 32.3384$		$\sum r_1 = 24.5526$

The total feed flow is calculated according to Equation C.9.

$$F_{0,tot} = \frac{250\,\text{Nml/min}}{22{,}414\,\text{Nl/mol}} = 11{,}1537\,\frac{\text{mmol}}{\text{min}} \cdot \frac{60\,\text{min/h}}{1000} = 0{,}669222\,\text{mol/h} \tag{C.9}$$

The inert feed flow is calculated from Equation C.10

$$F_{0,N2} = X_{0,N2} \cdot F_{0,tot} = 0{,}03 \cdot 0{,}669222\,\text{mol/h} = 0{,}02007666\,\text{mol/h} \tag{C.10}$$

Now the flow F_1 can be calculated from Equation C.11, and similar for F_0, for all of the components i and j.

$$F_{1,i} = r_{1,i} \cdot F_{1,N2} \qquad \text{where} \qquad F_{1,N2} = F_{0,N2} \tag{C.11}$$

The selectivity of the outgoing components (j) can then be calculated according to Equation C.12, where n is the carbon number.

$$S_j = \frac{n \cdot (F_{1,j} - F_{0,j})}{F_{0,CO} - F_{1,CO}} \tag{C.12}$$

As an example the selectivity of CH_4 is calculated. The flows in Table C.4 are calculated from the Equation C.11, where the reactions rates are taken from Table C.3.

Table C.4: Calculated flow values for CO and CH_4

Flow	Calculated value [mol/h]
$F_{1,CO}$	0.1659019412
$F_{0,CO}$	0.2161800586
$F_{1,CH4}$	$4.95839123 \cdot 10^{-3}$
$F_{0,CH4}$	$2.085698482 \cdot 10^{-10}$

By applying the values from Table C.4 to Equation C.12, the selectivity of CH_4 is given by Equation C.13.

$$S_{CH4} = \frac{1 \cdot (F_{1,CH4} - F_{0,CH4})}{F_{0,CO} - F_{1,CO}} = 0{,}0986 = 9{,}86\,\% \tag{C.13}$$

The selectivity of C_{5+} can be calculated from Equation C.14 after the selectivities of C2-C4 and CO_2 are calculated.

$$S_{C5+} = 100\,\% - \sum_{j=1}^{4} S_j - S_{CO2} \tag{C.14}$$

Site Time Yield

The Site Time Yield (STY) can be calculated from Equation C.15. All the parameters given in Table C.5 are used, together with the dispersion and conversion of each catalyst given in Table C.6, in order to calculate STY. The resulting values of STY of each catalyst are also given in Table C.6.

$$STY = \frac{F_{0,CO}}{w_{cat.} \cdot V_m} \times \frac{\eta_{CO} \cdot M_{Co}}{w_m \cdot D} \tag{C.15}$$

Table C.5: Experimental data for sample calculations of the Site Time Yield

Parameter	Value	Unit	Explanation
$w_{cat.}$	1.0	g	Weight of catalyst
V_m	22 414	ml/mol	Volume of one mole of ideal gas at ambient conditions
M_{Co}	58.93	g/mol	Molar mass of cobalt
w_m	0.20	-	Weight fraction of cobalt in the catalyst
$F_{0,CO}$	80.75	ml/min	Molar feed flow of carbon monoxide

Table C.6: Calculated site time yields for each sample with dispersion measured from H_2 chemisorption and conversion measured at 23 hours of running

Sample	Dispersion	Conversion (%)	STY (s^{-1})
Co/Al_2O_3	0.040	6.3	0.028
$Co/Re/Al_2O_3$	0.072	23.3	0.057
$Co/Pt/Al_2O_3$	0.081	17.9	0.039
$Co/Ru/Al_2O_3$	0.084	16.9	0.036

C.1 Identification of GC peaks

In order for the calculations to be correct, it is important that all C_1-C_4 components are correctly identified (in addition to H_2, CO and N_2). The identification of the C_{5+} components is not critical for the calculations, but C_5 and C_6 (in the gas phase) are reported.[98] An example of a chromatogram is shown in Figure C.2

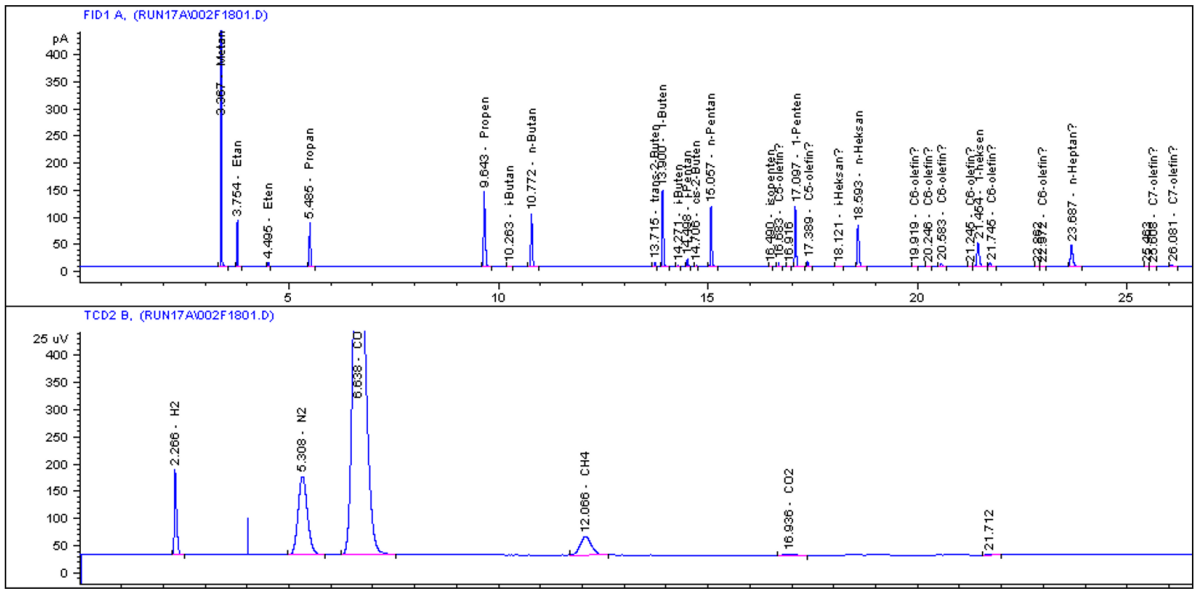

Figure C.2: Example of chromatogram, section 0 - 27 min (FID: HP-PLOT Al_2O_3 "M, TCD: CarboSieve. The figure is obtained from SINTEF's manual of the FT setup.[98]

D XRD: Phase and Refinement Information

This appendix contains the structural information of the phases (Table D.1), obtained from the PDF-4 database by ICDD[95], and the refinement parameters (Table D.2) used for the Pawley analysis in Topas.

Table D.1: Structural information of the phases

Structure	Crystal system	Space group	Lattice parameters (Å)		Database nr.
			a	c	
Co_3O_4	Cubic	Fd-3m (227)	8.084		00-042-1467
γ-Al_2O_3	Cubic	Fd-3m (227)	7.911		00-056-0457
Rutile (TiO_2)	Tetragonal	P42/mnm (136)	4.594	2.959	04-003-0648
Anatase (TiO_2)	Tetragonal	I41/amd (141)	3.78536	9.4936	00-064-0863

Table D.2: Refinement parameters used in Topas

Emission profile	Background	Instrument details	Corrections	Miscellaneous
WL(Å) = 1.534007	Order = 10*	Prim. radius (nm) = 280	Sample displ. (mm): -0.255 (refine)	Conv. steps = 1
WL(Å) = 1.540678		Sec. radius (nm) = 280	LP factor: 0 (fix)	
WL(Å) = 1.541121		Linear PSD	Zero error: -0.1042 (fix)	
WL(Å) = 1.54474		2Th angular range of LPSD (^{0})=3		
WL(Å) = 1.544866		FDS angle (^{0}) = 0.3		
WL(Å) = 1.476639		Beam spill, sample length (nm) = 20		
WL(Å) = 1.489223				
WL(Å) = 1.392387				

*This relatively high order is set due to the shape of the diffractograms.

E Raw Data

This appendix contains the raw data from the N_2-physisorption (E.1), H_2-chemisorption (E.2), pawley fit in Topas (E.3), and XRF (E.4) measurements.

E.1 N_2 Physisorption: Adsorption/Desorption Curves

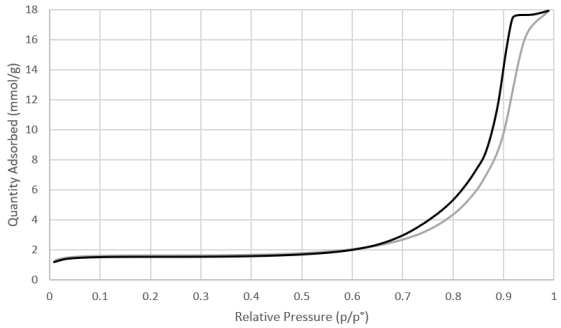

(a) γ-Al_2O_3

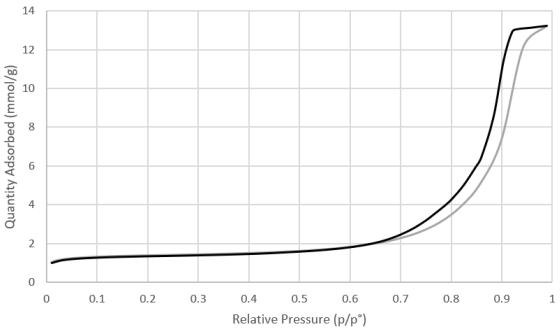

(b) Co/Al_2O_3

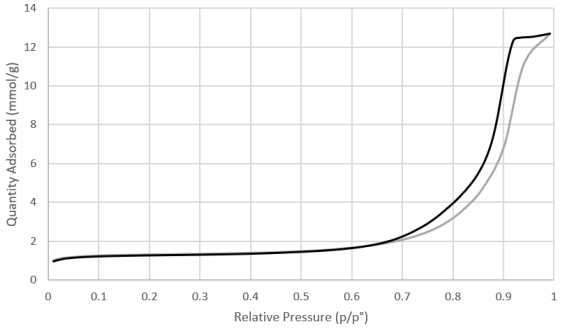

(c) $Co/Pt/Cl/Al_2O_3$

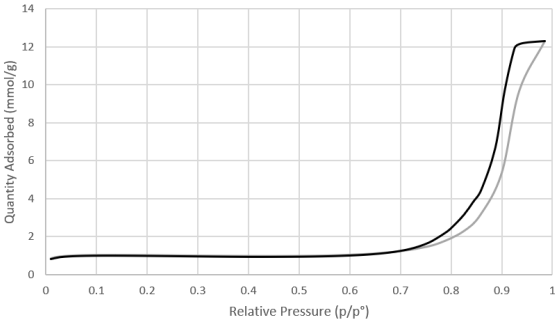

(d) $Co/Pt/Al_2O_3$

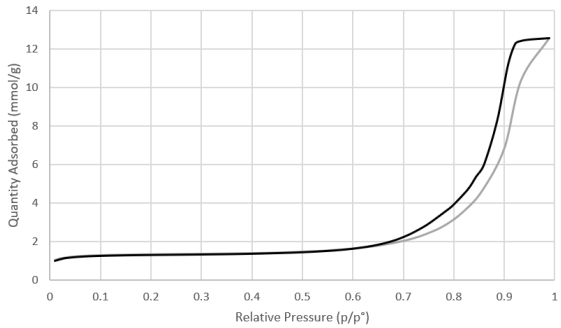

(e) $Co/Re/Al_2O_3$

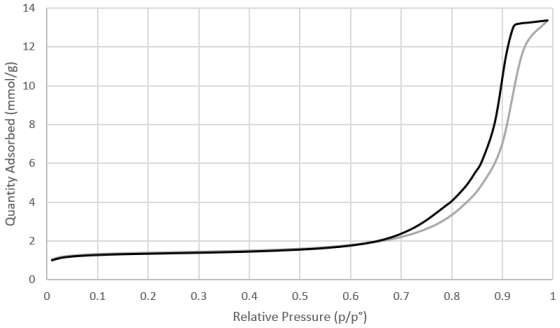

(f) $Co/Ru/Al_2O_3$

Figure E.1: Adsorption (grey)/desorption (black) curves for the catalysts supported on Al_2O_3 and the bare support γ-Al_2O_3, obtained from N_2-physisorption.

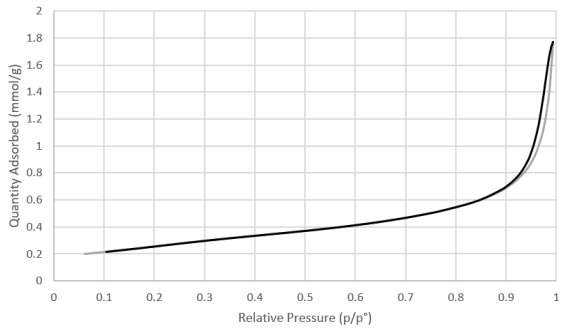

(a) TiO_2

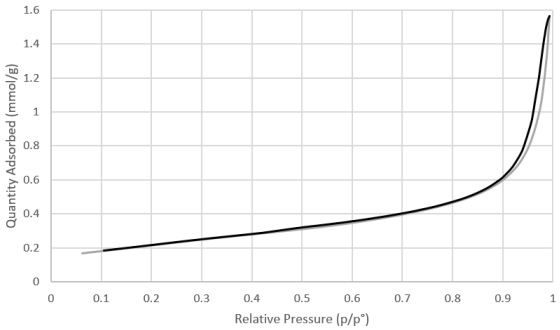

(b) Co/TiO_2

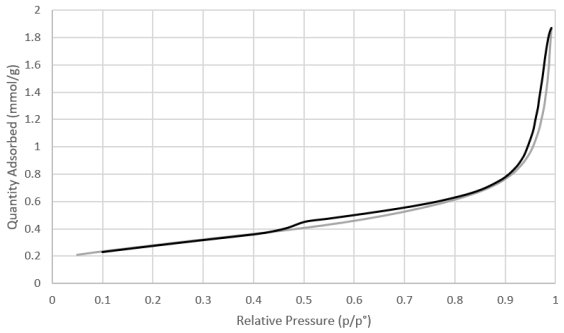

(c) $Co/Pt/TiO_2$

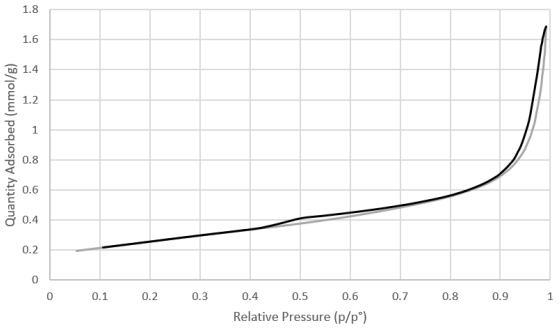

(d) $Co/Re/TiO_2$

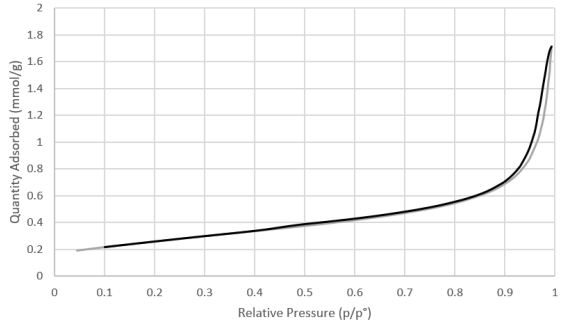

(e) $Co/Ru/TiO_2$

Figure E.2: Adsorption (grey)/desorption (black) curves for the catalysts supported on TiO_2 and the bare support TiO_2, obtained from N_2-physisorption.

E.2 H_2 Chemisorption Curves

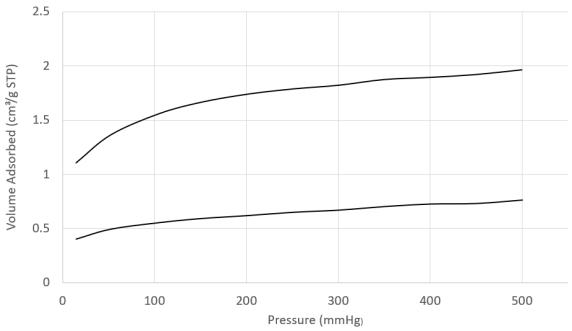

(a) Co/Al_2O_3

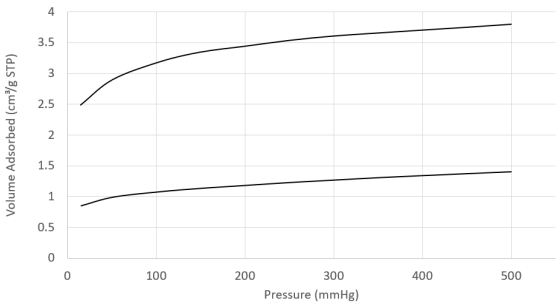

(b) $Co/Pt/Al_2O_3$

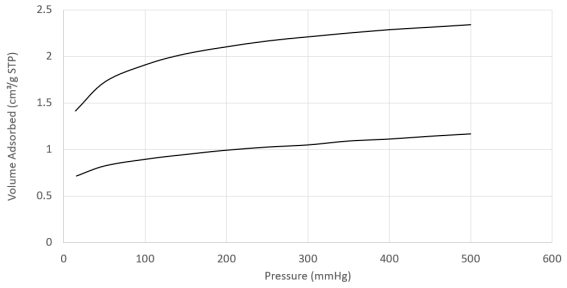

(c) $Co/Pt/Cl/Al_2O_3$

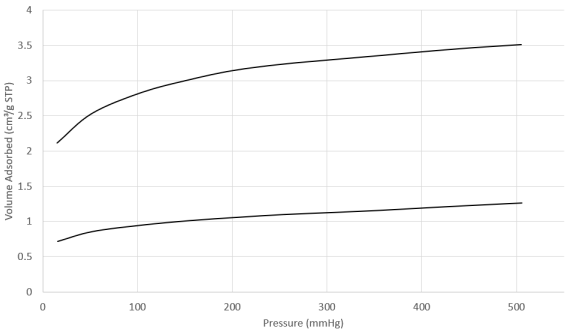

(d) $Co/Re/Al_2O_3$

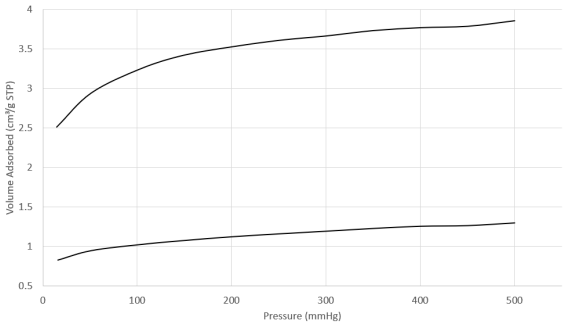

(e) $Co/Ru/Al_2O_3$

Figure E.3: Chemisorption isotherm plots for the catalysts supported on Al_2O_3

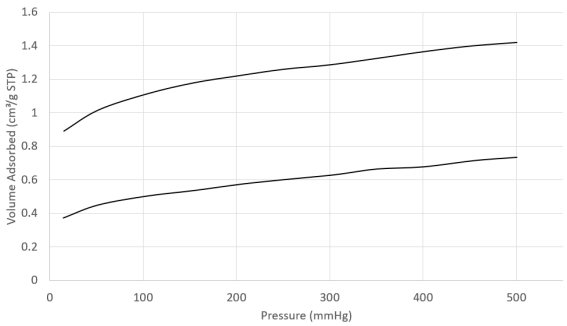

(a) Co/TiO_2

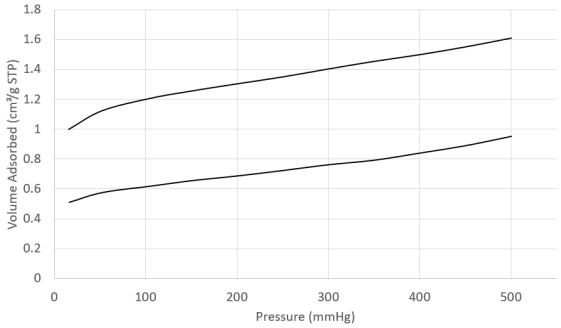

(b) $Co/Pt/TiO_2$

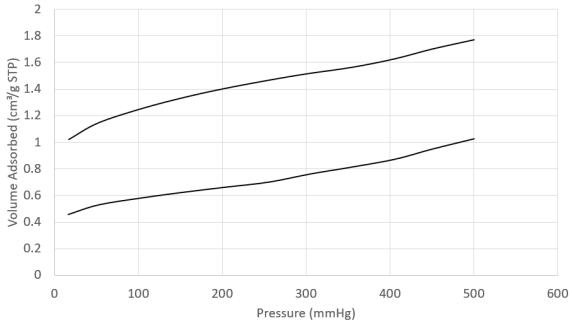

(c) $Co/Re/TiO_2$

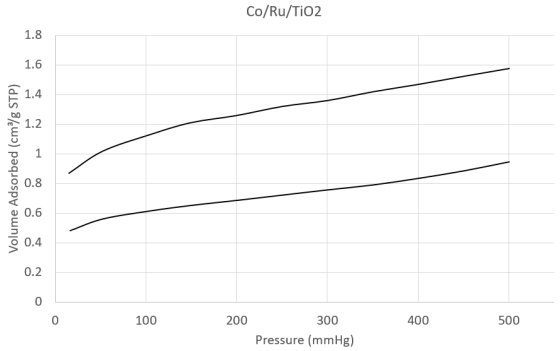

(d) $Co/Ru/TiO_2$

Figure E.4: Chemisorption isotherm plots for the catalysts supported on TiO_2

E.3 Pawley Fit

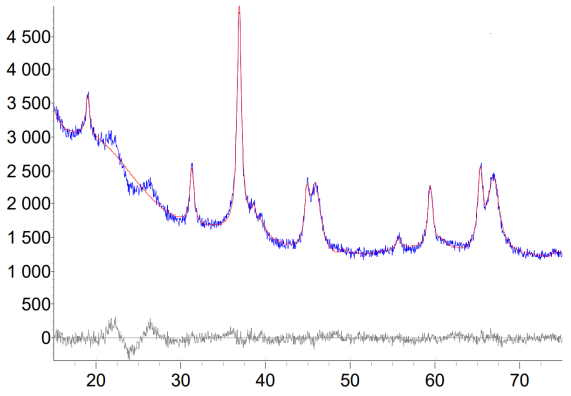

(a) Co/Al_2O_3

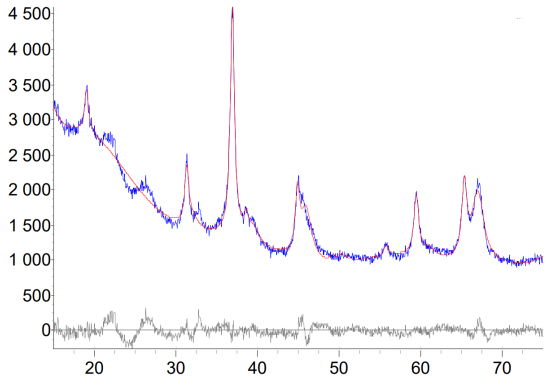

(b) $Co/Pt/Al_2O_3$

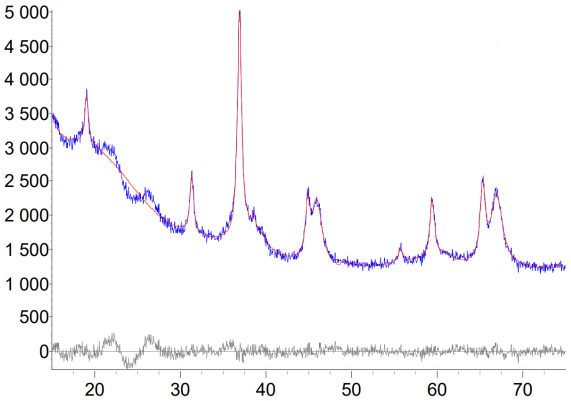

(c) $Co/Pt/Cl/Al_2O_3$

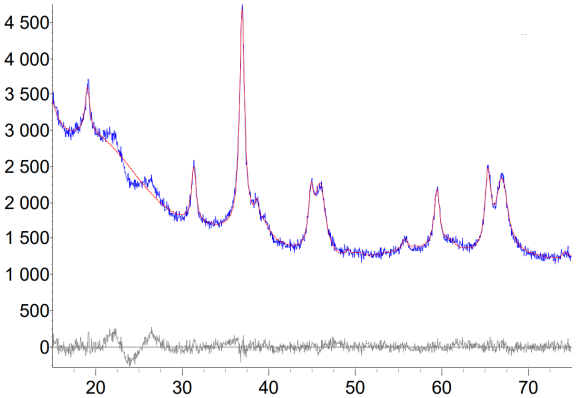

(d) $Co/Re/Al_2O_3$

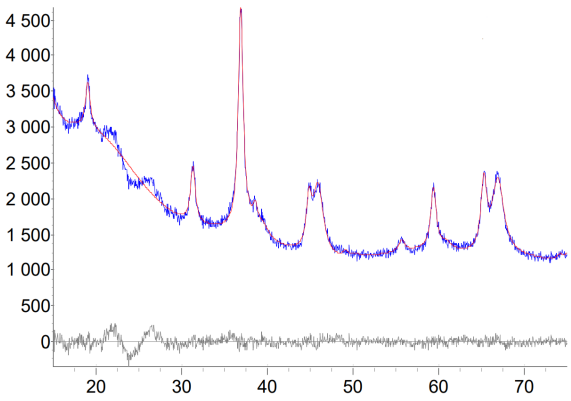

(e) $Co/Ru/Al_2O_3$

Figure E.5: The observed (blue), calculated (red) and difference (grey) profiles for the catalysts supported on Al_2O_3

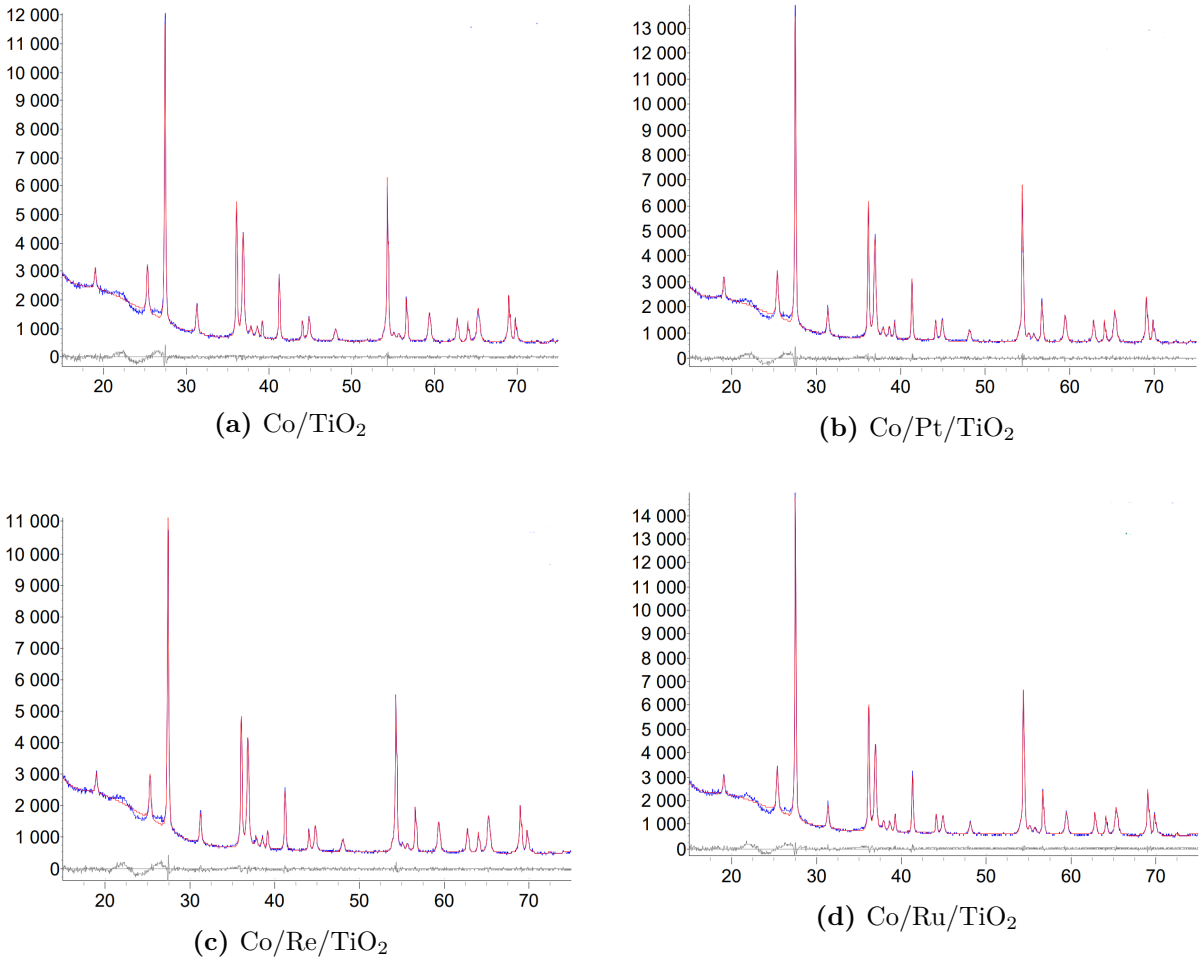

(a) Co/TiO_2 **(b)** $Co/Pt/TiO_2$

(c) $Co/Re/TiO_2$ **(d)** $Co/Ru/TiO_2$

Figure E.6: The observed (blue), calculated (red) and difference (grey) profiles for the catalysts supported on TiO_2

E.4 XRF Results

The obtained XRF results are given in the tables below, where Table E.1 shows the results for the three prepared samples of the catalyst $Co/Re/Al_2O_3$. The remaining tables show the results from the catalysts analyzed by XRF three times. The standard deviation was calculated using the formula E.1, where N is number of measurements, $\overline{x}$ is the average value, and x_i is one measured value in the population.

$$\sigma = \sqrt{\frac{(\sum_{i=1}^{N}(\overline{x} - x_i)^2}{N}} \tag{E.1}$$

Table E.1: The obtained XRF results for the three prepared pellets of the catalyst $Co/Re/Al_2O_3$.

Pellet	Co [wt%]	Al [wt%]	Re [wt%]	K [wt%]	Ag [wt%]	S [wt%]
1	25.2	72.6	0.91	1.20	-	-
2	27.5	69.9	0.74	1.81	0.96	-
3	34.9	62.2	0.94	1.20	-	0.18
Average value	29.2 ± 4.1	68.2 ± 4.4	0.86 ± 0.09	1.40 ± 0.29	0.96 ± 0	0.18 ± 0

Table E.2: XRF results of the pellet containing catalyst Co/Al_2O_3

Run	Co [wt%]	Al [wt%]	K [wt%]	Ca [wt%]	Fe [wt%]
1	23.8	74.3	1.20	0.37	0.27
2	24.3	73.9	1.74	-	-
3	24.4	73.9	1.41	0.32	-
Average value	24.2 ± 0.26	74.0 ± 0.2	1.45 ± 0.22	0.35 ± 0.03	0.27 ± 0

Table E.3: XRF results of the pellet containing catalyst $Co/Ru/Al_2O_3$

Run	Co [wt%]	Al [wt%]	Ru [wt%]	K [wt%]	S [wt%]	Cl [wt%]
1	23.8	74.8	0.37	0.96	0.10	-
2	23.6	74.8	0.33	1.19	-	0.02
3	24.5	73.8	0.34	1.26	0.13	-
Average value	24.0 ± 0.4	74.5 ± 0.5	0.35 ± 0.02	1.14 ± 0.13	0.12 ± 0.02	0.02 ± 0

Table E.4: XRF results of the pellet containing catalyst $Co/Pt/Cl/Al_2O_3$

Run	Co [wt%]	Al [wt%]	Pt [wt%]	K [wt%]	Mg [wt%]	Ca [wt%]
1	25.9	71.3	0.77	1.0	0.81	0.17
2	26.1	70.4	0.67	1.38	1.16	0.20
3	26.9	71.0	0.91	1.25	-	-
Average value	26.3 ± 0.4	70.9 ± 0.4	0.78 ± 0.10	1.21 ± 0.16	0.99 ± 0.18	0.19 ± 0.02

Table E.5: XRF results of the pellet containing catalyst $Co/Pt/Al_2O_3$

Run	Co [wt%]	Al [wt%]	Pt [wt%]	K [wt%]	Mg [wt%]	Si [wt%]
1	26.6	70.1	0.63	1.14	0.82	0.56
2	28.0	69.0	0.68	1.40	-	0.56
3	28.5	68.7	0.85	1.15	-	0.60
Average value	27.7 ± 0.8	69.3 ± 0.6	0.72 ± 0.09	1.2 ± 0.1	0.82 ± 0	0.57 ± 0.02

Table E.6: XRF results of the pellet containing catalyst Co/TiO_2

Run	Co [wt%]	Ti [wt%]	K [wt%]	Ca [wt%]	Al [wt%]	Cl [wt%]	Si [wt%]
1	33.3	65.9	0.77	0.11	-	-	-
2	33.6	65.3	0.75	-	0.32	0.06	-
3	32.6	66.2	0.87	-	-	-	0.25
Average value	33.2 ± 0.4	65.8 ± 0.4	0.80 ± 0.05	0.11 ± 0	0.32 ± 0	0.06 ± 0	0.25 ± 0

Table E.7: XRF results of the pellet containing catalyst $Co/Re/TiO_2$

Run	Co [wt%]	Ti [wt%]	Re [wt%]	K [wt%]	Si [wt%]
1	31.7	66.2	1.34	0.73	-
2	31.9	66.2	1.14	0.65	0.19
3	31.0	67.1	1.20	0.66	-
Average value	31.5 ± 0.4	66.5 ± 0.4	1.22 ± 0.08	0.68 ± 0.04	0.19 ± 0

Table E.8: XRF results of the pellet containing catalyst Co/Ru/TiO_2

Run	Co [wt%]	Ti [wt%]	Ru [wt%]	K [wt%]	Si [wt%]	S [wt%]
1	29.4	69.0	0.59	0.75	0.29	-
2	28.8	69.6	0.78	0.82	-	-
3	29.5	69.0	0.70	0.75	-	0.09
Average value	29.2 ± 0.3	69.2 ± 0.3	0.69 ± 0.08	0.77 ± 0.03	0.29 ± 0	0.09 ± 0

Table E.9: XRF results of the pellet containing catalyst Co/Pt/TiO_2

Run	Co [wt%]	Ti [wt%]	Pt [wt%]	K [wt%]	Al [wt%]	Si [wt%]	Fe [wt%]
1	31.0	67.1	1.09	0.68	-	-	-
2	32.2	65.9	1.01	0.56	0.34	-	-
3	32.4	65.3	1.04	0.65	-	0.29	0.24
Average value	31.9 ± 0.6	66.1 ± 0.7	1.05 ± 0.03	0.63 ± 0.05	0.34 ± 0	0.29 ± 0	0.24 ± 0

F Catalyst Performance Results for Catalysts Supported on Al_2O_3

This appendix contains all of the catalyst performance results for the catalysts supported on Al_2O_3. The appendix contains 3 different tables for each catalyst analysed in the FTS set-up. The first table contains inlet compositions of N_2, CO and H_2 and total selectivities. The second table include hydrocarbon selectivities ("CO_2-free") and olefin/parafin ratios, while the third table consists of reaction rates. TOS is an abbreviation for time on stream and is given in each of the tables.

Table F.1: Space velocities, inlet compositions, CO and H_2 conversions, and total selectivities for the catalyst Co/Al_2O_3

		Inlet comp. (%)			Conversion (%)		Total selectivities (%)								
TOS	GHSV	N_2	CO	H_2	CO	H_2	CH_4	C2=	C2-	C3=	C3-	1-C4=	n-C4-	C4tot	S_{CO2}	C2-C4	S_{C5+}
4.7	15000	3	32.3	64.7	6	5.8	12.81	0.6	0.88	4.72	1.15	4.66	1.73	6.4	6.96	13.75	66.48
8	15000	3	32.3	64.7	5.8	5.9	13.03	0.6	0.85	4.65	1.11	4.66	1.7	6.36	4.42	13.57	68.98
11.4	15000	3	32.3	64.7	6	6.2	12.63	0.57	0.81	4.44	1.05	4.48	1.62	6.11	3.34	12.98	71.05
14.7	15000	3	32.3	64.7	6.2	6.4	12.48	0.56	0.8	4.33	1.02	4.38	1.58	5.96	2.71	12.67	72.14
18.1	15000	3	32.3	64.7	6	6.3	12.54	0.55	0.8	4.32	1.02	4.36	1.57	5.93	2.41	12.62	72.43
21.4	15000	3	32.3	64.7	6.1	6.4	12.64	0.55	0.8	4.33	1.02	4.38	1.57	5.95	2.23	12.65	72.48
24.8	15000	3	32.3	64.7	6.3	6.5	12.2	0.53	0.78	4.15	0.98	4.21	1.51	5.72	1.98	12.16	73.66
34.9	2400	3	32.3	64.7	29	30.2	8.18	0.15	0.72	2.5	0.8	1.93	0.9	2.92	0.7	7.09	84.03
38.2	2400	3	32.3	64.7	37.7	39.2	7.9	0.12	0.79	2.61	0.91	2	1.04	3.16	0.63	7.59	83.88
41.6	2400	3	32.3	64.7	40.4	42	7.93	0.12	0.83	2.76	0.99	2.21	1.22	3.57	0.61	8.27	83.19
44.9	2400	3	32.3	64.7	40.9	42.6	7.96	0.12	0.86	2.86	1.03	2.39	1.35	3.89	0.61	8.76	82.67
48.3	1800	3	32.3	64.7	40.8	42.5	7.99	0.12	0.88	2.91	1.06	2.49	1.43	4.08	0.6	9.05	82.36
51.7	1800	3	32.3	64.7	42.1	43.9	7.9	0.12	0.87	2.85	1.04	2.44	1.41	4.02	0.59	8.90	82.61
55	1800	3	32.3	64.7	43.6	45.4	7.85	0.11	0.88	2.84	1.05	2.4	1.41	3.98	0.58	8.86	82.71
58.4	1800	3	32.3	64.7	44.9	46.8	7.77	0.11	0.88	2.81	1.05	2.37	1.41	3.94	0.58	8.79	82.86
61.8	1800	3	32.3	64.7	47.1	49	7.69	0.1	0.88	2.76	1.05	2.29	1.38	3.83	0.58	8.62	83.11
65.1	1800	3	32.3	64.7	48.7	50.7	7.66	0.1	0.89	2.76	1.07	2.27	1.39	3.83	0.58	8.65	83.11
68.5	1800	3	32.3	64.7	49.5	51.5	7.65	0.1	0.9	2.79	1.09	2.29	1.42	3.88	0.58	8.76	83.01

Table F.2: Hydrocarbon selectivities ("CO_2-free") and olefin/parafin ratios for the catalyst Co/Al_2O_3

	HC-selectivities ("CO_2-free")												Olefin/Parafin		
TOS	CH_4	C2=	C2-	C2tot	C3=	C3-	C3tot	1-C4=	n-C4-	C4tot	C2-C4	S_{C5+}	C2=/C2-	C3=/C3-	C4=/C4-
4.7	13.77	0.64	0.95	1.59	5.07	1.24	6.31	5.01	1.86	6.88	14.78	71.45	0.68	4.10	2.69
8	13.63	0.63	0.89	1.52	4.87	1.16	6.03	4.88	1.78	6.65	14.20	72.17	0.71	4.19	2.74
11.4	13.07	0.59	0.84	1.43	4.59	1.09	5.68	4.63	1.68	6.32	13.43	73.51	0.70	4.23	2.77
14.7	12.83	0.58	0.82	1.40	4.45	1.05	5.50	4.50	1.62	6.13	13.02	74.15	0.70	4.25	2.77
18.1	12.85	0.56	0.82	1.38	4.43	1.05	5.47	4.47	1.61	6.08	12.93	74.22	0.69	4.24	2.78
21.4	12.93	0.56	0.82	1.38	4.43	1.04	5.47	4.48	1.61	6.09	12.94	74.13	0.69	4.25	2.79
24.8	12.45	0.54	0.80	1.34	4.23	1.00	5.23	4.30	1.54	5.84	12.41	75.15	0.68	4.23	2.79
34.9	8.24	0.15	0.73	0.88	2.52	0.81	3.32	1.94	0.91	2.94	7.14	84.62	0.21	3.13	2.14
38.2	7.95	0.12	0.80	0.92	2.63	0.92	3.54	2.01	1.05	3.18	7.64	84.41	0.15	2.87	1.92
41.6	7.98	0.12	0.84	0.96	2.78	1.00	3.77	2.22	1.23	3.59	8.32	83.70	0.14	2.79	1.81
44.9	8.01	0.12	0.87	0.99	2.88	1.04	3.91	2.40	1.36	3.91	8.81	83.18	0.14	2.78	1.77
48.3	8.04	0.12	0.89	1.01	2.93	1.07	3.99	2.51	1.44	4.10	9.10	82.86	0.14	2.75	1.74
51.7	7.95	0.12	0.88	1.00	2.87	1.05	3.91	2.45	1.42	4.04	8.95	83.10	0.14	2.74	1.73
55	7.90	0.11	0.89	1.00	2.86	1.06	3.91	2.41	1.42	4.00	8.91	83.19	0.13	2.70	1.70
58.4	7.82	0.11	0.89	1.00	2.83	1.06	3.88	2.38	1.42	3.96	8.84	83.34	0.13	2.68	1.68
61.8	7.73	0.10	0.89	0.99	2.78	1.06	3.83	2.30	1.39	3.85	8.67	83.59	0.11	2.63	1.66
65.1	7.70	0.10	0.90	1.00	2.78	1.08	3.85	2.28	1.40	3.85	8.70	83.59	0.11	2.58	1.63
68.5	7.69	0.10	0.91	1.01	2.81	1.10	3.90	2.30	1.43	3.90	8.81	83.49	0.11	2.56	1.61

Table F.3: Reaction rates for the catalyst Co/Al_2O_3

TOS	Rates									
	molCO/g*h	g/g*h	g/g*h	g/g*h	g/g*h	g/g*h	g/g*h	g/g*h	g/g*h	g/g*h
	r_{CO}	r_{C1}	r_{C2}	r_{C3}	r_{C4}	r_{C2-C4}	r_{C5+}	r_{HCtot}	r_{CO2}
4.7	0.0130	0.0266	0.0028	0.0108	0.0117	0.0253	0.1207	0.1726	0.0397
8	0.0125	0.0261	0.0027	0.0102	0.0113	0.0241	0.1211	0.1713	0.0244
11.4	0.0130	0.0262	0.0026	0.0101	0.0112	0.0239	0.1290	0.1791	0.0191
14.7	0.0134	0.0268	0.0027	0.0101	0.0113	0.0241	0.1354	0.1862	0.0160
18.1	0.0130	0.0260	0.0026	0.0098	0.0109	0.0232	0.1315	0.1807	0.0138
21.4	0.0132	0.0267	0.0026	0.0100	0.0111	0.0237	0.1338	0.1841	0.0129
24.8	0.0136	0.0266	0.0026	0.0099	0.0110	0.0235	0.1404	0.1905	0.0119
34.9	0.0100	0.0131	0.0013	0.0047	0.0041	0.0101	0.1180	0.1413	0.0031
38.2	0.0130	0.0165	0.0018	0.0065	0.0058	0.0141	0.1531	0.1837	0.0036
41.6	0.0140	0.0177	0.0020	0.0074	0.0071	0.0165	0.1627	0.1969	0.0038
44.9	0.0141	0.0180	0.0021	0.0078	0.0078	0.0177	0.1637	0.1994	0.0038
48.3	0.0106	0.0135	0.0016	0.0060	0.0061	0.0137	0.1220	0.1492	0.0028
51.7	0.0109	0.0138	0.0016	0.0060	0.0062	0.0139	0.1263	0.1540	0.0028
55	0.0113	0.0142	0.0017	0.0062	0.0064	0.0143	0.1310	0.1595	0.0029
58.4	0.0116	0.0145	0.0017	0.0064	0.0065	0.0146	0.1351	0.1642	0.0030
61.8	0.0122	0.0150	0.0018	0.0066	0.0066	0.0150	0.1422	0.1722	0.0031
65.1	0.0126	0.0155	0.0019	0.0069	0.0069	0.0156	0.1470	0.1781	0.0032
68.5	0.0128	0.0157	0.0019	0.0071	0.0071	0.0161	0.1492	0.1810	0.0033

Table F.4: Space velocities, inlet compositions, CO and H_2 conversions, and total selectivities for the catalyst $Co/Ru/Al_2O_3$

		Inlet comp. (%)			Conversion (%)		Total selectivities (%)										
TOS	GHSV	N_2	CO	H_2	CO	H_2	CH_4	C2=	C2-	C3=	C3-	1-C4=	n-C4-	C4tot	S_{CO2}	C2-C4	S_{C5+}
2.2	15000	3	32.3	64.7	16.8	15.6	12.22	0.19	0.81	2.99	0.96	2.16	1.03	3.28	9.74	8.23	69.81
5.5	15000	3	32.3	64.7	20.8	21.6	11.61	0.16	0.82	3.17	1.02	3.05	1.59	4.87	1.89	10.04	76.46
8.9	15000	3	32.3	64.7	18.9	19.9	12.12	0.17	0.85	3.28	1.04	3.18	1.65	5.05	1.31	10.39	76.18
12.2	15000	3	32.3	64.7	18.1	19.1	12.34	0.17	0.87	3.29	1.06	3.21	1.67	5.11	1.08	10.50	76.08
15.6	15000	3	32.3	64.7	17.6	18.7	12.3	0.17	0.87	3.26	1.04	3.18	1.66	5.05	0.92	10.39	76.39
18.9	15000	3	32.3	64.7	16.8	17.8	12.77	0.17	0.9	3.37	1.08	3.29	1.71	5.22	0.85	10.74	75.64
22.3	15000	3	32.3	64.7	16.9	18	12.43	0.17	0.88	3.29	1.04	3.22	1.66	5.09	0.78	10.47	76.32
25.6	5400	3	32.3	64.7	16.7	17.8	12.43	0.17	0.87	3.28	1.04	3.21	1.65	5.07	0.74	10.43	76.40
29	5400	3	32.3	64.7	37	39.1	10.27	0.09	0.79	2.62	1.04	2.25	1.44	3.88	0.43	8.42	80.88
32.3	5400	3	32.3	64.7	45.3	47.6	9.58	0.08	0.74	2.35	0.97	1.98	1.3	3.45	0.39	7.59	82.44
35.7	5400	3	32.3	64.7	53.5	56.1	9.07	0.07	0.75	2.34	1.04	1.97	1.41	3.57	0.37	7.77	82.79
39.1	5400	3	32.3	64.7	54.4	57.2	9.03	0.07	0.76	2.4	1.08	2.12	1.57	3.89	0.37	8.20	82.40
42.4	5400	3	32.3	64.7	54	56.7	9.07	0.07	0.77	2.43	1.09	2.19	1.64	4.05	0.36	8.41	82.16
45.8	5400	3	32.3	64.7	53.3	56	9.13	0.07	0.77	2.44	1.1	2.22	1.66	4.1	0.36	8.48	82.03
49.2	5700	3	32.3	64.7	51.2	53.8	9.28	0.07	0.78	2.51	1.12	2.33	1.74	4.3	0.36	8.78	81.58
52.5	5700	3	32.3	64.7	49.4	52	9.41	0.07	0.79	2.52	1.11	2.35	1.74	4.32	0.37	8.81	81.41
55.9	5700	3	32.3	64.7	48.7	51.3	9.45	0.07	0.78	2.48	1.09	2.22	1.62	4.05	0.37	8.47	81.71
59.2	5700	3	32.3	64.7	48.3	50.9	9.54	0.07	0.79	2.51	1.1	2.26	1.65	4.13	0.36	8.60	81.50
62.6	5700	3	32.3	64.7	48	50.5	9.61	0.07	0.8	2.53	1.11	2.29	1.68	4.2	0.36	8.71	81.32
66	5700	3	32.3	64.7	47.6	50.1	9.68	0.08	0.8	2.55	1.12	2.31	1.71	4.25	0.35	8.80	81.17
69.3	5700	3	32.3	64.7	47.2	49.7	9.74	0.08	0.81	2.56	1.13	2.33	1.72	4.29	0.35	8.87	81.04

Table F.5: Hydrocarbon selectivities ("CO_2-free") and olefin/parafin ratios for the catalyst $Co/Ru/Al_2O_3$

	HC-selectivities ("CO_2-free")												Olefin/Parafin		
TOS	CH_4	C2=	C2-	C2tot	C3=	C3-	C3tot	1-C4=	n-C4-	C4tot	C2-C4	S_{C5+}	C2=/C2-	C3=/C3-	C4=/C4-
2.2	13.54	0.21	0.90	1.11	3.31	1.06	4.38	2.39	1.14	3.63	9.12	77.34	0.23	3.11	2.10
5.5	11.83	0.16	0.84	1.00	3.23	1.04	4.27	3.11	1.62	4.96	10.23	77.93	0.20	3.11	1.92
8.9	12.28	0.17	0.86	1.03	3.32	1.05	4.38	3.22	1.67	5.12	10.53	77.19	0.20	3.15	1.93
12.2	12.47	0.17	0.88	1.05	3.33	1.07	4.40	3.25	1.69	5.17	10.61	76.91	0.20	3.10	1.92
15.6	12.41	0.17	0.88	1.05	3.29	1.05	4.34	3.21	1.68	5.10	10.49	77.10	0.20	3.13	1.92
18.9	12.88	0.17	0.91	1.08	3.40	1.09	4.49	3.32	1.72	5.26	10.83	76.29	0.19	3.12	1.92
22.3	12.53	0.17	0.89	1.06	3.32	1.05	4.36	3.25	1.67	5.13	10.55	76.92	0.19	3.16	1.94
25.6	12.52	0.17	0.88	1.05	3.30	1.05	4.35	3.23	1.66	5.11	10.51	76.97	0.20	3.15	1.95
29	10.31	0.09	0.79	0.88	2.63	1.04	3.68	2.26	1.45	3.90	8.46	81.23	0.11	2.52	1.56
32.3	9.62	0.08	0.74	0.82	2.36	0.97	3.33	1.99	1.31	3.46	7.62	82.76	0.11	2.42	1.52
35.7	9.10	0.07	0.75	0.82	2.35	1.04	3.39	1.98	1.42	3.58	7.80	83.10	0.09	2.25	1.40
39.1	9.06	0.07	0.76	0.83	2.41	1.08	3.49	2.13	1.58	3.90	8.23	82.71	0.09	2.22	1.35
42.4	9.10	0.07	0.77	0.84	2.44	1.09	3.53	2.20	1.65	4.06	8.44	82.46	0.09	2.23	1.34
45.8	9.16	0.07	0.77	0.84	2.45	1.10	3.55	2.23	1.67	4.11	8.51	82.33	0.09	2.22	1.34
49.2	9.31	0.07	0.78	0.85	2.52	1.12	3.64	2.34	1.75	4.32	8.81	81.87	0.09	2.24	1.34
52.5	9.44	0.07	0.79	0.86	2.53	1.11	3.64	2.36	1.75	4.34	8.84	81.71	0.09	2.27	1.35
55.9	9.49	0.07	0.78	0.85	2.49	1.09	3.58	2.23	1.63	4.07	8.50	82.01	0.09	2.28	1.37
59.2	9.57	0.07	0.79	0.86	2.52	1.10	3.62	2.27	1.66	4.14	8.63	81.79	0.09	2.28	1.37
62.6	9.64	0.07	0.80	0.87	2.54	1.11	3.65	2.30	1.69	4.22	8.74	81.61	0.09	2.28	1.36
66	9.71	0.08	0.80	0.88	2.56	1.12	3.68	2.32	1.72	4.26	8.83	81.46	0.10	2.28	1.35
69.3	9.77	0.08	0.81	0.89	2.57	1.13	3.70	2.34	1.73	4.31	8.90	81.32	0.10	2.27	1.35

Table F.6: Reaction rates for the catalyst $Co/Ru/Al_2O_3$

TOS	Rates									
	molCO/g*h	g/g*h	g/g*h	g/g*h	g/g*h	g/g*h	g/g*h	g/g*h	g/g*h	g/g*h
	r_{CO}	r_{C1}	r_{C2}	r_{C3}	r_{C4}	r_{C2-C4}	r_{C5+}	r_{HCtot}	r_{CO2}
2.2	0.0363	0.0710	0.0054	0.0203	0.0169	0.0426	0.3549	0.4685	0.1556
5.5	0.0450	0.0835	0.0065	0.0267	0.0310	0.0643	0.4813	0.6291	0.0374
8.9	0.0409	0.0792	0.0062	0.0250	0.0292	0.0604	0.4357	0.5754	0.0235
12.2	0.0391	0.0772	0.0060	0.0241	0.0283	0.0585	0.4167	0.5525	0.0186
15.6	0.0380	0.0749	0.0059	0.0232	0.0272	0.0563	0.4069	0.5380	0.0154
18.9	0.0363	0.0742	0.0058	0.0229	0.0269	0.0555	0.3846	0.5143	0.0136
22.3	0.0365	0.0727	0.0057	0.0224	0.0263	0.0545	0.3903	0.5174	0.0125
25.6	0.0130	0.0258	0.0020	0.0080	0.0093	0.0193	0.1390	0.1841	0.0042
29	0.0288	0.0473	0.0038	0.0150	0.0159	0.0346	0.3260	0.4079	0.0054
32.3	0.0353	0.0540	0.0043	0.0166	0.0173	0.0382	0.4069	0.4991	0.0060
35.7	0.0416	0.0604	0.0051	0.0200	0.0211	0.0462	0.4825	0.5892	0.0068
39.1	0.0423	0.0612	0.0052	0.0209	0.0234	0.0496	0.4883	0.5991	0.0069
42.4	0.0420	0.0610	0.0053	0.0210	0.0242	0.0505	0.4833	0.5948	0.0067
45.8	0.0415	0.0606	0.0052	0.0209	0.0242	0.0502	0.4763	0.5872	0.0066
49.2	0.0421	0.0624	0.0053	0.0217	0.0257	0.0527	0.4803	0.5955	0.0067
52.5	0.0406	0.0611	0.0052	0.0209	0.0249	0.0511	0.4625	0.5746	0.0066
55.9	0.0400	0.0605	0.0051	0.0203	0.0230	0.0484	0.4576	0.5665	0.0065
59.2	0.0397	0.0606	0.0051	0.0204	0.0233	0.0487	0.4527	0.5620	0.0063
62.6	0.0394	0.0606	0.0051	0.0204	0.0235	0.0491	0.4489	0.5585	0.0062
66	0.0391	0.0606	0.0051	0.0204	0.0236	0.0491	0.4443	0.5540	0.0060
69.3	0.0388	0.0604	0.0051	0.0203	0.0236	0.0491	0.4399	0.5494	0.0060

Table F.7: Space velocities, inlet compositions, CO and H_2 conversions, and total selectivities for the catalyst $Co/Re/Al_2O_3$

		Inlet comp. (%)			Conversion (%)		Total selectivities (%)										
TOS	GHSV	N_2	CO	H_2	CO	H_2	CH_4	C2=	C2-	C3=	C3-	1-C4=	n-C4-	C4tot	S_{CO2}	C2-C4	S_{C5+}
3	15000	3	32.3	64.7	25.7	25.3	9.37	0.13	0.62	2.27	0.71	1.56	0.76	2.42	4.68	6.15	79.80
6.3	15000	3	32.3	64.7	26.6	27.6	9.3	0.13	0.66	2.59	0.81	2.28	1.14	3.58	1.29	7.77	81.64
9.7	15000	3	32.3	64.7	25.4	26.6	9.51	0.13	0.69	2.68	0.84	2.49	1.28	3.95	0.95	8.29	81.25
13.1	15000	3	32.3	64.7	24.6	25.8	9.65	0.13	0.7	2.71	0.86	2.56	1.33	4.08	0.78	8.48	81.09
16.4	15000	3	32.3	64.7	24	25.2	9.74	0.13	0.71	2.73	0.87	2.59	1.36	4.15	0.67	8.59	81.00
19.8	15000	3	32.3	64.7	23.5	24.7	9.88	0.13	0.72	2.76	0.88	2.64	1.39	4.24	0.62	8.73	80.77
23.1	15000	3	32.3	64.7	23.3	24.5	9.86	0.13	0.72	2.76	0.88	2.65	1.4	4.26	0.58	8.75	80.81
29.8	7500	3	32.3	64.7	50	52	7.8	0.07	0.61	1.78	0.68	1.15	0.66	1.91	0.34	5.05	86.81
33.2	7500	3	32.3	64.7	51.2	53.4	7.73	0.07	0.64	2.09	0.81	1.51	0.92	2.58	0.34	6.19	85.74
36.5	7500	3	32.3	64.7	50.9	53	7.75	0.07	0.65	2.2	0.85	1.76	1.09	3.01	0.35	6.78	85.12
39.9	7500	3	32.3	64.7	50.7	52.8	7.75	0.07	0.66	2.22	0.86	1.86	1.17	3.22	0.35	7.03	84.87
43.3	7500	3	32.3	64.7	50.2	52.3	7.8	0.08	0.66	2.26	0.88	1.95	1.24	3.39	0.35	7.27	84.58
50	7500	3	32.3	64.7	49.3	51.4	7.83	0.08	0.67	2.28	0.89	2.05	1.32	3.57	0.34	7.49	84.34
53.3	7500	3	32.3	64.7	49	51.2	7.88	0.08	0.67	2.3	0.9	2.07	1.34	3.62	0.34	7.57	84.21
56.7	7500	3	32.3	64.7	48.9	51	7.87	0.08	0.67	2.24	0.88	2.03	1.32	3.56	0.34	7.43	84.36
60.1	7500	3	32.3	64.7	48.5	50.7	7.91	0.08	0.67	2.27	0.89	2.04	1.34	3.59	0.34	7.50	84.25
63.4	7500	3	32.3	64.7	48.3	50.4	7.94	0.08	0.68	2.28	0.9	2.06	1.35	3.61	0.34	7.55	84.17
66.8	7500	3	32.3	64.7	47.9	50.1	7.98	0.08	0.68	2.3	0.9	2.08	1.37	3.66	0.33	7.62	84.07

Table F.8: Hydrocarbon selectivities ("CO_2-free") and olefin/parafin ratios for the catalyst $Co/Re/Al_2O_3$

	HC-selectivities ("CO_2-free")										Olefin/Parafin		
TOS	CH_4	C2=	C2-	C2tot	C3=	C3-	C3tot	1-C4=	n-C4-	C4tot	C2-C4	S_{C5+}	C2=/C2-	C3=/C3-	C4=/C4-
3	9.83	0.14	0.65	0.79	2.38	0.74	3.13	1.64	0.80	2.54	6.45	83.72	0.21	3.20	2.05
6.3	9.42	0.13	0.67	0.80	2.62	0.82	3.44	2.31	1.15	3.63	7.87	82.71	0.20	3.20	2.00
9.7	9.60	0.13	0.70	0.83	2.71	0.85	3.55	2.51	1.29	3.99	8.37	82.03	0.19	3.19	1.95
13.1	9.73	0.13	0.71	0.84	2.73	0.87	3.60	2.58	1.34	4.11	8.55	81.73	0.19	3.15	1.92
16.4	9.81	0.13	0.71	0.85	2.75	0.88	3.62	2.61	1.37	4.18	8.65	81.55	0.18	3.14	1.90
19.8	9.94	0.13	0.72	0.86	2.78	0.89	3.66	2.66	1.40	4.27	8.78	81.27	0.18	3.14	1.90
23.1	9.92	0.13	0.72	0.85	2.78	0.89	3.66	2.67	1.41	4.28	8.80	81.28	0.18	3.14	1.89
29.8	7.83	0.07	0.61	0.68	1.79	0.68	2.47	1.15	0.66	1.92	5.07	87.11	0.11	2.62	1.74
33.2	7.76	0.07	0.64	0.71	2.10	0.81	2.91	1.52	0.92	2.59	6.21	86.03	0.11	2.58	1.64
36.5	7.78	0.07	0.65	0.72	2.21	0.85	3.06	1.77	1.09	3.02	6.80	85.42	0.11	2.59	1.61
39.9	7.78	0.07	0.66	0.73	2.23	0.86	3.09	1.87	1.17	3.23	7.05	85.17	0.11	2.58	1.59
43.3	7.83	0.08	0.66	0.74	2.27	0.88	3.15	1.96	1.24	3.40	7.30	84.88	0.12	2.57	1.57
50	7.86	0.08	0.67	0.75	2.29	0.89	3.18	2.06	1.32	3.58	7.52	84.63	0.12	2.56	1.55
53.3	7.91	0.08	0.67	0.75	2.31	0.90	3.21	2.08	1.34	3.63	7.60	84.50	0.12	2.56	1.54
56.7	7.90	0.08	0.67	0.75	2.25	0.88	3.13	2.04	1.32	3.57	7.46	84.65	0.12	2.55	1.54
60.1	7.94	0.08	0.67	0.75	2.28	0.89	3.17	2.05	1.34	3.60	7.53	84.54	0.12	2.55	1.52
63.4	7.97	0.08	0.68	0.76	2.29	0.90	3.19	2.07	1.35	3.62	7.58	84.46	0.12	2.53	1.53
66.8	8.01	0.08	0.68	0.76	2.31	0.90	3.21	2.09	1.37	3.67	7.65	84.35	0.12	2.56	1.52

Table F.9: Reaction rates for the catalyst $Co/Re/Al_2O_3$

TOS	Rates									
	molCO/g*h	g/g*h	g/g*h	g/g*h	g/g*h	g/g*h	g/g*h	g/g*h	g/g*h	g/g*h
	r_{CO}	r_{C1}	r_{C2}	r_{C3}	r_{C4}	r_{C2-C4}	r_{C5+}	r_{HCtot}	r_{CO2}
3	0.0556	0.0833	0.0062	0.0235	0.0190	0.0487	0.6206	0.7526	0.1144
6.3	0.0575	0.0856	0.0067	0.0277	0.0292	0.0636	0.6572	0.8063	0.0326
9.7	0.0549	0.0835	0.0067	0.0274	0.0307	0.0648	0.6245	0.7729	0.0230
13.1	0.0532	0.0821	0.0066	0.0269	0.0307	0.0642	0.6037	0.7500	0.0182
16.4	0.0519	0.0808	0.0065	0.0265	0.0305	0.0634	0.5883	0.7326	0.0153
19.8	0.0508	0.0803	0.0064	0.0262	0.0305	0.0631	0.5744	0.7178	0.0139
23.1	0.0504	0.0795	0.0064	0.0260	0.0304	0.0627	0.5698	0.7120	0.0129
29.8	0.0540	0.0674	0.0055	0.0189	0.0146	0.0390	0.6568	0.7632	0.0081
33.2	0.0553	0.0684	0.0059	0.0228	0.0203	0.0489	0.6642	0.7816	0.0083
36.5	0.0550	0.0682	0.0059	0.0238	0.0235	0.0532	0.6556	0.7770	0.0085
39.9	0.0548	0.0679	0.0060	0.0240	0.0250	0.0550	0.6511	0.7740	0.0084
43.3	0.0543	0.0677	0.0060	0.0242	0.0261	0.0563	0.6425	0.7664	0.0084
50	0.0533	0.0668	0.0060	0.0240	0.0270	0.0569	0.6291	0.7528	0.0080
53.3	0.0530	0.0668	0.0059	0.0241	0.0272	0.0572	0.6244	0.7483	0.0079
56.7	0.0529	0.0665	0.0059	0.0234	0.0267	0.0560	0.6242	0.7468	0.0079
60.1	0.0524	0.0663	0.0059	0.0235	0.0267	0.0561	0.6183	0.7407	0.0078
63.4	0.0522	0.0663	0.0059	0.0236	0.0268	0.0562	0.6151	0.7377	0.0078
66.8	0.0518	0.0661	0.0059	0.0235	0.0269	0.0563	0.6093	0.7317	0.0075
62.6	0.0394	0.0606	0.0051	0.0204	0.0235	0.0491	0.4489	0.5585	0.0062
66	0.0391	0.0606	0.0051	0.0204	0.0236	0.0491	0.4443	0.5540	0.0060
69.3	0.0388	0.0604	0.0051	0.0203	0.0236	0.0491	0.4399	0.5494	0.0060

Table F.10: Space velocities, inlet compositions, CO and H_2 conversions, and total selectivities for the catalyst $Co/Pt/Al_2O_3$

		Inlet comp. (%)			Conversion (%)		Total selectivities (%)										
TOS	GHSV	N_2	CO	H_2	CO	H_2	CH_4	C2=	C2-	C3=	C3-	1-C4=	n-C4-	C4tot	S_{CO2}	C2-C4	S_{C5+}
3.8	15000	3	32.3	64.7	21.1	21.6	11.11	0.19	0.93	3.63	1.22	3.27	1.78	5.34	3.13	11.31	74.45
7.2	15000	3	32.3	64.7	19.9	20.9	11.43	0.19	0.97	3.76	1.26	3.48	1.9	5.64	1.51	11.82	75.24
10.5	15000	3	32.3	64.7	19.1	20.2	11.6	0.19	0.99	3.77	1.28	3.49	1.93	5.7	1.17	11.93	75.30
13.9	15000	3	32.3	64.7	18.6	19.7	11.72	0.18	1.01	3.77	1.3	3.48	1.95	5.72	0.98	11.98	75.32
17.3	15000	3	32.3	64.7	18.3	19.5	11.82	0.18	1.02	3.79	1.31	3.49	1.97	5.74	0.85	12.04	75.29
20.6	15000	3	32.3	64.7	18.3	19.4	11.68	0.18	1.02	3.74	1.29	3.44	1.94	5.66	0.75	11.89	75.68
23.9	15000	3	32.3	64.7	17.9	19.1	11.72	0.18	1.02	3.74	1.29	3.45	1.95	5.67	0.73	11.90	75.65
27.3	6000	3	32.3	64.7	31.7	33.4	10.13	0.11	0.93	2.96	1.21	2.3	1.48	3.99	0.51	9.20	80.16
30.7	6000	3	32.3	64.7	40.7	42.8	9.45	0.1	0.9	2.96	1.26	2.48	1.73	4.46	0.45	9.68	80.42
34	6000	3	32.3	64.7	49.6	52	8.81	0.08	0.88	2.81	1.26	2.29	1.69	4.22	0.44	9.25	81.50
37.4	6000	3	32.3	64.7	50.5	53	8.72	0.08	0.89	2.85	1.29	2.41	1.81	4.48	0.45	9.59	81.24
40.7	6000	3	32.3	64.7	50.4	52.9	8.75	0.08	0.9	2.88	1.31	2.46	1.87	4.61	0.44	9.78	81.03
44.1	6000	3	32.3	64.7	50.2	52.6	8.75	0.08	0.91	2.88	1.32	2.48	1.9	4.67	0.43	9.86	80.96
47.5	6000	3	32.3	64.7	49.8	52.3	8.78	0.08	0.91	2.89	1.33	2.49	1.92	4.71	0.42	9.92	80.88
50.8	6000	3	32.3	64.7	49.3	51.8	8.82	0.08	0.92	2.9	1.34	2.51	1.95	4.74	0.42	9.98	80.78
54.2	6000	3	32.3	64.7	49.3	51.8	8.83	0.08	0.91	2.82	1.32	2.37	1.85	4.49	0.43	9.62	81.12
57.6	6000	3	32.3	64.7	49.7	52.1	8.85	0.08	0.92	2.82	1.33	2.34	1.85	4.47	0.42	9.62	81.11
60.9	6000	3	32.3	64.7	49.5	52	8.89	0.08	0.93	2.85	1.35	2.4	1.92	4.61	0.41	9.82	80.88
64.3	6000	3	32.3	64.7	49.4	51.9	8.93	0.08	0.93	2.88	1.37	2.43	1.96	4.69	0.41	9.95	80.71
67.7	6000	3	32.3	64.7	49.1	51.6	8.96	0.08	0.94	2.89	1.38	2.45	1.98	4.73	0.4	10.02	80.62

Table F.11: Hydrocarbon selectivities ("CO_2-free") and olefin/parafin ratios for the catalyst $Co/Pt/Al_2O_3$

	HC-selectivities ("CO_2-free")												Olefin/Parafin		
TOS	CH_4	C2=	C2-	C2tot	C3=	C3-	C3tot	1-C4=	n-C4-	C4tot	C2-C4	S_{C5+}	C2=/C2-	C3=/C3-	C4=/C4-
3.8	11.47	0.20	0.96	1.16	3.75	1.26	5.01	3.38	1.84	5.51	11.68	76.86	0.20	2.98	1.84
7.2	11.61	0.19	0.98	1.18	3.82	1.28	5.10	3.53	1.93	5.73	12.00	76.39	0.20	2.98	1.83
10.5	11.74	0.19	1.00	1.19	3.81	1.30	5.11	3.53	1.95	5.77	12.07	76.19	0.19	2.95	1.81
13.9	11.84	0.18	1.02	1.20	3.81	1.31	5.12	3.51	1.97	5.78	12.10	76.07	0.18	2.90	1.78
17.3	11.92	0.18	1.03	1.21	3.82	1.32	5.14	3.52	1.99	5.79	12.14	75.94	0.18	2.89	1.77
20.6	11.77	0.18	1.03	1.21	3.77	1.30	5.07	3.47	1.95	5.70	11.98	76.25	0.18	2.90	1.77
23.9	11.81	0.18	1.03	1.21	3.77	1.30	5.07	3.48	1.96	5.71	11.99	76.21	0.18	2.90	1.77
27.3	10.18	0.11	0.93	1.05	2.98	1.22	4.19	2.31	1.49	4.01	9.25	80.57	0.12	2.45	1.55
30.7	9.49	0.10	0.90	1.00	2.97	1.27	4.24	2.49	1.74	4.48	9.72	80.78	0.11	2.35	1.43
34	8.85	0.08	0.88	0.96	2.82	1.27	4.09	2.30	1.70	4.24	9.29	81.86	0.09	2.23	1.36
37.4	8.76	0.08	0.89	0.97	2.86	1.30	4.16	2.42	1.82	4.50	9.63	81.61	0.09	2.21	1.33
40.7	8.79	0.08	0.90	0.98	2.89	1.32	4.21	2.47	1.88	4.63	9.82	81.39	0.09	2.20	1.32
44.1	8.79	0.08	0.91	0.99	2.89	1.33	4.22	2.49	1.91	4.69	9.90	81.31	0.09	2.18	1.31
47.5	8.82	0.08	0.91	0.99	2.90	1.34	4.24	2.50	1.93	4.73	9.96	81.22	0.09	2.17	1.30
50.8	8.86	0.08	0.92	1.00	2.91	1.35	4.26	2.52	1.96	4.76	10.02	81.12	0.09	2.16	1.29
54.2	8.87	0.08	0.91	0.99	2.83	1.33	4.16	2.38	1.86	4.51	9.66	81.47	0.09	2.14	1.28
57.6	8.89	0.08	0.92	1.00	2.83	1.34	4.17	2.35	1.86	4.49	9.66	81.45	0.09	2.12	1.26
60.9	8.93	0.08	0.93	1.01	2.86	1.36	4.22	2.41	1.93	4.63	9.86	81.21	0.09	2.11	1.25
64.3	8.97	0.08	0.93	1.01	2.89	1.38	4.27	2.44	1.97	4.71	9.99	81.04	0.09	2.10	1.24
67.7	9.00	0.08	0.94	1.02	2.90	1.39	4.29	2.46	1.99	4.75	10.06	80.94	0.09	2.09	1.24

Table F.12: Reaction rates for the catalyst $Co/Pt/Al_2O_3$

TOS	Rates									
	molCO/g*h	g/g*h	g/g*h	g/g*h	g/g*h	g/g*h	g/g*h	g/g*h	g/g*h	g/g*h
	r_{CO}	r_{C1}	r_{C2}	r_{C3}	r_{C4}	r_{C2-C4}	r_{C5+}	r_{HCtot}	r_{CO2}
3.8	0.0456	0.0811	0.0076	0.0314	0.0345	0.0735	0.4754	0.6299	0.0628
7.2	0.0430	0.0787	0.0074	0.0306	0.0344	0.0724	0.4531	0.6042	0.0286
10.5	0.0413	0.0766	0.0072	0.0296	0.0334	0.0702	0.4352	0.5820	0.0213
13.9	0.0402	0.0754	0.0071	0.0289	0.0326	0.0686	0.4240	0.5680	0.0173
17.3	0.0396	0.0748	0.0070	0.0286	0.0322	0.0679	0.4170	0.5596	0.0148
20.6	0.0396	0.0739	0.0070	0.0282	0.0317	0.0670	0.4191	0.5601	0.0131
23.9	0.0387	0.0726	0.0069	0.0276	0.0311	0.0656	0.4098	0.5480	0.0124
27.3	0.0274	0.0444	0.0042	0.0162	0.0155	0.0360	0.3076	0.3880	0.0062
30.7	0.0352	0.0532	0.0052	0.0211	0.0223	0.0486	0.3962	0.4981	0.0070
34	0.0429	0.0605	0.0061	0.0248	0.0257	0.0567	0.4893	0.6065	0.0083
37.4	0.0437	0.0609	0.0063	0.0257	0.0278	0.0598	0.4966	0.6174	0.0086
40.7	0.0436	0.0610	0.0064	0.0260	0.0286	0.0609	0.4944	0.6163	0.0084
44.1	0.0434	0.0608	0.0064	0.0259	0.0288	0.0612	0.4920	0.6139	0.0082
47.5	0.0431	0.0605	0.0064	0.0258	0.0288	0.0610	0.4876	0.6091	0.0080
50.8	0.0426	0.0602	0.0064	0.0257	0.0287	0.0608	0.4821	0.6030	0.0079
54.2	0.0426	0.0602	0.0063	0.0251	0.0272	0.0586	0.4841	0.6029	0.0081
57.6	0.0430	0.0608	0.0064	0.0254	0.0273	0.0591	0.4880	0.6079	0.0079
60.9	0.0428	0.0609	0.0064	0.0256	0.0281	0.0601	0.4846	0.6056	0.0077
64.3	0.0427	0.0610	0.0064	0.0258	0.0285	0.0608	0.4826	0.6044	0.0077
67.7	0.0425	0.0609	0.0065	0.0258	0.0286	0.0608	0.4792	0.6008	0.0075
69.3	0.0388	0.0604	0.0051	0.0203	0.0236	0.0491	0.4399	0.5494	0.0060

G Catalyst Performance Results for Catalysts Supported on TiO_2

This appendix contains all of the catalyst performance results for the catalysts supported on TiO_2. The appendix contains 3 different tables for each catalyst analysed in the FTS set-up. The first table contains inlet compositions of N_2, CO and H_2 and total selectivities. The second table include hydrocarbon selectivities ("CO_2-free") and olefin/parafin ratios, while the third table consists of reaction rates. TOS is an abbreviation for time on stream and is given in each of the tables.

Table G.1: Space velocities, inlet compositions, CO and H_2 conversions, and total selectivities for the catalyst Co/TiO_2

		Inlet comp. (%)			Conversion (%)		Total selectivities (%)										
TOS	GHSV	N_2	CO	H_2	CO	H_2	CH_4	C2=	C2-	C3=	C3-	1-C4=	n-C4-	C4tot	S_{CO2}	C2-C4	S_{C5+}
3.2	7500	3	32.3	64.6	18.6	19.2	7.84	0.15	0.81	2.2	0.64	1.69	0.83	2.72	3.14	6.52	82.50
6.6	7500	3	32.3	64.6	17.5	18.2	8.09	0.15	0.78	2.16	0.61	1.72	0.81	2.71	1.45	6.41	84.05
9.9	7500	3	32.3	64.6	16.5	17.2	8.37	0.16	0.77	2.1	0.62	1.7	0.82	2.67	1.12	6.32	84.19
13.3	7500	3	32.3	64.6	16	16.7	8.35	0.16	0.76	2.08	0.6	1.69	0.81	2.64	0.89	6.24	84.52
16.6	7500	3	32.3	64.6	15.6	16.3	8.45	0.16	0.76	2.09	0.6	1.71	0.81	2.66	0.75	6.27	84.53
20	7500	3	32.3	64.6	15.2	15.9	8.5	0.16	0.75	2.09	0.6	1.72	0.8	2.63	0.68	6.23	84.59
23.4	7500	3	32.3	64.6	15.3	16.0	8.4	0.16	0.74	2.06	0.59	1.7	0.79	2.59	0.63	6.14	84.83
25.4	2370	3	32.3	64.6	15.2	15.9	8.39	0.17	0.73	2.05	0.58	1.68	0.78	2.56	0.61	6.09	84.91
28.7	2370	3	32.3	64.6	27.1	28.4	6.65	0.09	0.56	1.32	0.45	0.93	0.48	1.49	0.4	3.91	89.04
32.1	2370	3	32.3	64.6	56	58.7	5.28	0.04	0.49	1.02	0.45	0.63	0.45	1.16	0.27	3.16	91.29
35.4	2370	3	32.3	64.6	69.1	72.5	4.96	0.03	0.47	1	0.46	0.64	0.49	1.22	0.27	3.18	91.59
38.8	2370	3	32.3	64.6	74.1	77.7	4.83	0.03	0.46	1	0.47	0.67	0.53	1.3	0.27	3.26	91.64
42.1	2370	3	32.3	64.6	75.9	79.6	4.77	0.03	0.46	1	0.47	0.7	0.56	1.35	0.26	3.31	91.66
45.5	3000	3	32.3	64.6	76.3	80.0	4.77	0.03	0.45	1.01	0.48	0.72	0.58	1.41	0.26	3.38	91.59
48.8	3000	3	32.3	64.6	55.4	58.1	5.46	0.06	0.5	1.24	0.52	1.02	0.75	1.91	0.25	4.23	90.06
52.2	3000	3	32.3	64.6	44.3	46.5	6.11	0.07	0.54	1.39	0.54	1.14	0.78	2.07	0.25	4.61	89.03
55.5	3000	3	32.3	64.6	44.4	46.6	6.22	0.07	0.56	1.4	0.56	1.12	0.77	2.03	0.24	4.62	88.92
58.9	3000	3	32.3	64.6	48.6	51.0	6.03	0.07	0.55	1.33	0.54	1.03	0.72	1.88	0.23	4.37	89.37
62.3	3000	3	32.3	64.6	50.6	53.1	5.92	0.06	0.53	1.29	0.52	0.98	0.68	1.79	0.22	4.19	89.67
65.6	3000	3	32.3	64.6	52.3	54.9	5.82	0.06	0.53	1.27	0.52	0.97	0.67	1.76	0.21	4.14	89.83
68.9	3000	3	32.3	64.6	52.4	55.0	5.81	0.06	0.53	1.27	0.52	0.98	0.68	1.77	0.2	4.15	89.84

Table G.2: Hydrocarbon selectivities ("CO_2-free") and olefin/parafin ratios for the catalyst Co/TiO_2

	HC-selectivities ("CO_2-free")												Olefin/Parafin		
TOS	CH_4	C2=	C2-	C2tot	C3=	C3-	C3tot	1-C4=	n-C4-	C4tot	C2-C4	S_{C5+}	C2=/C2-	C3=/C3-	C4=/C4-
3.2	8.09	0.15	0.84	0.99	2.27	0.66	2.93	1.74	0.86	2.81	6.73	85.17	0.19	3.44	2.04
6.6	8.21	0.15	0.79	0.94	2.19	0.62	2.81	1.75	0.82	2.75	6.50	85.29	0.19	3.54	2.12
9.9	8.46	0.16	0.78	0.94	2.12	0.63	2.75	1.72	0.83	2.70	6.39	85.14	0.21	3.39	2.07
13.3	8.42	0.16	0.77	0.93	2.10	0.61	2.70	1.71	0.82	2.66	6.30	85.28	0.21	3.47	2.09
16.6	8.51	0.16	0.77	0.93	2.11	0.60	2.71	1.72	0.82	2.68	6.32	85.17	0.21	3.48	2.11
20	8.56	0.16	0.76	0.92	2.10	0.60	2.71	1.73	0.81	2.65	6.27	85.17	0.21	3.48	2.15
23.4	8.45	0.16	0.74	0.91	2.07	0.59	2.67	1.71	0.80	2.61	6.18	85.37	0.22	3.49	2.15
25.4	8.44	0.17	0.73	0.91	2.06	0.58	2.65	1.69	0.78	2.58	6.13	85.43	0.23	3.53	2.15
28.7	6.68	0.09	0.56	0.65	1.33	0.45	1.78	0.93	0.48	1.50	3.93	89.40	0.16	2.93	1.94
32.1	5.29	0.04	0.49	0.53	1.02	0.45	1.47	0.63	0.45	1.16	3.17	91.54	0.08	2.27	1.40
35.4	4.97	0.03	0.47	0.50	1.00	0.46	1.46	0.64	0.49	1.22	3.19	91.84	0.06	2.17	1.31
38.8	4.84	0.03	0.46	0.49	1.00	0.47	1.47	0.67	0.53	1.30	3.27	91.89	0.07	2.13	1.26
42.1	4.78	0.03	0.46	0.49	1.00	0.47	1.47	0.70	0.56	1.35	3.32	91.90	0.07	2.13	1.25
45.5	4.78	0.03	0.45	0.48	1.01	0.48	1.49	0.72	0.58	1.41	3.39	91.83	0.07	2.10	1.24
48.8	5.47	0.06	0.50	0.56	1.24	0.52	1.76	1.02	0.75	1.91	4.24	90.29	0.12	2.38	1.36
52.2	6.13	0.07	0.54	0.61	1.39	0.54	1.93	1.14	0.78	2.08	4.62	89.25	0.13	2.57	1.46
55.5	6.23	0.07	0.56	0.63	1.40	0.56	1.96	1.12	0.77	2.03	4.63	89.13	0.13	2.50	1.45
58.9	6.04	0.07	0.55	0.62	1.33	0.54	1.87	1.03	0.72	1.88	4.38	89.58	0.13	2.46	1.43
62.3	5.93	0.06	0.53	0.59	1.29	0.52	1.81	0.98	0.68	1.79	4.20	89.87	0.11	2.48	1.44
65.6	5.83	0.06	0.53	0.59	1.27	0.52	1.79	0.97	0.67	1.76	4.15	90.02	0.11	2.44	1.45
68.9	5.82	0.06	0.53	0.59	1.27	0.52	1.79	0.98	0.68	1.77	4.16	90.02	0.11	2.44	1.44

Table G.3: Reaction rates for the catalyst Co/TiO_2

TOS	Rates									
	molCO/g*h	g/g*h	g/g*h	g/g*h	g/g*h	g/g*h	g/g*h	g/g*h	g/g*h	g/g*h
	r_{CO}	r_{C1}	r_{C2}	r_{C3}	r_{C4}	r_{C2-C4}	r_{C5+}	r_{HCtot}	r_{CO2}
3.2	0.0201	0.0252	0.0029	0.0081	0.0077	0.0187	0.2322	0.2761	0.0278
6.6	0.0189	0.0245	0.0026	0.0074	0.0073	0.0173	0.2226	0.2643	0.0121
9.9	0.0178	0.0239	0.0025	0.0069	0.0067	0.0161	0.2102	0.2501	0.0088
13.3	0.0173	0.0231	0.0024	0.0066	0.0065	0.0154	0.2046	0.2431	0.0068
16.6	0.0169	0.0228	0.0023	0.0064	0.0064	0.0151	0.1995	0.2374	0.0056
20	0.0164	0.0223	0.0022	0.0063	0.0061	0.0146	0.1946	0.2315	0.0049
23.4	0.0165	0.0222	0.0022	0.0062	0.0061	0.0145	0.1964	0.2331	0.0046
25.4	0.0052	0.0070	0.0007	0.0019	0.0019	0.0045	0.0617	0.0732	0.0014
28.7	0.0093	0.0098	0.0009	0.0023	0.0020	0.0052	0.1154	0.1304	0.0016
32.1	0.0191	0.0162	0.0015	0.0040	0.0032	0.0087	0.2444	0.2693	0.0023
35.4	0.0236	0.0187	0.0018	0.0049	0.0041	0.0108	0.3026	0.3321	0.0028
38.8	0.0253	0.0196	0.0019	0.0053	0.0047	0.0118	0.3247	0.3561	0.0030
42.1	0.0259	0.0198	0.0019	0.0054	0.0050	0.0123	0.3326	0.3647	0.0030
45.5	0.0330	0.0252	0.0024	0.0070	0.0066	0.0160	0.4230	0.4641	0.0038
48.8	0.0240	0.0209	0.0020	0.0060	0.0065	0.0145	0.3020	0.3374	0.0026
52.2	0.0192	0.0187	0.0017	0.0052	0.0056	0.0126	0.2387	0.2701	0.0021
55.5	0.0192	0.0191	0.0018	0.0053	0.0055	0.0127	0.2390	0.2707	0.0020
58.9	0.0210	0.0203	0.0019	0.0056	0.0056	0.0131	0.2629	0.2963	0.0021
62.3	0.0219	0.0207	0.0019	0.0056	0.0056	0.0131	0.2746	0.3084	0.0021
65.6	0.0226	0.0211	0.0020	0.0057	0.0057	0.0134	0.2844	0.3188	0.0021
68.9	0.0227	0.0211	0.0020	0.0058	0.0057	0.0134	0.2849	0.3194	0.0020

Table G.4: Space velocities, inlet compositions, CO and H_2 conversions, and total selectivities for the catalyst $Co/Ru/TiO_2$

		Inlet comp. (%)			Conversion (%)		Total selectivities (%)										
TOS	GHSV	N_2	CO	H_2	CO	H_2	CH_4	C2=	C2-	C3=	C3-	1-C4=	n-C4-	C4tot	S_{CO2}	C2-C4	S_{C5+}
4.9	7500	3	32.3	64.6	19.3	20.1	8.1	0.13	0.51	1.74	0.53	1.63	0.76	2.53	2.01	5.44	84.45
8.3	7500	3	32.3	64.6	15.5	16.2	9.06	0.15	0.54	1.83	0.59	1.8	0.88	2.76	1.46	5.87	83.61
11.6	7500	3	32.3	64.6	13.8	14.4	9.42	0.16	0.53	1.87	0.6	1.86	0.9	2.83	1.21	5.99	83.38
15	7500	3	32.3	64.6	12.8	13.4	9.75	0.17	0.53	1.91	0.61	1.92	0.92	2.92	1.05	6.14	83.06
18.3	7500	3	32.3	64.6	12.1	12.6	9.93	0.18	0.53	1.93	0.61	1.96	0.93	2.96	0.95	6.21	82.91
21.7	7500	3	32.3	64.6	11.5	12.0	10.06	0.19	0.53	1.94	0.61	1.99	0.94	2.99	0.88	6.26	82.80
27	1740	3	32.3	64.6	11.1	11.6	10.21	0.19	0.53	1.99	0.62	2.01	0.94	3.01	0.86	6.34	82.59
30.4	1740	3	32.3	64.6	13.3	13.9	9.41	0.16	0.48	1.7	0.55	1.64	0.76	2.46	0.77	5.35	84.47
33.8	1740	3	32.3	64.6	32.1	33.6	6.21	0.06	0.29	0.74	0.28	0.57	0.28	0.88	0.45	2.25	91.09
37.1	1740	3	32.3	64.6	55.9	58.6	5.24	0.03	0.25	0.48	0.21	0.28	0.15	0.45	0.38	1.42	92.96
40.4	1740	3	32.3	64.6	70.4	73.8	5	0.02	0.24	0.44	0.21	0.22	0.13	0.37	0.37	1.28	93.35
43.8	1740	3	32.3	64.6	77.5	81.2	4.96	0.02	0.25	0.46	0.24	0.21	0.14	0.38	0.38	1.35	93.31
47.1	2700	3	32.3	64.6	81.1	85.0	5.19	0.02	0.31	0.63	0.36	0.32	0.25	0.6	0.41	1.92	92.48
50.5	2700	3	32.3	64.6	65.7	68.9	6.07	0.04	0.39	0.97	0.57	0.81	0.71	1.61	0.39	3.58	89.96
53.9	2700	3	32.3	64.6	52	54.5	7.08	0.05	0.46	1.25	0.72	1.15	1	2.29	0.34	4.77	87.81
57.2	2700	3	32.3	64.6	43.8	45.9	7.69	0.06	0.48	1.33	0.74	1.34	1.14	2.62	0.3	5.23	86.78
60.6	2700	3	32.3	64.6	40.6	42.6	8	0.07	0.48	1.35	0.74	1.39	1.16	2.69	0.29	5.33	86.38
63.9	2700	3	32.3	64.6	41.2	43.2	8.02	0.07	0.47	1.24	0.68	1.28	1.06	2.47	0.28	4.93	86.77
67.3	2700	3	32.3	64.6	40.7	42.7	8.06	0.07	0.47	1.22	0.66	1.24	1.03	2.4	0.27	4.82	86.85
70.6	2700	3	32.3	64.6	39.8	41.7	8.16	0.07	0.47	1.23	0.66	1.25	1.03	2.4	0.26	4.83	86.75

Table G.5: Hydrocarbon selectivities ("CO_2-free") and olefin/parafin ratios for the catalyst Co/Ru/TiO_2

	HC-selectivities ("CO_2-free")												Olefin/Parafin		
TOS	CH_4	C2=	C2-	C2tot	C3=	C3-	C3tot	1-C4=	n-C4-	C4tot	C2-C4	S_{C5+}	C2=/C2-	C3=/C3-	C4=/C4-
4.9	8.27	0.13	0.52	0.65	1.78	0.54	2.32	1.66	0.78	2.58	5.55	86.18	0.25	3.28	2.14
8.3	9.19	0.15	0.55	0.70	1.86	0.60	2.46	1.83	0.89	2.80	5.96	84.85	0.28	3.10	2.05
11.6	9.54	0.16	0.54	0.70	1.89	0.61	2.50	1.88	0.91	2.86	6.06	84.40	0.30	3.12	2.07
15	9.85	0.17	0.54	0.71	1.93	0.62	2.55	1.94	0.93	2.95	6.21	83.94	0.32	3.13	2.09
18.3	10.03	0.18	0.54	0.72	1.95	0.62	2.56	1.98	0.94	2.99	6.27	83.71	0.34	3.16	2.11
21.7	10.15	0.19	0.53	0.73	1.96	0.62	2.57	2.01	0.95	3.02	6.32	83.54	0.36	3.18	2.12
27	10.30	0.19	0.53	0.73	2.01	0.63	2.63	2.03	0.95	3.04	6.39	83.31	0.36	3.21	2.14
30.4	9.48	0.16	0.48	0.64	1.71	0.55	2.27	1.65	0.77	2.48	5.39	85.13	0.33	3.09	2.16
33.8	6.24	0.06	0.29	0.35	0.74	0.28	1.02	0.57	0.28	0.88	2.26	91.50	0.21	2.64	2.04
37.1	5.26	0.03	0.25	0.28	0.48	0.21	0.69	0.28	0.15	0.45	1.43	93.31	0.12	2.29	1.87
40.4	5.02	0.02	0.24	0.26	0.44	0.21	0.65	0.22	0.13	0.37	1.28	93.70	0.08	2.10	1.69
43.8	4.98	0.02	0.25	0.27	0.46	0.24	0.70	0.21	0.14	0.38	1.36	93.67	0.08	1.92	1.50
47.1	5.21	0.02	0.31	0.33	0.63	0.36	0.99	0.32	0.25	0.60	1.93	92.86	0.06	1.75	1.28
50.5	6.09	0.04	0.39	0.43	0.97	0.57	1.55	0.81	0.71	1.62	3.59	90.31	0.10	1.70	1.14
53.9	7.10	0.05	0.46	0.51	1.25	0.72	1.98	1.15	1.00	2.30	4.79	88.11	0.11	1.74	1.15
57.2	7.71	0.06	0.48	0.54	1.33	0.74	2.08	1.34	1.14	2.63	5.25	87.04	0.13	1.80	1.18
60.6	8.02	0.07	0.48	0.55	1.35	0.74	2.10	1.39	1.16	2.70	5.35	86.63	0.15	1.82	1.20
63.9	8.04	0.07	0.47	0.54	1.24	0.68	1.93	1.28	1.06	2.48	4.94	87.01	0.15	1.82	1.21
67.3	8.08	0.07	0.47	0.54	1.22	0.66	1.89	1.24	1.03	2.41	4.83	87.09	0.15	1.85	1.20
70.6	8.18	0.07	0.47	0.54	1.23	0.66	1.89	1.25	1.03	2.41	4.84	86.98	0.15	1.86	1.21

Table G.6: Reaction rates for the catalyst $Co/Ru/TiO_2$

TOS	Rates									
	molCO/g*h	g/g*h	g/g*h	g/g*h	g/g*h	g/g*h	g/g*h	g/g*h	g/g*h	g/g*h
	r_{CO}	r_{C1}	r_{C2}	r_{C3}	r_{C4}	r_{C2-C4}	r_{C5+}	r_{HCtot}	r_{CO2}
4.9	0.0209	0.0270	0.0020	0.0067	0.0075	0.0162	0.2466	0.2898	0.0184
8.3	0.0168	0.0243	0.0017	0.0057	0.0065	0.0140	0.1961	0.2344	0.0108
11.6	0.0149	0.0225	0.0015	0.0052	0.0060	0.0127	0.1741	0.2093	0.0079
15	0.0138	0.0216	0.0014	0.0049	0.0057	0.0121	0.1609	0.1945	0.0064
18.3	0.0131	0.0208	0.0014	0.0047	0.0055	0.0116	0.1518	0.1841	0.0055
21.7	0.0124	0.0200	0.0013	0.0045	0.0053	0.0111	0.1441	0.1752	0.0048
27	0.0028	0.0045	0.0003	0.0010	0.0012	0.0025	0.0322	0.0392	0.0011
30.4	0.0033	0.0050	0.0003	0.0011	0.0012	0.0025	0.0394	0.0470	0.0011
33.8	0.0080	0.0080	0.0004	0.0012	0.0010	0.0026	0.1026	0.1132	0.0016
37.1	0.0140	0.0118	0.0006	0.0014	0.0009	0.0029	0.1824	0.1970	0.0023
40.4	0.0177	0.0141	0.0007	0.0016	0.0009	0.0032	0.2307	0.2481	0.0029
43.8	0.0194	0.0154	0.0008	0.0019	0.0010	0.0038	0.2539	0.2730	0.0032
47.1	0.0316	0.0262	0.0016	0.0045	0.0027	0.0087	0.4085	0.4435	0.0057
50.5	0.0256	0.0248	0.0016	0.0056	0.0059	0.0131	0.3220	0.3599	0.0044
53.9	0.0202	0.0229	0.0015	0.0057	0.0066	0.0138	0.2487	0.2855	0.0030
57.2	0.0170	0.0210	0.0014	0.0050	0.0064	0.0128	0.2070	0.2408	0.0022
60.6	0.0158	0.0202	0.0013	0.0047	0.0060	0.0120	0.1910	0.2233	0.0020
63.9	0.0160	0.0206	0.0013	0.0044	0.0056	0.0113	0.1947	0.2266	0.0020
67.3	0.0158	0.0204	0.0013	0.0042	0.0054	0.0109	0.1925	0.2239	0.0019
70.6	0.0155	0.0202	0.0012	0.0042	0.0053	0.0107	0.1881	0.2190	0.0018

Table G.7: Space velocities, inlet compositions, CO and H_2 conversions, and total selectivities for the catalyst $Co/Re/TiO_2$

		Inlet comp. (%)			Conversion (%)		Total selectivities (%)										
TOS	GHSV	N_2	CO	H_2	CO	H_2	CH_4	C2=	C2-	C3=	C3-	1-C4=	n-C4-	C4tot	S_{CO2}	C2-C4	S_{C5+}
5.7	7500	3	32.3	64.6	25.4	26.5	6.56	0.11	0.53	1.54	0.45	1.29	0.63	2.03	1.25	4.66	87.53
9.1	7500	3	32.3	64.6	23	24.0	6.85	0.12	0.53	1.55	0.45	1.33	0.63	2.06	0.88	4.71	87.56
12.4	7500	3	32.3	64.6	21.8	22.8	6.92	0.12	0.52	1.55	0.44	1.33	0.62	2.05	0.7	4.68	87.70
15.8	7500	3	32.3	64.6	21	22.0	6.89	0.12	0.51	1.54	0.43	1.34	0.6	2.03	0.6	4.63	87.88
19.2	7500	3	32.3	64.6	20.2	21.2	6.98	0.13	0.51	1.55	0.43	1.36	0.6	2.03	0.54	4.65	87.83
22.5	7500	3	32.3	64.6	20.3	21.3	6.98	0.13	0.51	1.54	0.42	1.35	0.6	2.01	0.5	4.61	87.91
27.9	3180	3	32.3	64.6	38.4	40.3	5.52	0.06	0.41	1.03	0.34	0.75	0.38	1.19	0.29	3.03	91.16
31.2	3180	3	32.3	64.6	62.7	65.8	4.73	0.04	0.38	0.94	0.37	0.71	0.45	1.23	0.25	2.96	92.06
34.6	3180	3	32.3	64.6	66.2	69.4	4.56	0.04	0.36	0.92	0.36	0.73	0.47	1.28	0.26	2.96	92.22
37.9	3180	3	32.3	64.6	66.6	69.8	4.48	0.04	0.35	0.91	0.35	0.74	0.47	1.29	0.27	2.94	92.31
41.3	3180	3	32.3	64.6	66.3	69.5	4.44	0.04	0.35	0.91	0.35	0.75	0.47	1.29	0.28	2.94	92.34
44.6	3180	3	32.3	64.6	65.6	68.8	4.42	0.04	0.35	0.9	0.35	0.75	0.47	1.3	0.3	2.94	92.34
48	3750	3	32.3	64.6	52.3	54.8	4.81	0.06	0.36	1.04	0.37	0.94	0.55	1.58	0.28	3.41	91.50
51.3	3750	3	32.3	64.6	44.9	47.1	5.18	0.07	0.38	1.11	0.36	0.99	0.54	1.62	0.24	3.54	91.04
54.7	3750	3	32.3	64.6	45.6	47.8	5.19	0.07	0.38	1.08	0.35	0.93	0.5	1.51	0.22	3.39	91.20
58.1	3750	3	32.3	64.6	46.5	48.8	5.19	0.07	0.38	1.08	0.35	0.91	0.49	1.48	0.21	3.36	91.24
61.4	3750	3	32.3	64.6	47.4	49.7	5.15	0.07	0.38	1.07	0.35	0.91	0.48	1.47	0.21	3.34	91.30
64.8	3750	3	32.3	64.6	48.3	50.7	5.1	0.07	0.37	1.06	0.35	0.9	0.48	1.46	0.21	3.31	91.38
68.1	3750	3	32.3	64.6	48.1	50.5	5.11	0.07	0.37	1.05	0.35	0.9	0.48	1.46	0.2	3.30	91.39

Table G.8: Hydrocarbon selectivities ("CO_2-free") and olefin/parafin ratios for the catalyst Co/Re/TiO_2

	HC-selectivities ("CO_2-free")												Olefin/Parafin		
TOS	CH_4	C2=	C2-	C2tot	C3=	C3-	C3tot	1-C4=	n-C4-	C4tot	C2-C4	S_{C5+}	C2=/C2-	C3=/C3-	C4=/C4-
5.7	6.64	0.11	0.54	0.65	1.56	0.46	2.02	1.31	0.64	2.06	4.72	88.64	0.21	3.42	2.05
9.1	6.91	0.12	0.53	0.66	1.56	0.45	2.02	1.34	0.64	2.08	4.75	88.34	0.23	3.44	2.11
12.4	6.97	0.12	0.52	0.64	1.56	0.44	2.00	1.34	0.62	2.06	4.71	88.32	0.23	3.52	2.15
15.8	6.93	0.12	0.51	0.63	1.55	0.43	1.98	1.35	0.60	2.04	4.66	88.41	0.24	3.58	2.23
19.2	7.02	0.13	0.51	0.64	1.56	0.43	1.99	1.37	0.60	2.04	4.68	88.31	0.25	3.60	2.27
22.5	7.02	0.13	0.51	0.64	1.55	0.42	1.97	1.36	0.60	2.02	4.63	88.35	0.25	3.67	2.25
27.9	5.54	0.06	0.41	0.47	1.03	0.34	1.37	0.75	0.38	1.19	3.04	91.43	0.15	3.03	1.97
31.2	4.74	0.04	0.38	0.42	0.94	0.37	1.31	0.71	0.45	1.23	2.97	92.29	0.11	2.54	1.58
34.6	4.57	0.04	0.36	0.40	0.92	0.36	1.28	0.73	0.47	1.28	2.97	92.46	0.11	2.56	1.55
37.9	4.49	0.04	0.35	0.39	0.91	0.35	1.26	0.74	0.47	1.29	2.95	92.56	0.11	2.60	1.57
41.3	4.45	0.04	0.35	0.39	0.91	0.35	1.26	0.75	0.47	1.29	2.95	92.60	0.11	2.60	1.60
44.6	4.43	0.04	0.35	0.39	0.90	0.35	1.25	0.75	0.47	1.30	2.95	92.62	0.11	2.57	1.60
48	4.82	0.06	0.36	0.42	1.04	0.37	1.41	0.94	0.55	1.58	3.42	91.76	0.17	2.81	1.71
51.3	5.19	0.07	0.38	0.45	1.11	0.36	1.47	0.99	0.54	1.62	3.55	91.26	0.18	3.08	1.83
54.7	5.20	0.07	0.38	0.45	1.08	0.35	1.43	0.93	0.50	1.51	3.40	91.40	0.18	3.09	1.86
58.1	5.20	0.07	0.38	0.45	1.08	0.35	1.43	0.91	0.49	1.48	3.37	91.43	0.18	3.09	1.86
61.4	5.16	0.07	0.38	0.45	1.07	0.35	1.42	0.91	0.48	1.47	3.35	91.49	0.18	3.06	1.90
64.8	5.11	0.07	0.37	0.44	1.06	0.35	1.41	0.90	0.48	1.46	3.32	91.57	0.19	3.03	1.88
68.1	5.12	0.07	0.37	0.44	1.05	0.35	1.40	0.90	0.48	1.46	3.31	91.57	0.19	3.00	1.88

Table G.9: Reaction rates for the catalyst Co/Re/TiO_2

TOS	Rates									
	molCO/g*h	g/g*h	g/g*h	g/g*h	g/g*h	g/g*h	g/g*h	g/g*h	g/g*h	g/g*h
	r_{CO}	r_{C1}	r_{C2}	r_{C3}	r_{C4}	r_{C2-C4}	r_{C5+}	r_{HCtot}	r_{CO2}
5.7	0.0275	0.0288	0.0026	0.0077	0.0079	0.0182	0.3364	0.3835	0.0151
9.1	0.0249	0.0272	0.0024	0.0070	0.0073	0.0167	0.3047	0.3487	0.0096
12.4	0.0236	0.0261	0.0022	0.0066	0.0068	0.0157	0.2893	0.3311	0.0073
15.8	0.0227	0.0250	0.0021	0.0063	0.0065	0.0150	0.2792	0.3192	0.0060
19.2	0.0218	0.0244	0.0021	0.0061	0.0063	0.0145	0.2685	0.3073	0.0052
22.5	0.0219	0.0245	0.0021	0.0061	0.0062	0.0144	0.2700	0.3089	0.0048
27.9	0.0176	0.0155	0.0012	0.0034	0.0030	0.0076	0.2246	0.2477	0.0022
31.2	0.0287	0.0217	0.0018	0.0053	0.0050	0.0122	0.3703	0.4042	0.0032
34.6	0.0303	0.0221	0.0018	0.0055	0.0055	0.0128	0.3917	0.4266	0.0035
37.9	0.0305	0.0219	0.0018	0.0055	0.0056	0.0128	0.3944	0.4291	0.0036
41.3	0.0304	0.0216	0.0018	0.0054	0.0056	0.0128	0.3928	0.4271	0.0037
44.6	0.0301	0.0213	0.0017	0.0053	0.0055	0.0126	0.3886	0.4225	0.0040
48	0.0283	0.0218	0.0018	0.0057	0.0063	0.0138	0.3620	0.3975	0.0035
51.3	0.0243	0.0201	0.0016	0.0051	0.0056	0.0122	0.3093	0.3416	0.0026
54.7	0.0246	0.0205	0.0016	0.0050	0.0053	0.0119	0.3146	0.3470	0.0024
58.1	0.0251	0.0209	0.0017	0.0051	0.0053	0.0120	0.3210	0.3539	0.0023
61.4	0.0256	0.0211	0.0017	0.0052	0.0053	0.0122	0.3274	0.3607	0.0024
64.8	0.0261	0.0213	0.0017	0.0052	0.0054	0.0123	0.3339	0.3675	0.0024
68.1	0.0260	0.0213	0.0017	0.0052	0.0054	0.0122	0.3326	0.3661	0.0023
70.6	0.0155	0.0202	0.0012	0.0042	0.0053	0.0107	0.1881	0.2190	0.0018

Table G.10: Space velocities, inlet compositions, CO and H_2 conversions, and total selectivities for the catalyst $Co/Pt/TiO_2$

		Inlet comp. (%)			Conversion (%)		Total selectivities (%)										
TOS	GHSV	N_2	CO	H_2	CO	H_2	CH_4	C2=	C2-	C3=	C3-	1-C4=	n-C4-	C4tot	S_{CO2}	C2-C4	S_{C5+}
4.1	7500	3	32.3	64.6	26	27.0	7.46	0.08	0.62	1.5	0.56	1.19	0.75	2.09	2.38	4.85	85.31
7.4	7500	3	32.3	64.6	21.4	22.3	7.82	0.09	0.61	1.51	0.54	1.25	0.74	2.12	1.57	4.87	85.74
10.8	7500	3	32.3	64.6	20.3	21.2	7.91	0.1	0.59	1.5	0.52	1.26	0.72	2.1	1.25	4.81	86.03
14.1	7500	3	32.3	64.6	19.5	20.4	8.08	0.1	0.59	1.51	0.52	1.28	0.72	2.12	1.08	4.84	86.00
17.5	7500	3	32.3	64.6	19	19.9	8.14	0.1	0.59	1.51	0.52	1.29	0.72	2.12	0.96	4.84	86.06
20.8	7500	3	32.3	64.6	18.7	19.6	8.12	0.1	0.58	1.49	0.51	1.29	0.71	2.08	0.89	4.76	86.23
24.2	7500	3	32.3	64.6	18.4	19.2	8.28	0.1	0.58	1.5	0.51	1.3	0.72	2.12	0.85	4.81	86.06
26.2	2850	3	32.3	64.6	18.2	19.0	8.33	0.1	0.59	1.51	0.51	1.3	0.72	2.12	0.84	4.83	86.00
29.6	2850	3	32.3	64.6	39.6	41.4	5.95	0.04	0.41	0.82	0.37	0.57	0.37	0.99	1.02	2.63	90.40
32.9	2850	3	32.3	64.6	67.6	70.6	4.9	0.02	0.37	0.68	0.39	0.44	0.41	0.92	1.16	2.38	91.56
36.3	2850	3	32.3	64.6	76.7	80.0	4.64	0.02	0.36	0.67	0.41	0.45	0.46	0.99	1.28	2.45	91.63
39.6	2850	3	32.3	64.6	79.4	82.8	4.52	0.02	0.35	0.67	0.42	0.47	0.5	1.05	1.35	2.51	91.62
43	2850	3	32.3	64.6	80.2	83.7	4.44	0.02	0.35	0.67	0.42	0.48	0.51	1.08	1.37	2.54	91.65
46.3	3900	3	32.3	64.6	74.3	77.5	4.49	0.03	0.36	0.73	0.44	0.58	0.61	1.3	1.38	2.86	91.27
49.7	3900	3	32.3	64.6	50.6	52.9	5.2	0.06	0.42	0.97	0.45	0.83	0.69	1.64	0.82	3.54	90.44
53	3900	3	32.3	64.6	43.3	45.3	5.59	0.07	0.43	1.04	0.44	0.88	0.65	1.65	0.6	3.63	90.18
56.4	3900	3	32.3	64.6	40.8	42.7	5.75	0.07	0.43	1.04	0.42	0.86	0.59	1.56	0.55	3.52	90.18
59.7	3900	3	32.3	64.6	39.6	41.5	5.85	0.07	0.44	1.05	0.42	0.86	0.58	1.53	0.54	3.51	90.10
63.1	3900	3	32.3	64.6	47.2	49.4	5.52	0.06	0.42	0.98	0.41	0.77	0.55	1.41	0.55	3.28	90.65
66.4	3900	3	32.3	64.6	47.8	50.1	5.49	0.06	0.42	0.97	0.41	0.78	0.55	1.43	0.54	3.29	90.68
69.8	3900	3	32.3	64.6	47.6	49.9	5.49	0.06	0.42	0.97	0.41	0.79	0.55	1.43	0.54	3.29	90.68

Table G.11: Hydrocarbon selectivities ("CO_2-free") and olefin/parafin ratios for the catalyst Co/Pt/TiO_2

	HC-selectivities ("CO_2-free")												Olefin/Parafin		
TOS	CH_4	C2=	C2-	C2tot	C3=	C3-	C3tot	1-C4=	n-C4-	C4tot	C2-C4	S_{C5+}	C2=/C2-	C3=/C3-	C4=/C4-
4.1	7.64	0.08	0.64	0.72	1.54	0.57	2.11	1.22	0.77	2.14	4.97	87.39	0.13	2.68	1.59
7.4	7.94	0.09	0.62	0.71	1.53	0.55	2.08	1.27	0.75	2.15	4.95	87.11	0.15	2.80	1.69
10.8	8.01	0.10	0.60	0.70	1.52	0.53	2.05	1.28	0.73	2.13	4.87	87.12	0.17	2.88	1.75
14.1	8.17	0.10	0.60	0.70	1.53	0.53	2.05	1.29	0.73	2.14	4.89	86.94	0.17	2.90	1.78
17.5	8.22	0.10	0.60	0.70	1.52	0.53	2.05	1.30	0.73	2.14	4.89	86.89	0.17	2.90	1.79
20.8	8.19	0.10	0.59	0.69	1.50	0.51	2.02	1.30	0.72	2.10	4.80	87.00	0.17	2.92	1.82
24.2	8.35	0.10	0.58	0.69	1.51	0.51	2.03	1.31	0.73	2.14	4.85	86.80	0.17	2.94	1.81
26.2	8.40	0.10	0.59	0.70	1.52	0.51	2.04	1.31	0.73	2.14	4.87	86.73	0.17	2.96	1.81
29.6	6.01	0.04	0.41	0.45	0.83	0.37	1.20	0.58	0.37	1.00	2.66	91.33	0.10	2.22	1.54
32.9	4.96	0.02	0.37	0.39	0.69	0.39	1.08	0.45	0.41	0.93	2.41	92.63	0.05	1.74	1.07
36.3	4.70	0.02	0.36	0.38	0.68	0.42	1.09	0.46	0.47	1.00	2.48	92.82	0.06	1.63	0.98
39.6	4.58	0.02	0.35	0.38	0.68	0.43	1.10	0.48	0.51	1.06	2.54	92.87	0.06	1.60	0.94
43	4.50	0.02	0.35	0.38	0.68	0.43	1.11	0.49	0.52	1.10	2.58	92.92	0.06	1.60	0.94
46.3	4.55	0.03	0.37	0.40	0.74	0.45	1.19	0.59	0.62	1.32	2.90	92.55	0.08	1.66	0.95
49.7	5.24	0.06	0.42	0.48	0.98	0.45	1.43	0.84	0.70	1.65	3.57	91.19	0.14	2.16	1.20
53	5.62	0.07	0.43	0.50	1.05	0.44	1.49	0.89	0.65	1.66	3.65	90.72	0.16	2.36	1.35
56.4	5.78	0.07	0.43	0.50	1.05	0.42	1.47	0.86	0.59	1.57	3.54	90.68	0.16	2.48	1.46
59.7	5.88	0.07	0.44	0.51	1.06	0.42	1.48	0.86	0.58	1.54	3.53	90.59	0.16	2.50	1.48
63.1	5.55	0.06	0.42	0.48	0.99	0.41	1.40	0.77	0.55	1.42	3.30	91.15	0.14	2.39	1.40
66.4	5.52	0.06	0.42	0.48	0.98	0.41	1.39	0.78	0.55	1.44	3.31	91.17	0.14	2.37	1.42
69.8	5.52	0.06	0.42	0.48	0.98	0.41	1.39	0.79	0.55	1.44	3.31	91.17	0.14	2.37	1.44

Table G.12: Reaction rates for the catalyst $Co/Pt/TiO_2$

TOS	Rates									
	molCO/g*h	g/g*h	g/g*h	g/g*h	g/g*h	g/g*h	g/g*h	g/g*h	g/g*h	g/g*h
	r_{CO}	r_{C1}	r_{C2}	r_{C3}	r_{C4}	r_{C2-C4}	r_{C5+}	r_{HCtot}	r_{CO2}
4.1	0.0281	0.0335	0.0029	0.0082	0.0083	0.0195	0.3356	0.3886	0.0294
7.4	0.0231	0.0289	0.0024	0.0067	0.0070	0.0161	0.2776	0.3227	0.0160
10.8	0.0219	0.0278	0.0022	0.0063	0.0065	0.0151	0.2643	0.3071	0.0121
14.1	0.0211	0.0272	0.0022	0.0061	0.0063	0.0146	0.2537	0.2956	0.0100
17.5	0.0205	0.0267	0.0021	0.0059	0.0062	0.0142	0.2474	0.2883	0.0087
20.8	0.0202	0.0263	0.0020	0.0057	0.0060	0.0137	0.2440	0.2840	0.0079
24.2	0.0199	0.0263	0.0020	0.0057	0.0060	0.0137	0.2396	0.2796	0.0074
26.2	0.0075	0.0100	0.0008	0.0021	0.0022	0.0052	0.0900	0.1051	0.0028
29.6	0.0163	0.0155	0.0011	0.0028	0.0023	0.0061	0.2058	0.2274	0.0073
32.9	0.0278	0.0218	0.0016	0.0042	0.0036	0.0095	0.3559	0.3871	0.0142
36.3	0.0315	0.0234	0.0018	0.0049	0.0044	0.0111	0.4041	0.4386	0.0177
39.6	0.0326	0.0236	0.0018	0.0051	0.0049	0.0118	0.4183	0.4536	0.0194
43	0.0329	0.0234	0.0018	0.0051	0.0051	0.0120	0.4226	0.4580	0.0199
46.3	0.0418	0.0300	0.0024	0.0070	0.0077	0.0171	0.5336	0.5807	0.0254
49.7	0.0284	0.0237	0.0020	0.0057	0.0066	0.0144	0.3601	0.3981	0.0103
53	0.0243	0.0218	0.0018	0.0051	0.0057	0.0126	0.3072	0.3416	0.0064
56.4	0.0229	0.0211	0.0017	0.0048	0.0051	0.0115	0.2895	0.3221	0.0055
59.7	0.0223	0.0208	0.0017	0.0046	0.0048	0.0112	0.2807	0.3127	0.0053
63.1	0.0265	0.0234	0.0019	0.0052	0.0053	0.0124	0.3367	0.3725	0.0064
66.4	0.0269	0.0236	0.0019	0.0053	0.0055	0.0126	0.3410	0.3773	0.0064
69.8	0.0268	0.0235	0.0019	0.0052	0.0054	0.0126	0.3396	0.3757	0.0064

H Risk Assessment

Detailed Risk Report

ID	40074	**Status**	**Date**
Risk Area	Risikovurdering: Helse, miljø og sikkerhet (HMS)	Created	15.09.2020
Created by	Vilde Rolland Svensen	Assessment started	15.09.2020
Responsible	Vilde Rolland Svensen	Measures decided	
		Closed	

Risk Assessment:

CAT, master student, 2021, Vilde Rolland Svensen

Valid from-to date:
9/15/2020 - 9/15/2023

Location:
NTNU Gløshaugen, Chemistry Hall D, K5-420, K5-425, K2-113, K5-317

Goal / purpose
Risk assess my work as master student

Background

In this project I will investigate the effect of promoters (Ru, Re and Pt) on cobalt catalysts for the Fischer-Tropsch synthesis. The project contains catalyst preparation, characterization and catalyst testing (FTS experiments).

List of instruments:
- High Temperature Furnace (HTF)
- Calcination furnace
- BET instrument
- XRF instrument
- Chemisorption instrument
- XRD instrument
- TPR instrument
- Fischer- Tropsch rig

List of methods:
- Incipient wetness impregnation
- Drying at 120 degrees celsius
- Calcination at 350-700 degrees celsius
- BET
- XRF
- Chemisorption
- XRD (XRD Contact person – Materials Dept - Maria Tsoutsouva (maria.tsoutsouva@ntnu.no))
- TPR
- Fischer-Tropsch Synthesis

About the Fischer-Tropsch rig:
- Rig nr. 1.6
- Temperature 200 - 230 ° C (typically 210 ° C)
- Pressure 20 - 30 bar (typically 20 bar)
- Emergency stop:
  General: CO detector if cut power on the rig at high alarm (60 ppm). Other emergency stop: Press the red emergency stop button on the fuse box inside the rig. Close any gas cylinders. Notify device manager.

List of chemicals (cleaning and waste handling):
- Perrhenic acid solution (acid liquid container in fume hood)
- Chloroplatinic acid (acid liquid container in fume hood)
- Tetraammine platinum nitrate (heavy metals container)
- Ruthenium(III)nitrosyl nitrate solution (heavy metals container)
- Cobalt(II) nitrate hexahydrate (heavy metals container)
- Aluminium oxide (minerale garbage)
- Titanium dioxide p25 (minerale garbage)
- Boric acid (Inorganic solid waste with heavy metals if pellet is made with catalyst, if not; without heavy metals)
- Liquid nitrogen (BET)
- H2 gas (Chemisorption and FTS)
- CO gas (FTS)
- Silicon carbide (minerale garbage)
- Nitric acid (acid liquid container in fume hood)
- Silveroxide (Inorganic solid waste)

Description and limitations

Focus on health and safety:
Read SDS
Proper training

Prerequesites, assumptions and simplifications

Regarding the risk assesment connected to the use of the FTS rig, I am referring to already done risk assesment for FTS experiment (SINTEF).
Flowsheet chart is also given in the SINTEF risk assessment.

Safety measures related to spread of covid19 infection:
- Avoid touching the face
- Disinfection before and after with ethanol/solvent on all surfaces you are in contact with (door knob – card reader with code panel – if you use common equipment - keyboard – mouse – screen – desk)
- Keep 1m distance from colleagues
- Use nitrile gloves when touching shared lab set-ups and equipment
- Wash hands as often as possible
- Update the IKP Lab activity 2020 Teams excel sheet about your weekly planning. A week in advance.

Attachments

Perrhenic acid solution.pdf
Nitrogen.pdf
Chloroplatinic acid solution.pdf
Kobolt(II)nitrat heksahydrat.pdf
Hydrogen.pdf
Karbonmonoksid.pdf
Aluminium oxide.pdf
Risikovurdering Rigg 1_6 okt 2019 (2) and flowchart.xlsm
Ruthenium(III) nitrosyl nitrate solution.pdf
Tetraamineplatinum(II) nitrate.pdf
Boric acid.pdf
TiO2.pdf
1.6_Apparatus card.pdf
SiC.pdf
Nitric acid.pdf
Ag2O.pdf

References

[Ingen registreringer]

Summary, result and final evaluation

The summary presents an overview of hazards and incidents, in addtition to risk result for each consequence area.

Hazard:	**Exposure of Chemicals**			
Incident:	**Exposure of carbonmonoxide**			
Consequence area:	Helse	Risk before measures:	Risiko after measures:	
	Ytre miljø	Risk before measures:	Risiko after measures:	
	Materielle verdier	Risk before measures:	Risiko after measures:	
Incident:	**Exposure of Cobalt(II) nitrate hexahydrate**			
Consequence area:	Helse	Risk before measures:	Risiko after measures:	
	Ytre miljø	Risk before measures:	Risiko after measures:	
	Materielle verdier	Risk before measures:	Risiko after measures:	
	Omdømme	Risk before measures:	Risiko after measures:	
Incident:	**Exposure of hydrogen**			
Consequence area:	Helse	Risk before measures:	Risiko after measures:	
	Ytre miljø	Risk before measures:	Risiko after measures:	
	Materielle verdier	Risk before measures:	Risiko after measures:	
Incident:	**Exposure of nitrogen**			
Consequence area:	Helse	Risk before measures:	Risiko after measures:	
Incident:	**Exposure of Chloroplatinic acid solution**			
Consequence area:	Helse	Risk before measures:	Risiko after measures:	

Hazard:	**Exposure of Chemicals**				
Incident:	**Exposure of Perrhenic acid solution**				
Consequence area:	Helse	Risk before measures:	Risiko after measures:		
Incident:	**Exposure of Aluminium Oxide**				
Consequence area:	Helse	Risk before measures:	Risiko after measures:		
Incident:	**Exposure of tetraamineplatinum(II) nitrate**				
Consequence area:	Helse	Risk before measures:	Risiko after measures:		
Incident:	**Exposure of Ruthenium(III) nitrosyl nitrate solution**				
Consequence area:	Helse	Risk before measures:	Risiko after measures:		
Incident:	**Exposure of boric acid**				
Consequence area:	Helse	Risk before measures:	Risiko after measures:		
Incident:	**Exposure of titanium dioxide**				
Consequence area:	Helse	Risk before measures:	Risiko after measures:		
Incident:	**Exposure of silicon carbide**				
Consequence area:	Helse	Risk before measures:	Risiko after measures:		
Incident:	**Exposure of nitric acid (68%)**				
Consequence area:	Helse	Risk before measures:	Risiko after measures:		

Hazard:	**Exposure of Chemicals**			
Incident:	**Exposure of silver oxide**			
Consequence area:	Helse	Risk before measures:	Risiko after measures:	
	Materielle verdier	Risk before measures:	Risiko after measures:	
Hazard:	**Calcination furnace**			
Incident:	**Burns**			
Consequence area:	Helse	Risk before measures:	Risiko after measures:	
Incident:	**Spills and accidents**			
Consequence area:	Materielle verdier	Risk before measures:	Risiko after measures:	
Incident:	**Fire**			
Consequence area:	Helse	Risk before measures:	Risiko after measures:	
	Materielle verdier	Risk before measures:	Risiko after measures:	
Hazard:	**Spread of covid19 infection**			
Incident:	**Spread of covid19 infection**			
Consequence area:	Helse	Risk before measures:	Risiko after measures:	
	Ytre miljø	Risk before measures:	Risiko after measures:	

Final evaluation

Organizational units and people involved

A risk assessment may apply to one or more organizational units, and involve several people. These are lsited below.

Organizational units which this risk assessment applies to

- NTNU

Participants

Readers

Edd Anders Blekkan

Estelle Marie M. Vanhaecke

Karin Wiggen Dragsten

Ingeborg-Helene Svenum

Anne Hoff

Gunn Torill Wikdahl

Others involved/stakeholders

[Ingen registreringer]

The following accept criteria have been decided for the risk area Risikovurdering: Helse, miljø og sikkerhet (HMS):

Helse	Materielle verdier	Omdømme	Ytre miljø
			

Overview of existing relevant measures which have been taken into account

The table below presents existing measures which have been take into account when assessing the likelihood and consequence of relevant incidents.

Hazard	Incident	Measures taken into account
Exposure of Chemicals	Exposure of carbonmonoxide	Personal measures
	Exposure of carbonmonoxide	Local exhaust
	Exposure of carbonmonoxide	Intrument/method training
	Exposure of carbonmonoxide	Gas detection alarm
	Exposure of carbonmonoxide	Procedures
	Exposure of carbonmonoxide	Previous risk assessment for intrument
	Exposure of carbonmonoxide	Apparatus card
	Exposure of carbonmonoxide	Gas trolley
	Exposure of Cobalt(II) nitrate hexahydrate	Personal measures
	Exposure of Cobalt(II) nitrate hexahydrate	Fume hood
	Exposure of Cobalt(II) nitrate hexahydrate	Local exhaust
	Exposure of Cobalt(II) nitrate hexahydrate	SDS
	Exposure of Cobalt(II) nitrate hexahydrate	Procedures
	Exposure of hydrogen	Personal measures
	Exposure of hydrogen	Local exhaust
	Exposure of hydrogen	Intrument/method training
	Exposure of hydrogen	Gas detection alarm
	Exposure of hydrogen	Previous risk assessment for intrument
	Exposure of hydrogen	Apparatus card
	Exposure of hydrogen	Gas trolley
	Exposure of nitrogen	Personal measures
	Exposure of nitrogen	Local exhaust
	Exposure of nitrogen	SDS
	Exposure of nitrogen	Intrument/method training
	Exposure of nitrogen	Procedures
	Exposure of Chloroplatinic acid solution	Personal measures
	Exposure of Chloroplatinic acid solution	Fume hood
	Exposure of Chloroplatinic acid solution	Local exhaust
	Exposure of Chloroplatinic acid solution	SDS
	Exposure of Chloroplatinic acid solution	Procedures
	Exposure of Perrhenic acid solution	Personal measures
	Exposure of Perrhenic acid solution	Fume hood
	Exposure of Perrhenic acid solution	Local exhaust

Exposure of Chemicals	Exposure of Perrhenic acid solution	SDS
	Exposure of Perrhenic acid solution	Procedures
	Exposure of Aluminium Oxide	Personal measures
	Exposure of Aluminium Oxide	Local exhaust
	Exposure of Aluminium Oxide	SDS
	Exposure of Aluminium Oxide	Procedures
	Exposure of tetraamineplatinum(II) nitrate	Personal measures
	Exposure of tetraamineplatinum(II) nitrate	Fume hood
	Exposure of tetraamineplatinum(II) nitrate	Local exhaust
	Exposure of tetraamineplatinum(II) nitrate	SDS
	Exposure of tetraamineplatinum(II) nitrate	Procedures
	Exposure of Ruthenium(III) nitrosyl nitrate solution	Personal measures
	Exposure of Ruthenium(III) nitrosyl nitrate solution	Local exhaust
	Exposure of Ruthenium(III) nitrosyl nitrate solution	SDS
	Exposure of Ruthenium(III) nitrosyl nitrate solution	Gas detection alarm
	Exposure of Ruthenium(III) nitrosyl nitrate solution	Procedures
	Exposure of boric acid	Personal measures
	Exposure of boric acid	Fume hood
	Exposure of boric acid	Local exhaust
	Exposure of boric acid	SDS
	Exposure of boric acid	Procedures
	Exposure of titanium dioxide	Personal measures
	Exposure of titanium dioxide	Local exhaust
	Exposure of titanium dioxide	SDS
	Exposure of titanium dioxide	Procedures
	Exposure of silicon carbide	Personal measures
	Exposure of silicon carbide	Local exhaust
	Exposure of silicon carbide	SDS
	Exposure of silicon carbide	Procedures
	Exposure of nitric acid (68%)	Personal measures
	Exposure of nitric acid (68%)	Fume hood
	Exposure of nitric acid (68%)	Local exhaust
	Exposure of nitric acid (68%)	SDS
	Exposure of nitric acid (68%)	Procedures
	Exposure of silver oxide	Personal measures
	Exposure of silver oxide	Fume hood
	Exposure of silver oxide	Local exhaust

Exposure of Chemicals	Exposure of silver oxide	SDS
	Exposure of silver oxide	Procedures
Calcination furnace	Burns	Personal measures
	Burns	Intrument/method training
	Burns	Procedures
	Burns	Apparatus card
	Spills and accidents	Personal measures
	Spills and accidents	Local exhaust
	Spills and accidents	Intrument/method training
	Spills and accidents	Procedures
	Spills and accidents	Apparatus card
	Fire	Personal measures
	Fire	Intrument/method training
	Fire	Procedures
	Fire	Apparatus card
Spread of covid19 infection	Spread of covid19 infection	Covid 19 measures
	Spread of covid19 infection	Covid 19 measures

Existing relevant measures with descriptions:

Personal measures

Lab coat
Safety goggles (mandatory in all laboratories)
Gloves (read sds in order to choose the correct gloves)
Gas mask (read sds in order to choose the correct filters)
Filter mask (read sds in order to choose the correct type)

Fume hood

[Ingen registreringer]

Local exhaust

[Ingen registreringer]

SDS

Safety data sheet for each chemical

Intrument/method training

Get the proper training of an instrument/method

Gas detection alarm

[Ingen registreringer]

Procedures

Normal procedures at the lab, for example waste handling and cleaning.

Previous risk assessment for intrument

[Ingen registreringer]

X

Apparatus card

[Ingen registreringer]

Gas trolley

[Ingen registreringer]

Covid 19 measures

- Avoid touching the face
- Disinfection before and after with ethanol/solvent on all surfaces you are in contact with (door knob / card reader with code panel / if you use common equipment / keyboard / mouse / screen / desk)
- Keep 1m distance from colleagues
- Use nitrile gloves when touching shared lab set-ups and equipment
- Wash hands as often as possible
- Update the IKP Lab activity 2020 Teams excel sheet about your weekly planning. A week in advance.

Risk analysis with evaluation of likelihood and consequence

This part of the report presents detailed documentation of hazards, incidents and causes which have been evaluated. A summary of hazards and associated incidents is listed at the beginning.

The following hazards and incidents has been evaluated in this risk assessment:

- **Exposure of Chemicals**
  - Exposure of carbonmonoxide
  - Exposure of Cobalt(II) nitrate hexahydrate
  - Exposure of hydrogen
  - Exposure of nitrogen
  - Exposure of Chloroplatinic acid solution
  - Exposure of Perrhenic acid solution
  - Exposure of Aluminium Oxide
  - Exposure of tetraamineplatinum(II) nitrate
  - Exposure of Ruthenium(III) nitrosyl nitrate solution
  - Exposure of boric acid
  - Exposure of titanium dioxide
  - Exposure of silicon carbide
  - Exposure of nitric acid (68%)
  - Exposure of silver oxide
- **Calcination furnace**
  - Burns
  - Spills and accidents
  - Fire
- **Spread of covid19 infection**
  - Spread of covid19 infection

Detailed view of hazards and incidents:

Hazard: Exposure of Chemicals

Incident: Exposure of carbonmonoxide

H220 Ekstremt brannfarlig gass.
H280 Inneholder gass under trykk; kan eksplodere ved oppvarming.
H331 Giftig ved innånding.
H360D Kan skade det ufødte barnet.
H372 Forårsaker organskader ved langvarig eller gjentatt eksponering.

Likelihood of the incident (common to all consequence areas): **Less likely (2)**

Kommentar:

Using the gas alarm system, leak test, local exhaust and given insturment training lowers the probability a lot. But there is always a change that it could be a small leak, but this will not be a dangerous amount of gas if the gas alarm system works.

Consequence area: Helse

Risk:

Assessed consequence: **Large (3)**

Comment: Considering the health sentences in the SDS for carbon monoxide there is a large consequence for the unwanted risk. It's toxic, can cause a fire, and is a gas under pressure which can cause explosion. If somebody is pregnant it can also cause harm to the unborn child.

Consequence area: Ytre miljø

Risk:

Assessed consequence: **Large (3)**

Comment: If fire is caused or an explosion this could cause large harm on the environment around.

Consequence area: Materielle verdier

Risk:

Assessed consequence: **Medium (2)**

Comment: If fire is caused or an explosion this could cause downtime in the lab for less than a week or a bit more.

Incident: Exposure of Cobalt(II) nitrate hexahydrate

H272 Kan forsterke brann; oksiderende.
H302 + H332 Farlig ved svelging eller innånding.
H317 Kan utløse en allergisk hudreaksjon.
H318 Gir alvorlig øyeskade.
H334 Kan gi allergi eller astmasymptomer eller pustevansker ved innånding.
H341 Mistenkes for å kunne forårsake genetiske skader.
H350 Kan forårsake kreft.
H360F Kan skade forplantningsevnen.
H410 Meget giftig, med langtidsvirkning, for liv i vann.

Likelihood of the incident (common to all consequence areas): **Unlikely (1)**

Kommentar:

Using personal measures, local exhaust, fume hood and procedures it is a very low risk that you will get exposed of this chemical.

Consequence area: Helse ***Risk:***

Assessed consequence: **Very large (4)**

Comment: Since this chemical can cause cancer I look at the risk as very large. It can also cause fire, give allergic reactions, cause genetical harm and damage the fertility.

Consequence area: Ytre miljø ***Risk:***

Assessed consequence: **Large (3)**

Comment: Fire can happen and not correct waste handling can cause harm to life in water.

Consequence area: Materielle verdier ***Risk:***

Assessed consequence: **Medium (2)**

Comment: If fire is caused could cause downtime in the lab for less than a week or a bit more.
If I get cancer the school can get sued.

Consequence area: Omdømme ***Risk:***

Assessed consequence: **Medium (2)**

Comment: If someone get cancer for being in the lab, this will not give a good reputation for the school

Incident: Exposure of hydrogen

H220 - Ekstremt brannfarlig gass.
H280 - Inneholder gass under trykk; kan eksplodere ved oppvarming

Likelihood of the incident (common to all consequence areas): **Less likely (2)**

Kommentar:

Using the gas alarm system, leak test, local exhaust and given insturment training lowers the probability a lot. But there is always a change that it could be a small leak, but this will not be a dangerous amount of gas if the gas alarm system works.

Consequence area: Helse

Risk:

Assessed consequence: **Large (3)**

Comment: The gas is very flammable and is under high pressure, this could therefore cause a fire or an explosion. It is therefore a big consequence.

Consequence area: Ytre miljø

Risk:

Assessed consequence: **Large (3)**

Comment: If fire is caused or an explosion this could cause large harm on the environment around.

Consequence area: Materielle verdier

Risk:

Assessed consequence: **Medium (2)**

Comment: If fire is caused or an explosion this could cause shutdown of the lab for less than a week or a bit more. Also need for new equipment if the plant is destroyed.

Incident: Exposure of nitrogen

H281: Inneholder nedkjølt gass; kan forårsake alvorlige forfrysninger.

Likelihood of the incident (common to all consequence areas): **Less likely (2)**

Kommentar:

Using personal measures (gloves), intrument training and local exhaust the probability to get exposed by the chemical is very low.

Consequence area: Helse

Risk:

Assessed consequence: **Medium (2)**

Comment: Exposure of this chemical can cause a frost-harm wich could need medical treatment, but has a short recovery time.

Incident: Exposure of Chloroplatinic acid solution

H302 Farlig ved svelging.
H314 Gir alvorlige etseskader på hud og øyne.
H317 Kan utløse en allergisk hudreaksjon.
H334 Kan gi allergi eller astmasymptomer eller pustevansker ved innånding.

Likelihood of the incident (common to all consequence areas): **Less likely (2)**

Kommentar:

Using personal measures (correct gloves) and procedures for waste handling it is a low probality that you will get exposed for the chemical.

Consequence area: Helse

Risk:

Assessed consequence: **Large (3)**

Comment: Since the chemical can give burns, allergic reactions and asthmasymptomes the consequence of exposure of this chemical is large and could give a long recovery time.

Incident: Exposure of Perrhenic acid solution

H314 Gir alvorlige etseskader på hud og øyne.

Likelihood of the incident (common to all consequence areas): **Likely (3)**

Kommentar:

Using personal measures (correct gloves) and procedures for waste handling it is a low probality that you will get exposed for the chemical.

Consequence area: Helse

Risk:

Assessed consequence: **Large (3)**

Comment: Since the chemical can give burns (acid) on skin and eyes, the consequence to exposure of this chemical is somewhere between middle and large, depending on how large the spill is.
Middle if small spill and short recovery time.
Large if large spill and long recovery time.

Incident: Exposure of Aluminium Oxide

Ikke et farlig stoff eller en farlig blanding i henhold til bestemmelse (EF) nr. 1272/2008.

Likelihood of the incident (common to all consequence areas): **Likely (3)**

Kommentar:

Using personal measures and procedures for waste handling it is a low probality that you will get exposed for the chemical.

Consequence area: Helse

Risk:

Assessed consequence: **Small (1)**

Comment: The chemical is not dangerous

Incident: Exposure of tetraamineplatinum(II) nitrate

H272 Kan forsterke brann; oksiderende.
H315 Irriterer huden.
H317 Kan utløse en allergisk hudreaksjon.
H319 Gir alvorlig øyeirritasjon.
H335 Kan forårsake irritasjon av luftveiene.

Likelihood of the incident (common to all consequence areas): **Less likely (2)**

Kommentar:

Using personal measures and procedures for waste handling it is a low probality that you will get exposed for the chemical.

Consequence area: Helse

Risk:

Assessed consequence: **Medium (2)**

Comment: Since the chemical can cause eyeirritation, lungirritation, give allergic reactions, it is maybe needed medical treatment, but the restitution is short.

Incident: Exposure of Ruthenium(III) nitrosyl nitrate solution

H290 Kan være etsende for metaller.
H314 Gir alvorlige etseskader på hud og øyne.
H332 Farlig ved innånding.

Lagre på en kjølig plass. Hold beholderen tett lukket på et tørt og godt ventilert sted. Åpne beholdere må lukkes med forsiktighet og lagres i oppreist stilling for å hindre lekkasje.

Likelihood of the incident (common to all consequence areas): **Less likely (2)**

Kommentar:

Using personal measures and procedures for waste handling it is a low probality that you will get exposed for the chemical.

Consequence area: Helse

Risk:

Assessed consequence: **Large (3)**

Comment: The chemical is corrosive, harmful by inhalation and can realease nitrous gases when exposed to high temperatures. The consequence is therefore big, and will need long restitution time and medical treatment if exposed.

Incident: Exposure of boric acid

H360FD Kan skade forplantningsevnen. Kan gi fosterskader.

Likelihood of the incident (common to all consequence areas): **Less likely (2)**

Kommentar:

Using personal measures (correct gloves) and procedures for waste handling it is a low probality that you will get exposed for the chemical.

Consequence area: Helse

Risk:

Assessed consequence: **Large (3)**

Comment: Since it can cause birth defects it is a large consequence

Incident: Exposure of titanium dioxide

Ikke et farlig stoff eller en farlig blanding i henhold til bestemmelse (EF) nr. 1272/2008.
Dette stoffet klassifiseres ikke som farlig i henhold til Direktiv 67/548/EØF.

Likelihood of the incident (common to all consequence areas): **Likely (3)**

Kommentar:

Using personal measures lower the risk of being exposed, but it can happen when working with large amounts.

Consequence area: Helse

Risk:

Assessed consequence: **Small (1)**

Comment: Not dangerous chemical

Incident: Exposure of silicon carbide

Ikke et farlig stoff eller en farlig blanding i henhold til bestemmelse (EF) nr. 1272/2008.

Likelihood of the incident (common to all consequence areas): **Likely (3)**

Kommentar:

Using personal measures lower the risk of being exposed, but it can happen when working with large amounts.

Consequence area: Helse

Risk:

Assessed consequence: **Small (1)**

Comment: Not dangerous chemical

Incident: Exposure of nitric acid (68%)

H272 Kan forsterke brann; oksiderende.
H290 Kan være etsende for metaller.
H314 Gir alvorlige etseskader på hud og øyne.
H331 Giftig ved innånding.

Likelihood of the incident (common to all consequence areas): **Unlikely (1)**

Kommentar:

Using personal measures, local exhaust, fume hood and procedures it is a very low risk that you will get exposed of this chemical.

Consequence area: Helse

Risk:

Assessed consequence: **Large (3)**

Comment: Since the chemical can give burns (acid) on skin and eyes, the consequence to exposure of this chemical is somewhere between middle and large, depending on how large the spill is.
Middle if small spill and short recovery time.
Large if large spill and long recovery time.

Incident: Exposure of silver oxide

H272 Kan forsterke brann; oksiderende.
H314 Gir alvorlige etseskader på hud og øyne.
EUH044 Eksplosjonsfarlig ved oppvarming i lukket rom.

Likelihood of the incident (common to all consequence areas): **Unlikely (1)**

Kommentar:

Using personal measures, local exhaust, fume hood and procedures it is a very low risk that you will get exposed of this chemical.

Consequence area: Helse

Risk:

Assessed consequence: **Medium (2)**

Comment: The chemical can cause severe burns to skin and eyes and can therefore require medical treatment. Short or long treatment time dependent of how bad the burn is.

Consequence area: Materielle verdier

Risk:

Assessed consequence: **Small (1)**

Comment: The chemical can intensify fire (oxidizing). The amounts used are small so if fire is caused it is easy to put out the fire.

Hazard: Calcination furnace

Incident: Burns

Likelihood of the incident (common to all consequence areas): **Less likely (2)**

Kommentar:

Using personal measures (like heat resistant gloves) and procedures the probability to get a serious burn is very low.

Consequence area: Helse

Risk:

Assessed consequence: **Medium (2)**

Comment: Burn on skin can give small recovery time, but could need medical treatment.

Incident: Spills and accidents

Likelihood of the incident (common to all consequence areas): **Less likely (2)**

Kommentar:

Using personal measures, local exhaust, procedures, and intrument training lowers the probability, but it can still happen an accident.

Consequence area: Materielle verdier

Risk:

Assessed consequence: **Medium (2)**

Comment: Getting a spill or accident on an instrument could cause a fire or destroy the instrument.

Incident: Fire

Due to the extremely high temperatures that lab furnaces operate at, there is always an increased risk of fire.

Likelihood of the incident (common to all consequence areas): **Unlikely (1)**

Kommentar:

Due to the extremely high temperatures that lab furnaces operate at, there is always an increased risk of fire. Using personal measures, intrument training, procedures, and fire alarm the probability for a big fire is very low.

Consequence area: Helse

Risk:

Assessed consequence: **Large (3)**

Comment: Could need medical treatment and long recovery time if a big fire is created.

Consequence area: Materielle verdier

Risk:

Assessed consequence: **Large (3)**

Comment: If fire is created this could destroy the builiding and the instruments.

Hazard: Spread of covid19 infection

Incident: Spread of covid19 infection

Likelihood of the incident (common to all consequence areas): **Unlikely (1)**

Kommentar:

[Ingen registreringer]

Consequence area: Helse

Risk:

Assessed consequence: **Medium (2)**

Comment: I am young and healthy with no underlyong sickness. Getting Covid19 would maybe need medical treatment, but not a long recovery time.

Consequence area: Ytre miljø

Risk:

Assessed consequence: **Very large (4)**

Comment: Spread of covid19 has a huge impact on the whole world. The consequence is therefore very big, spreading the virus to the wrong person could kill them.

Overview of risk mitiating measures which have been decided:

Below is an overview of risk mitigating measures, which are intended to contribute towards minimizing the likelihood and/or consequence of incidents:

Overview of risk mitigating measures which have been decided, with description:

Detailed view of assessed risk for each hazard/incident before and after mitigating measures

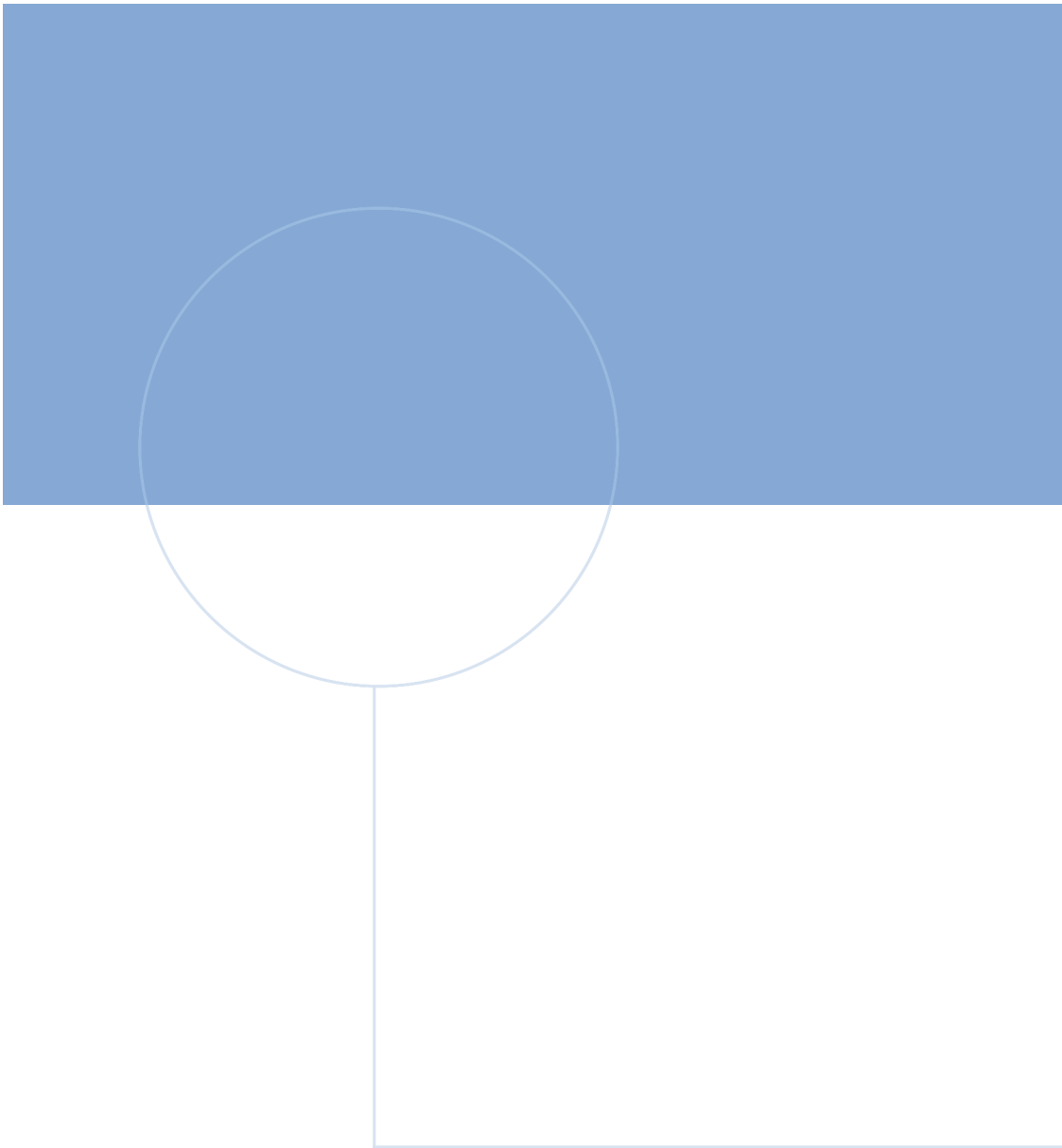

NTNU

Norwegian University of
Science and Technology